ORNL/TM-2017/292

HTV Post Irradiation Examination (PIE) Results and Analysis

Timothy D. Burchell

June 2017

DOCUMENT AVAILABILITY

Reports produced after January 1, 1996, are generally available free via US Department of Energy (DOE) SciTech Connect.

Website http://www.osti.gov/scitech/

Reports produced before January 1, 1996, may be purchased by members of the public from the following source:

National Technical Information Service
5285 Port Royal Road
Springfield, VA 22161
Telephone 703-605-6000 (1-800-553-6847)
TDD 703-487-4639
Fax 703-605-6900
E-mail info@ntis.gov
Website http://classic.ntis.gov/

Reports are available to DOE employees, DOE contractors, Energy Technology Data Exchange representatives, and International Nuclear Information System representatives from the following source:

Office of Scientific and Technical Information
PO Box 62
Oak Ridge, TN 37831
Telephone 865-576-8401
Fax 865-576-5728
E-mail reports@osti.gov
Website http://www.osti.gov/contact.html

This report was prepared as an account of work sponsored by an agency of the United States Government. Neither the United States Government nor any agency thereof, nor any of their employees, makes any warranty, express or implied, or assumes any legal liability or responsibility for the accuracy, completeness, or usefulness of any information, apparatus, product, or process disclosed, or represents that its use would not infringe privately owned rights. Reference herein to any specific commercial product, process, or service by trade name, trademark, manufacturer, or otherwise, does not necessarily constitute or imply its endorsement, recommendation, or favoring by the United States Government or any agency thereof. The views and opinions of authors expressed herein do not necessarily state or reflect those of the United States Government or any agency thereof.

ORNL/TM-2017/292

Materials Science & Technology Division

HTV POST IRRADIATION EXAMINATION (PIE) RESULTS AND ANALYSIS

Timothy D. Burchell

Date Published: June 2017

Prepared by
OAK RIDGE NATIONAL LABORATORY
Oak Ridge, TN 37831-6283
managed by
UT-BATTELLE, LLC
for the
US DEPARTMENT OF ENERGY
under contract DE-AC05-00OR22725

Contents

FIGURES

TABLES

ABBREVIATIONS AND ACRONYMS

AG	Against-grain
AGC	Advanced Graphite Creep
ASME	American Society for Mechanical Engineers
ATR	Advanced Test Reactor
dpa	Displacements per atom
HFIR	High Flux Isotope Reactor
HTR	High Temperature Reactor
HTV	High Temperature Vehicle
INL	Idaho National Laboratory
LAMDA	Low Activation Materials Development and Analysis
MPO	Memorandum Purchase Order
ORNL	Oak Ridge National Laboratory
PIE	Post Irradiation Examination
Pre-IE	Pre-Irradiation Examination
RT	Room Temperature
SiC	Silicon Carbide
s/c	sub capsule
TOF	Time of Flight
TM	Temperature Monitor
SiC	Silicon Carbide
WG	With-grain

ABSTRACT

This report is responsive to 2017 Idaho National Laboratory (INL) Memorandum Purchase Order (MPO) No. 00181805, statement of work 13687 "HTR Graphite R&D – FY ORNL 2017 MPO", Deliverable 12A "issue final report on the HTV PIE to INL", due June 15th 2017.

The HTV (High Temperature Vessel) was a HFIR (High Flux Isotope Reactor) high temperature target rod capsule in support of the DOE's (Department of Energy) High Temperature Reactor (HTR) program. The HTV capsule contained eight sub-capsules, each with nine graphite specimens. The sub-capsules were designed to operate at ~900°C, ~1200°C or ~1600°C. The actual irradiation temperature was established by interrogating SiC and graphite TMs during PIE (post-irradiation examination). Actual graphite specimen temperatures were estimated to be 869, 1189 and 1412°C. The capsule dose ranged from 1.49 dpa to 3.34 dpa, and varied with specimen position within the capsule the maximum dose occurring at the reactor mid-plane and the minimum dose occurring at the core periphery.

The irradiated graphite specimens were examined during PIE to establish their high temperature dimensional and elastic (Young's) modulus changes. The PIE results are reported and analyzed here. The dimensional and modulus changes were shown to have a strong thermal dependence.

The dimensional changes were small, being of the order of a few percent or less, ranging from a maximum shrinkage of -3.1% (PCEA WG, T_{irr}=1412°C) at 3.3 dpa) to +0.131% (2114 AG, T_{irr} = 869 at 3.2 dpa). The specimen volume shrinkages varied from –0.81 (2114, T_{irr} = 840 at 3.1 dpa) to -9.15% (PCEA, T_{irr}=1412°C at 3.3 dpa). The volume changes were larger at higher irradiation temperatures. Of the six grades examined, only 2114 moved into the net positive dimensional swelling situation. Significantly, the volume change for 2114 remained negative at the doses and temperature tested here. Dimensional and volume changes were explained in terms of the temperature dependence of the crystal growth rate, the anisotropy of the crystal growth (crystallographic c-axis growth and crystallographic a-direction shrinkage) and the thermal closure of aligned micro-porosity

The modulus changes were much larger, being of the order of a few tens of percent. A trend of lesser fractional increases of Young's Modulus with an increasing T_{irr} was noted. The minimum increase in Young's Modulus was 20% (H-451 WG, T_{irr}=1412°C at 3.3 dpa) and the maximum 71% (IG-110, T_{irr} = 840°C at 3.3 dpa). The rise in Young's modulus is attributed to dislocation pinning by lattice defects produced by neutron irradiation and the temperature dependency of this increase is related to the irradiation temperature influence on the number of defect available to pin dislocations.

1. OBJECTIVES

The objectives of the HTV experiment were fourfold:

1. To irradiate a selection of graphite grades as used in the AGC Creep capsules at high temperatures (deign temperature ~900°C, ~1200°C and ~1500°C) and to modest doses (~1.5 to 3.5 dpa) to provide swelling data for the AGC 5/6 capsules,

2. to demonstrate that the graphite grades examined here do not enter into net swelling at elevated temperature and thus would not become jammed in the creep capsule's channels,

3. to demonstrate the applicability of the linear visco-elastics creep law which will only apply in the shrinkage region before volume turn-around, and

4. to determine the extent of the Young's Modulus change at low dose (~1,5 to 3.5 dpa) and high temperatures (design temperatures ~900°C, ~1200°C and ~1500°C) and show that the Young's Modulus correction to creep data is small and can be neglected.

2. INTRODUCTION

The binding energy of a carbon atom in the graphite lattice is about 7 eV [1]. Impinging energetic particles such as fast neutrons, electrons, or ions can displace carbon atoms from their equilibrium positions. There have been many studies of the energy required to displace a carbon atom (E_d), as reviewed by Kelly [2] and Burchell [3]. The value of E_d is not well defined but lies between 24 and 60 eV. The latter value has gained wide acceptance and use in displacement damage calculations, but a value of 30 eV would be more appropriate [4].

The primary atomic displacement [primary knock-on carbon atoms (PKAs)] produced by energetic particle collisions produce further carbon atom displacements in a cascade effect. The cascade carbon atoms are referred to as secondary knock-on atoms (SKAs). The displaced SKAs tend to be clustered in small groups of 5-10 atoms and for most purposes it is satisfactory to treat the displacements as if they occur randomly. The total number of displaced carbon atoms will depend upon the energy of the PKA, which is itself a function of the neutron energy spectrum, and the neutron flux. Once displaced the carbon atoms recoil through the graphite lattice, displacing other carbon atoms and leaving vacant lattice sites. However, not all of the carbon atoms remain displaced. The displaced carbon atoms diffuse between the graphite layer planes in two dimensions and a high proportion will recombine with lattice vacancies. Others will coalesce to form C2, C3, or C4 linear molecules. These in turn may form the nucleus of a dislocation loop—essentially a new graphite plane. Interstitial clusters may, on further irradiation, be destroyed by a fast neutron or carbon knock-on atom (irradiation annealing). Adjacent lattice vacancies in the same graphitic layer are believed to collapse parallel to the

layers, thereby forming sinks for other vacancies which are increasingly mobile above 600°C, and hence can no longer recombine and annihilate interstitials.

A principal result of carbon atom displacements is crystallite dimensional change. Interstitial defects will cause crystallite growth perpendicular to the layer planes (c-axis direction), and relaxation in the plane due to coalescence of vacancies will cause a shrinkage parallel to the layer plane (a-axis direction). The damage mechanism and associated dimensional changes are illustrated in Figure 1 . Dimensional changes can be very large, as demonstrated in studies on well-ordered graphite materials, such as pyrolytic graphite, which has frequently been used to study the neutron-irradiation induced dimensional changes of the graphite crystallite (e.g., Kelly [5], Engle & Eatherly [6]).

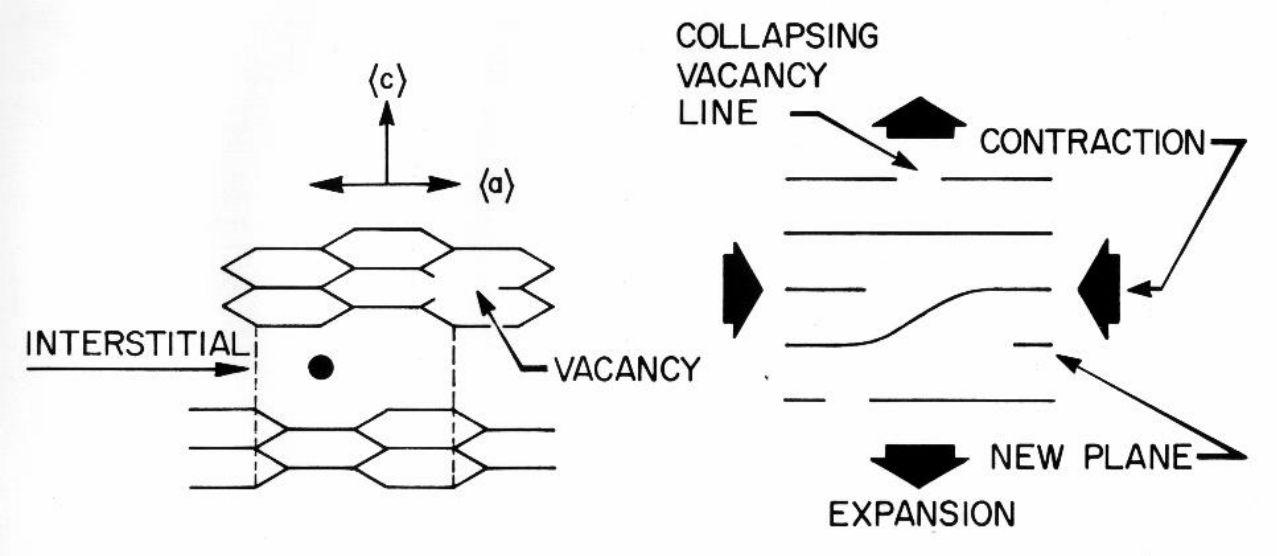

Figure 1 Neutron irradiation damage mechanism illustrating the induced crystal dimensional strains [3].

The dimensional changes that occur in nuclear (artificial) graphite up to the point of volume turn-around are a complex mixture of several factors and are strongly affected by the Irradiation temperature. These factors are:

- Crystal growth rates
- crystal orientation/anisotropy
- accommodation porosity
- degree of crystal perfection

The influence of each of these factors on nuclear graphites dimensional change is expanded upon below:

The crystal growth rates are a strong function of the irradiation temperature. Figure 2 shows the relationship between the growth rate and the irradiation temperature at a dose of 6.6 dpa and over the irradiation temperature range 300 - 1500°C [2]. Crystal growth reduces with increasing radiation temperature in the range 300 to ~900°C and the increases rapidly with increasing irradiation temperature to 1500°C. Because the irradiation temperatures here are in the latter range it is anticipated that the dimensional change data will reflect the reported tripling of the growth rates with increasing temperature [2].

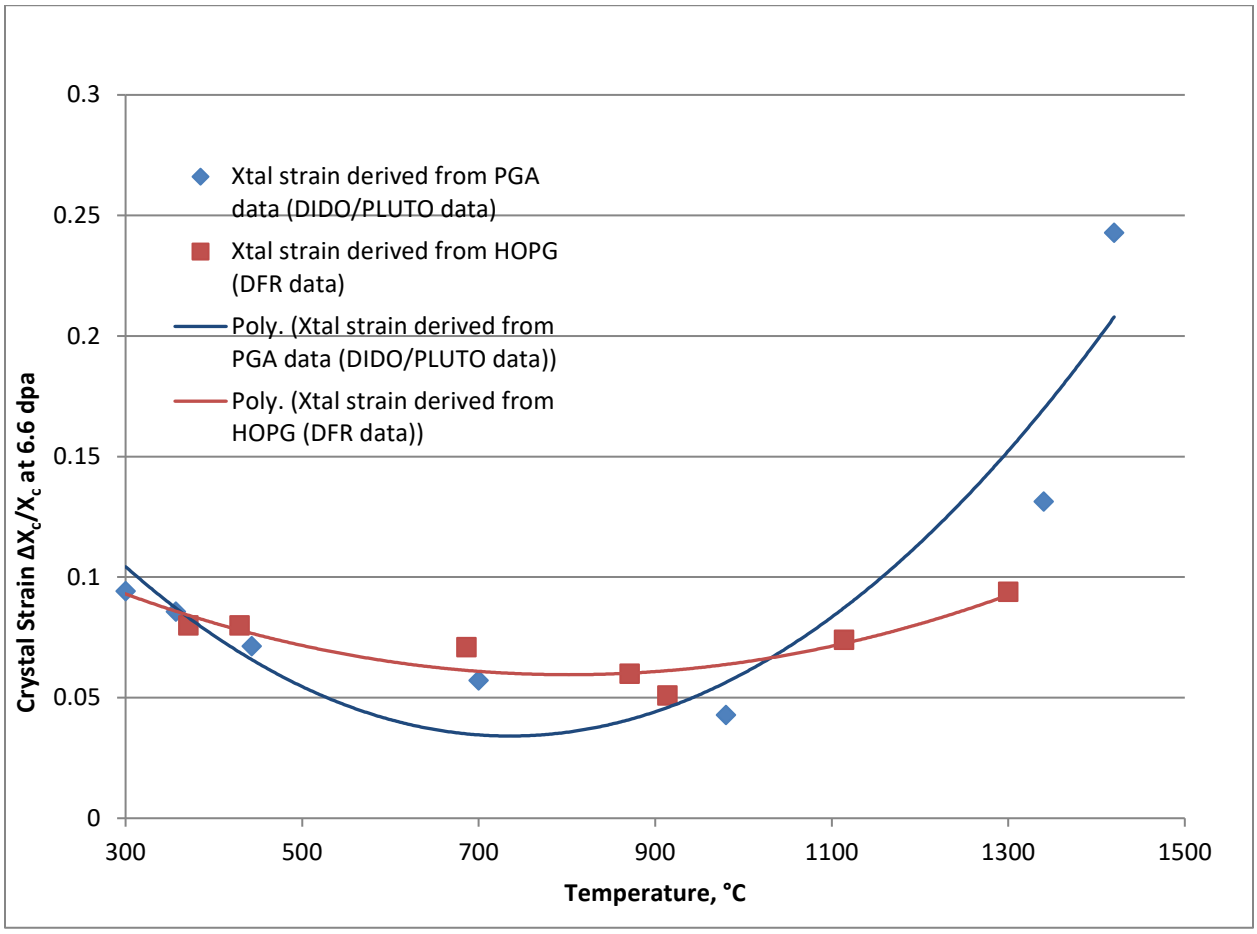

Figure 2 Variations of crystal growth rate with irradiation temperature [2]

Polygranular graphite exhibit a polycrystalline structure, usually with significant texture (anisotropy) resulting from the method of forming during manufacture. Consequently, structural and dimensional changes in polygranular graphite are a function of the crystallite dimensional changes and the graphite's texture. Significant anisotropy may occur in the neutron irradiation induced dimensional changes due to the alignment of the crystalline filler during forming (Figure 3). There is gross crystal anisotropy resulting from the crystallite a-axis shrinkage parallel to the basal plane and c-axis growth perpendicular to the crystallographic basal planes. Consequently, it is possible to discern a WG and AG direction. Note that extruded grades have their WG direction parallel to the forming direction and molded graphites have their AG directions parallel to the molding direction.

Moreover, in polygranular graphite, thermal shrinkage cracks that occur during manufacture that are preferentially aligned in the crystallographic a-direction and will initially accommodate the c-direction expansion, so mainly a-direction contraction will be observed. The graphite thus undergoes net volume shrinkage. With increasing neutron dose (displacements) the incompatibility of crystallite dimensional changes leads to the generation of new porosity oriented parallel to the basal planes, and the volume shrinkage rate falls, eventually reaching zero. The graphite now begins to swell at an increasing rate with increasing neutron dose. The graphite thus undergoes a volume change "turnaround" into net growth that continues until the generation of cracks and pores in the graphite, due to differential crystal strain, eventually causes total disintegration of the graphite. This "accommodation porosity" also manifests itself in the observed thermal expansion behavior of unirradiated graphite, which has an increasing coefficient of thermal expansion with increasing temperature.

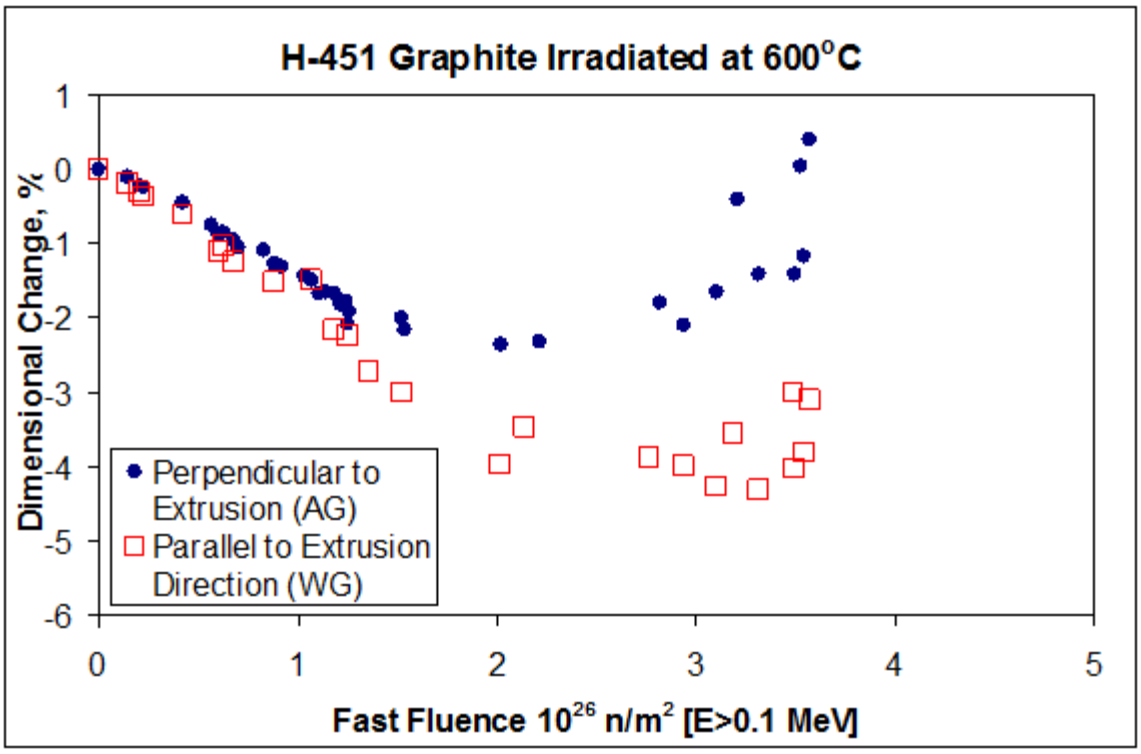

Figure 3 Dimensional change behavior of H-451 graphite at an irradiation temperature of 600°C. [7]

Price [8] conducted a study of the neutron-irradiation induced dimensional changes in pyrolytic graphite. He showed the crystallite shrinkage in the a-direction for neutron doses up to 12 displacements per atom (dpa) for samples that were graphitized at a temperature of 2200-3300°C prior to being irradiated at 1300-1500°C (Figure 4). The a-axis shrinkage increased linearly with dose for all of the samples, but the magnitude of the shrinkage at any given dose decreases with increasing graphitization temperature. Similar trends were noted for the c-axis expansion. The significant effect of graphitization temperature on irradiation induced dimensional change

accumulation can be attributed to thermally induced improvements in crystal perfection, thereby reducing the number of vacancy trapping sites in the lattice.

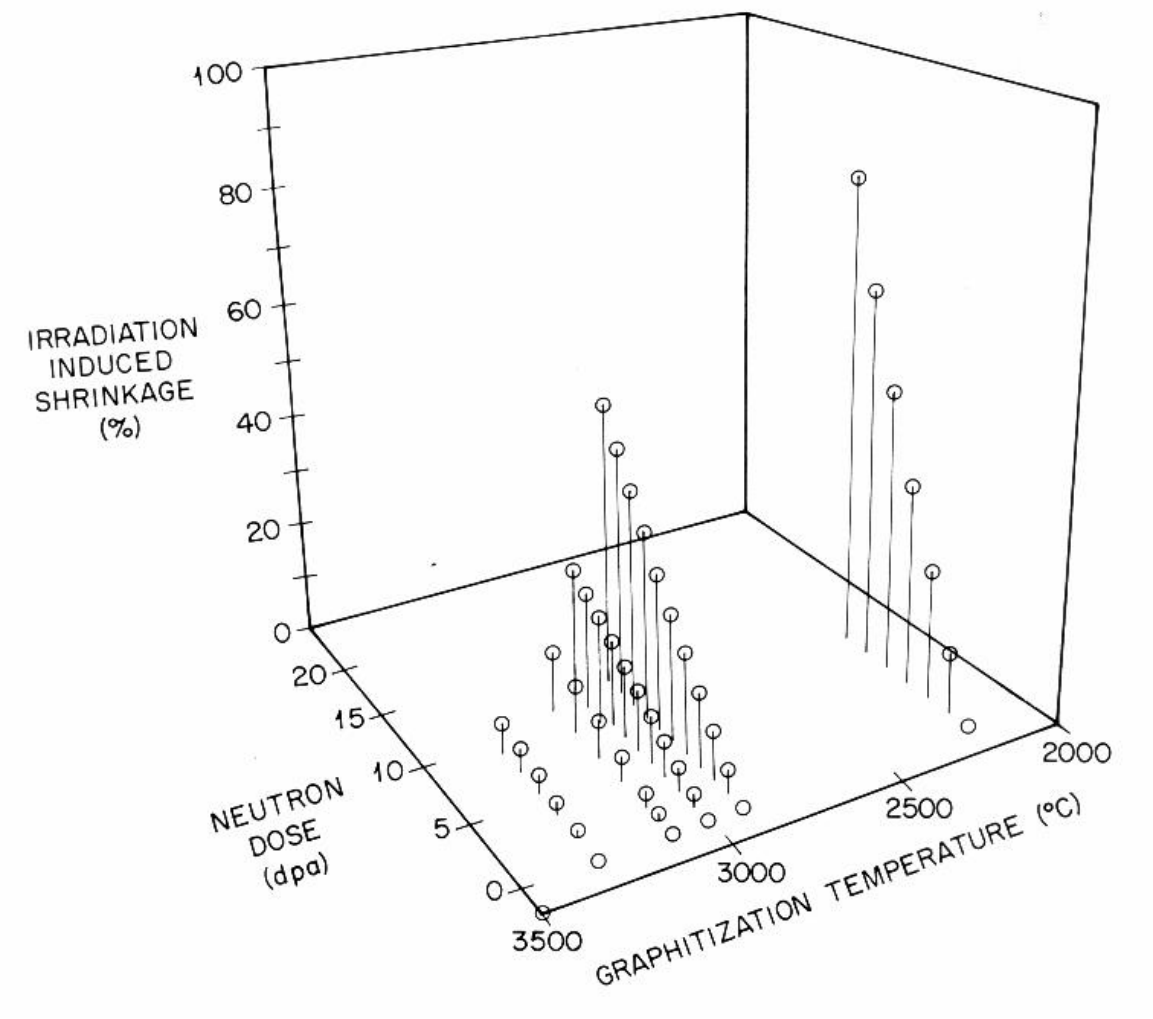

Figure 4 Neutron irradiation-induced a-axis shrinkage behavior of pyrolytic graphite showing the effects of graphitization temperature on the magnitude of the dimensional change [8].

As is shown here, the irradiation temperature has a significant effect on the extent and magnitude of the overall dimensional change.

The irradiation induced changes in Young's modulus show a complex dependency on neutron dose and irradiation temperature [5]. At irradiation temperatures below 300°C there is an initial increase in modulus to a peak, the magnitude of the peak depending upon the graphite grade. The initial increase is generally about 2.5 times the initial modulus and is attributed to the effect of dislocation pinning by lattice defects produced by neutron irradiation. The initial increase takes longer the higher the irradiation temperatures. The modulus then increases further, followed by a fall to a magnitude below the initial modulus with increasing dose, eventually reaching zero when the material can be expected to disintegrate. In irradiations above 300°C the initial rise

occurs to magnitudes which decrease with increasing irradiation temperature, and this is followed by a period of constancy in the modulus. Graphite then increases its modulus followed by the fall to zero. This is precisely the behavior seen in work in grade GraphNOL N3M conducted by Burchell and Eatherly [9] and is shown in Figure 5.

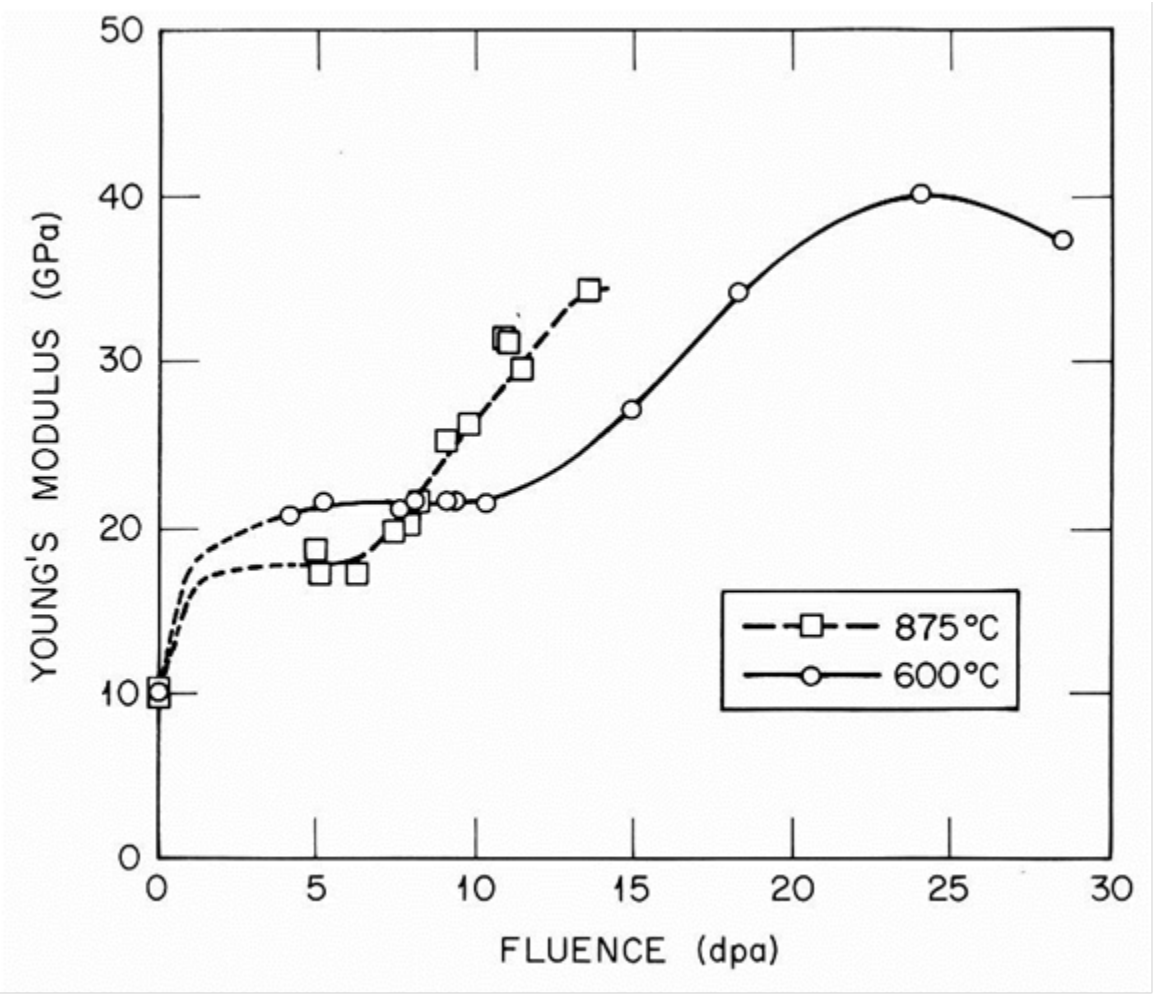

Figure 5 Neutron irradiation-induced Young's modulus changes for GraphNOL N3M at irradiation temperatures 600 and 875°C.

Increases of irradiation temperature reduce the dose at which the second rise and subsequent fall occurs. The final fall in modulus is associated with pore generation after volume turnaround.

3. EXPERIMENTAL

Post irradiation examination (PIE) experimental measurements of mass, dimensions and elastic modulus were made in the Low Activation Materials Development & Analysis (LAMDA) lab at Oak Ridge National Laboratory (ORNL), using identical methods as were used for the pre-irradiation examination (Pre-IE) [10]. Figure 6 shows the measurement locations used for the HTV specimen PIE. Mass and dimensional measurements were conducted in accordance with ASTM C559 [11], and the dynamic Young's modulus was determined from the longitudinal sonic velocity in accordance with C769-15 [12].

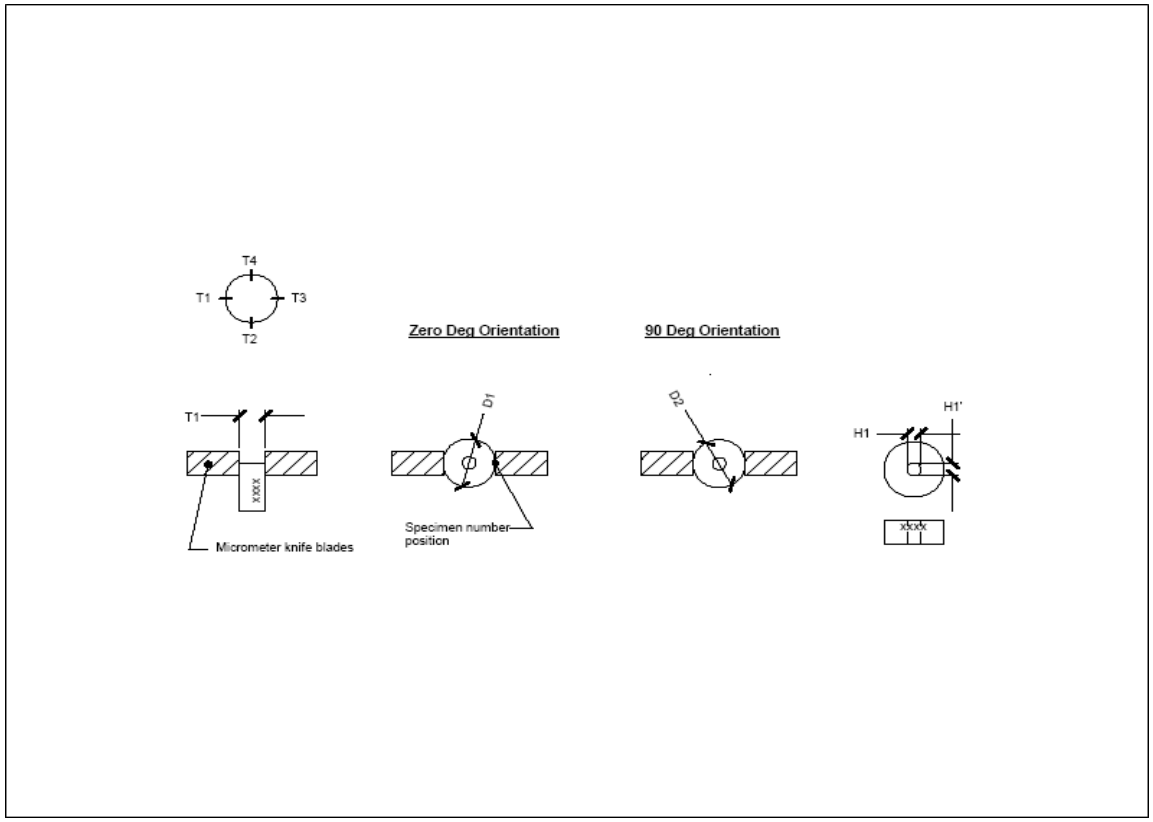

Figure 6 Measurement locations used for HTV specimen dimensional PIE

The graphite and SiC temperature monitors were read either by their expansion (sub capsules 2 and 4, T_{irr}~840°C (actual), SiC TM's only) in accordance with E228-11[13]. Sub-capsules 3,7 & 8 (Tirr~1189°C(actual)) and sub-capsules 1, 5 & 6 (Tirr~1412°C(actual)) had their resistivity read using the 4-pt probe method as described in C611-98 [14]. The isochronal annealing schedule for the SiC monitors from sub-capsules 3, 7 & 8, and sub-capsules 1, 5 & 6 is given in Table 1. The temperature monitors were heated to the annealing temperature at 5°C/min and held at the annealing temperature for at least 30 minutes before being furnace cooled to room temperature for resistivity determination. Since we have no interest in the absolute value of resistivity, only in the relative change in resistivity, the voltage reading was taken as the mean of five measurements in forward current mode only. Details of the equipment used for experimental PIE measurements are given in Table 2.

Table 1 Isochronal annealing schedule for HTV sub-capsules 3, 7 & 8, and sub-capsules 1, 5 & 6.

HTV TM ANNEALING TEMPERATURE SCHEDULE			
Sub Capsule*	Des Temp	Annealing Temp	Actions
3, 7, and 8	1200	1000	Anneal, cool to RT, measure resistivity
TM Nos.		1050	Anneal, cool to RT, measure resistivity
4A, 9A & 10A		1100	Anneal, cool to RT, measure resistivity
8B, 4B & 1B		1150	Anneal, cool to RT, measure resistivity
		1200	Anneal, cool to RT, measure resistivity
		1250	Anneal, cool to RT, measure resistivity
		1300	Anneal, cool to RT, measure resistivity
		1350	Anneal, cool to RT, measure resistivity
		1400	Anneal, cool to RT, measure resistivity
		1500	Anneal, cool to RT, measure resistivity
1, 5,and 6	1500	1200	Anneal, cool to RT, measure resistivity
TM Nos.		1300	Anneal, cool to RT, measure resistivity
1A, 7A & 8A		1400	Anneal, cool to RT, measure resistivity
7B, 5B & 6B		1450	Anneal, cool to RT, measure resistivity
		1500	Anneal, cool to RT, measure resistivity
		1550	Anneal, cool to RT, measure resistivity
		1600	Anneal, cool to RT, measure resistivity
		1650	Anneal, cool to RT, measure resistivity
		1700	Anneal, cool to RT, measure resistivity
		1750	Anneal, cool to RT, measure resistivity
		1800	Anneal, cool to RT, measure resistivity
	*2 TM's per sub cap		

Table 2 Experimental equipment used in the PIE measurement reported here

Property	ASTM Test Method	Equipment	Serial, Calibration or ID Number
Mass	C559	Metler Microbalance	ID# X-102919
Dimensions	C559	Mitutoyo Micrometer 0-1"	Cal #27047744
		Mitutoyo Digital Indicator for Dyer small hole gauge	Cal # 005069
Sonic Velocity/Young's Modulus	C769-15	National Instruments NI PXI-1033 Scope Interface	Cal # A001182 S/ # 1466F05
	C769-15	Olympus Panametrics NDT Signal Generator Model 5077PR	S/ # 90183908 Cal # A001182
Electrical Resistivity	C611-98	Keithley 2400 Source Meter Keithley 2182 Nano-voltmeter	S/N 0987875 S/N 0985274
Thermal Expansion	E228-11	Netzsch DIL 402 CD	S/# 219 7 038G

4. RESULTS

4.1 IRRADIATION CONDITIONS

4.1.1 Irradiation Doses

The actual HFIR cycle lengths for the HTV capsule were a little longer the planned. Consequently a scaling factor was used to calculate the correct capsule fluences/doses.

$$\varphi_{ACTUAL} = \varphi_{PLANNED} \times 1.054 \qquad \text{Equation 1}$$

This is scaling factor was based upon the actual dose (φ_{ACTUAL}) of 4183 MWd compared to the planned dose of 3970 MWd [15].

The core flux distribution is well characterized for the HFIR [16] and historical data for the flux distribution was used for planning and design purposes [15]. However, flux wires were included in HTV for a backup flux measurement. Post irradiation analysis of the Al/Co and Cu flux wires showed good agreement between the flux wire's measured activity and the calculated (using the historical flux distribution) activity (Figure 7 and Figure 8). Thus the assumed HFIR historical flux distribution used for the calculated activity wass verified by the data being in agreement in Figure 7 and Figure 8.

Other flux wires incorporated in HTV (Fe and Ti) were submitted for activity measurement, but the data were deemed unreliable, probably due to the decay of activity caused by the long delay after irradiation and the flux wire activity measurements.

Therefore, the actual dose to the graphite samples only needs to be corrected for the actual experiments duration per equation 1. The corrected (actual dose is given in the experimental data (appendix A and B) and is used here in all the data plots.

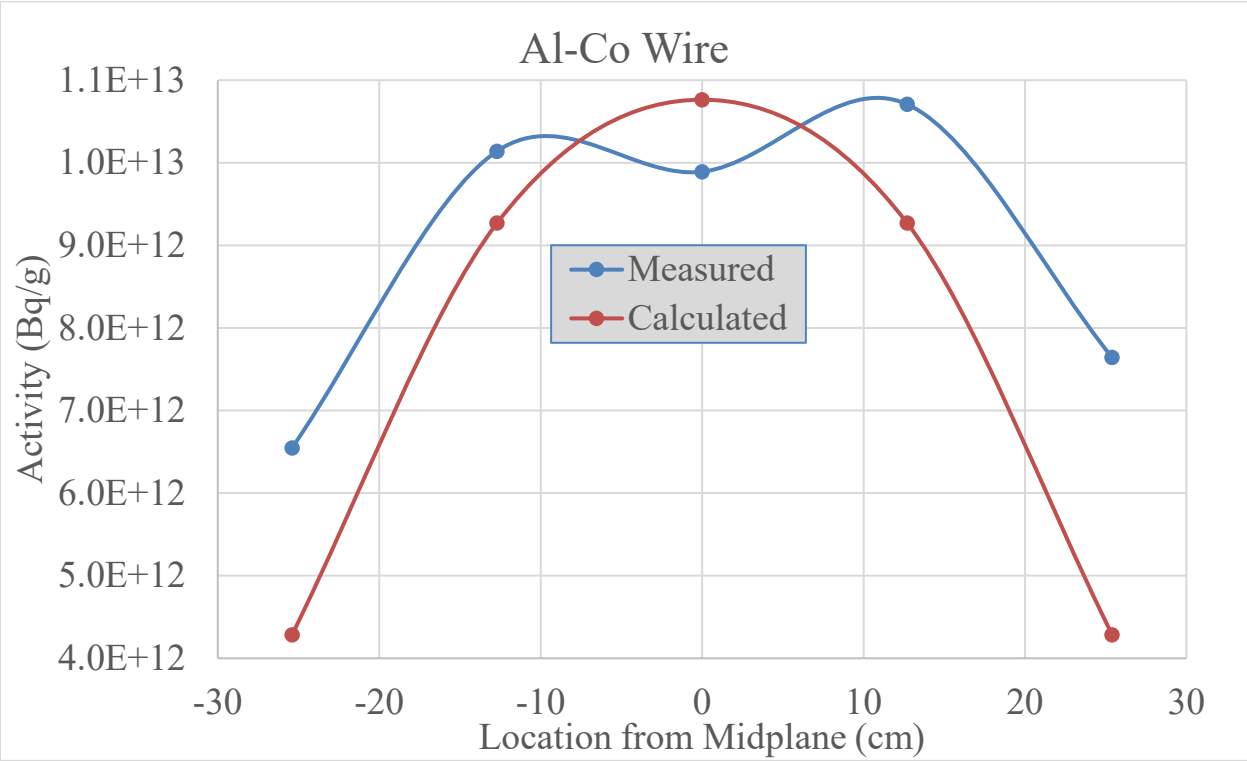

Figure 7 Comparison of calculated and measured activities for Al-Co flux wire from HFIR capsule HTV

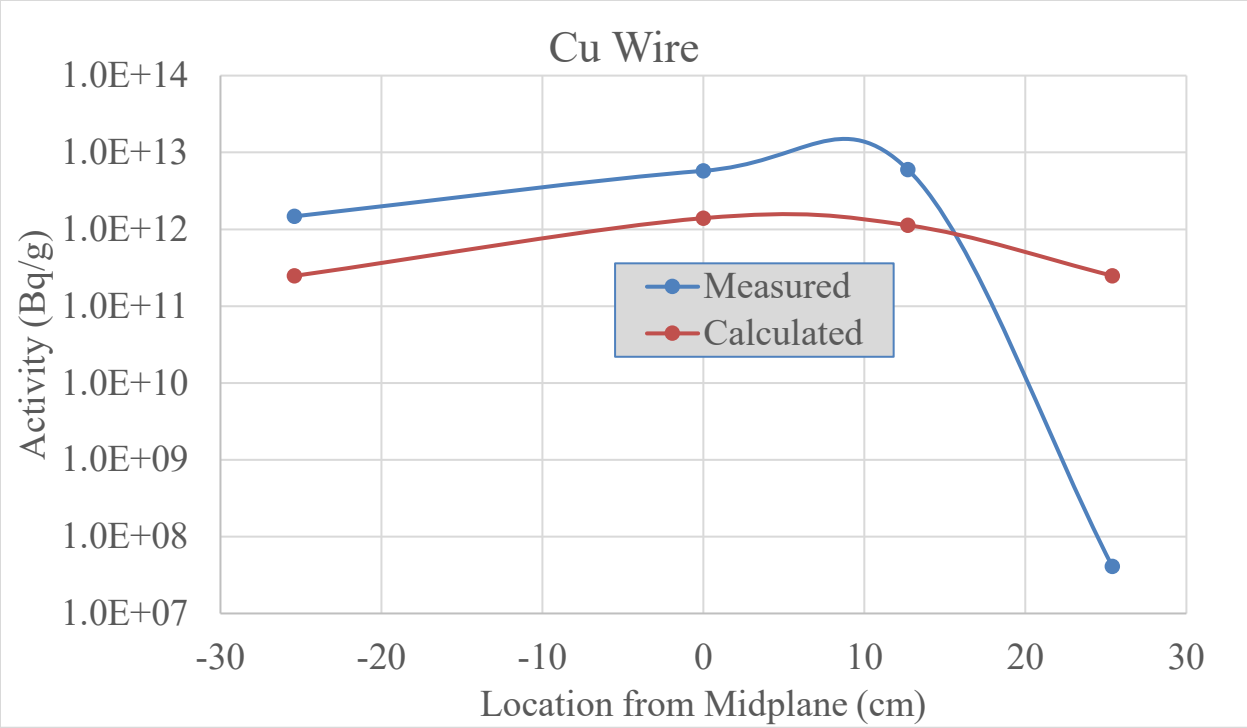

Figure 8 Comparison of calculated and measured activities for Cu flux wire from HFIR Capsule HTV

4.1.2 Irradiation Temperature

The irradiation temperatures of the HTV sub capsules were assessed by reading the temperature monitors via thermal expansion or isochronal annealing/electrical resistivity. The temperature monitors were individually marked as shown in Table 3.

Table 3 HTV temperature monitors ID marking scheme

HTV sub capsule	Location/Material	ID Mark	TM Serial No.
1	Upper/SiC	• |	1A
1	Lower/Graphite	• ||	7B
2	Upper/SiC	•• |	2A
2	Lower/SiC	•• ||	3A
3	Upper/SiC	••• |	4A
3	Lower/Graphite	••• ||	8B
4	Upper/SiC	•••• |	5A
4	Lower/SiC	•••• ||	6A
5	Upper/SiC	•| |	7A
5	Lower/Graphite	•| ||	5B
6	Upper/SiC	•|• |	8A
6	Lower/Graphite	•|• ||	6B
7	Upper/SiC	•||• |	9A
7	Lower/Graphite	•||• ||	4B
8	Upper/SiC	•|||• |	10A
8	Lower/Graphite	•|||• ||	1B

4.1.2.1 Thermal Expansion

Sub capsules 2 and 4 (design T_{irr} = 900°C (design)) each contained two SiC monitors. These SiC temperature monitors were interrogated using the thermal expansion analysis reported by Campbell *et al* [17]. The thermal expansion results (heating and cooling) are shown graphically for the monitors in Figure 9 to Figure 12. The graphical temperature analysis data is summarized in Table 4.

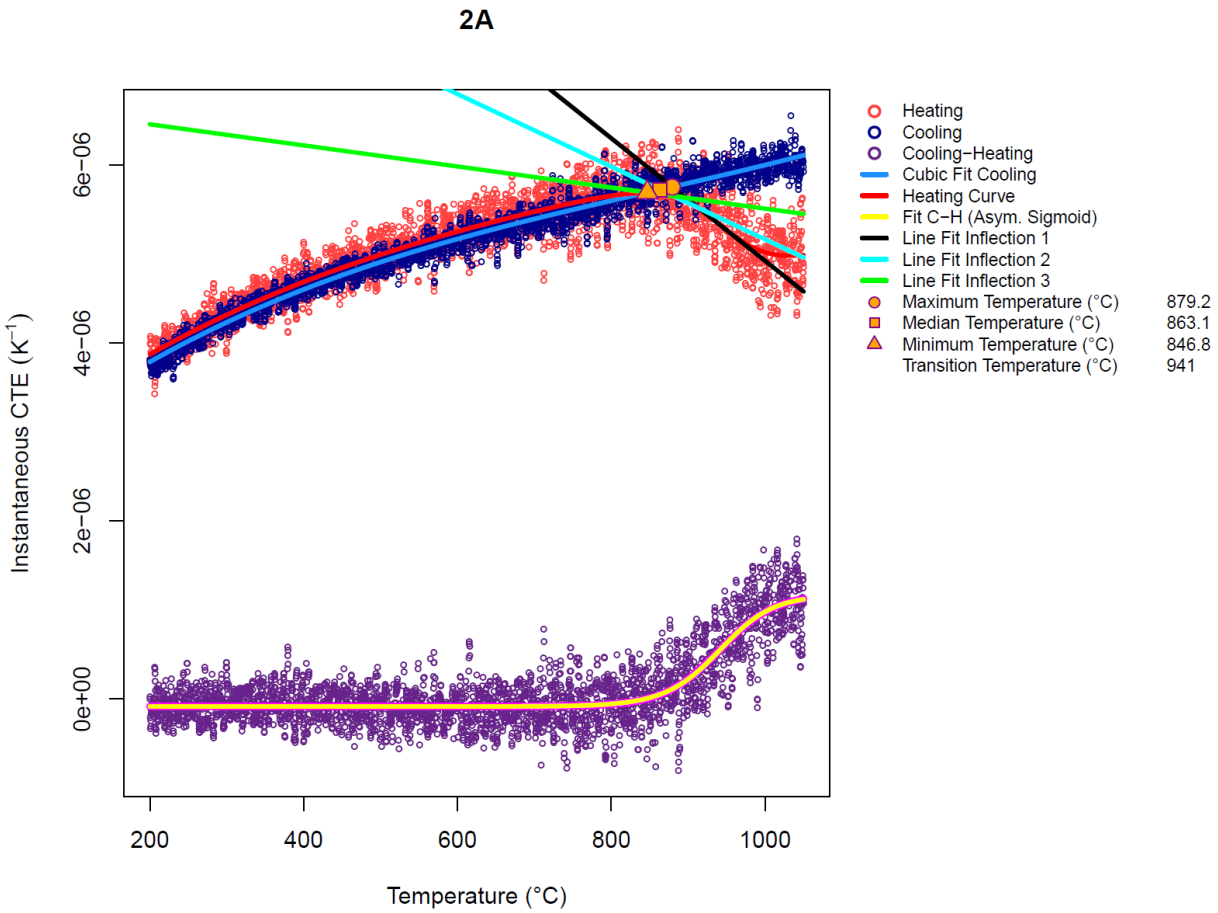

Figure 9 Analysis plot of temperature monitor 2A (HTV sub capsule 2)

A thermal analysis of the HTV Capsule was reported by McDuffee [18]. The temperature monitors in sub-capsules 2 and 4 (design irradiation temperature ~ 900°C) were expected to run 30-40°C hotter than the graphite specimens contained therein. Moreover, the graphite samples were expected to display a variation in their temperature of ~+2°C. The mean of the expansion TM data indicated median temperature was 869°C (Table 4). Taking into account the predicted [18] graphite specimen temperatures, it appears likely that sub capsules 2 and 4 ran cooler than design expectations and the graphite irradiation temperature was ~ (869-30°C), or ~840°C. From Figure 9 - Figure 12 and Table 4 it is seen that annealing occurs over a range of temperatures spanning 30-70°C. Thus we estimate the uncertainty in actual specimen irradiation temperature to be ±25°C. Based on the continuous expansion-annealing indicated temperatures, the irradiation temperature of the graphite specimens in sub-capsules 2 and 4 was 840±25°C.

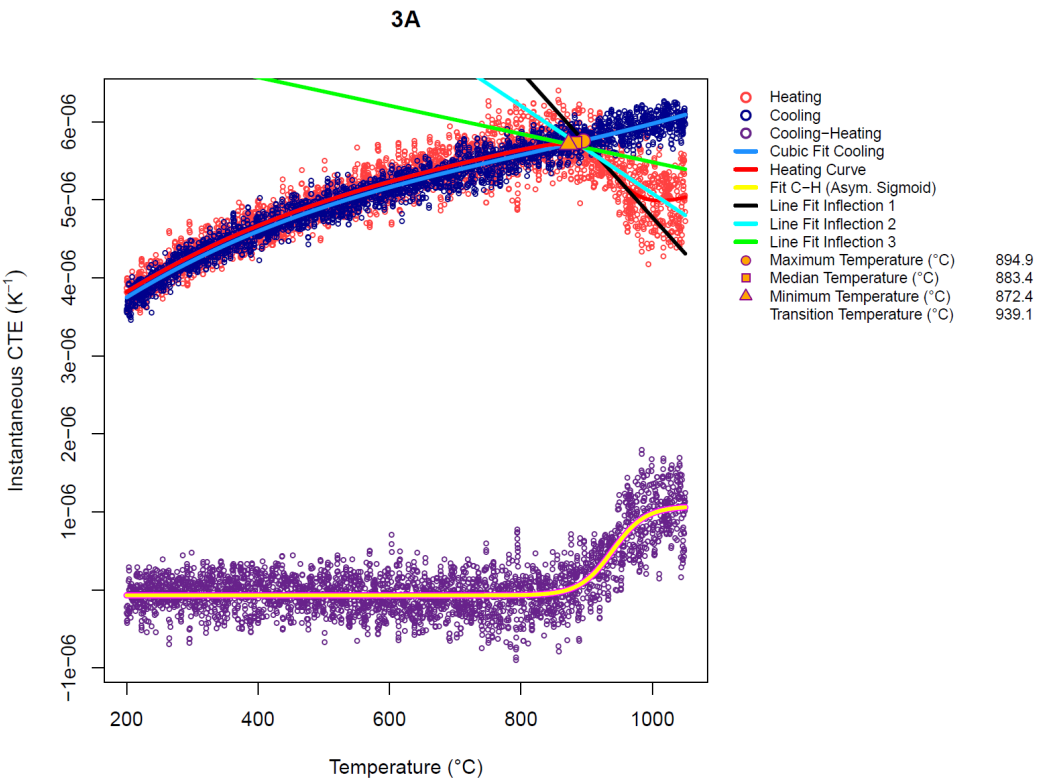

Figure 10 Analysis plot of temperature monitor 3A (HTV sub capsule 2)

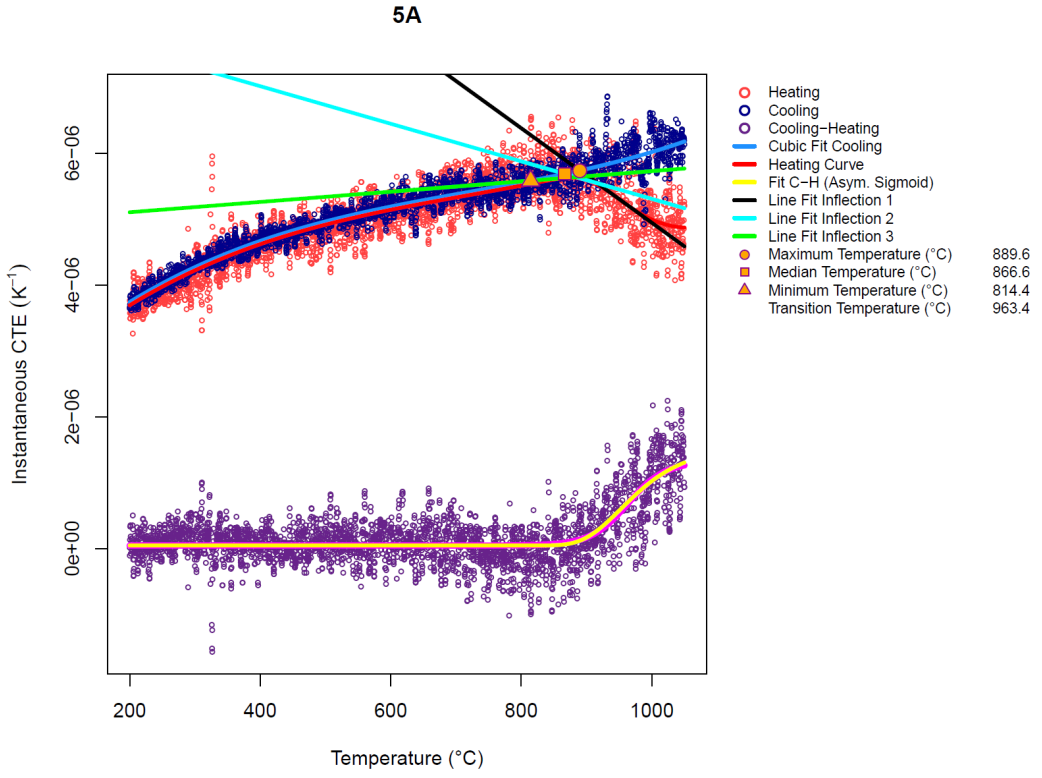

Figure 11 Analysis plot of temperature monitor 5A (HTV sub capsule 4)

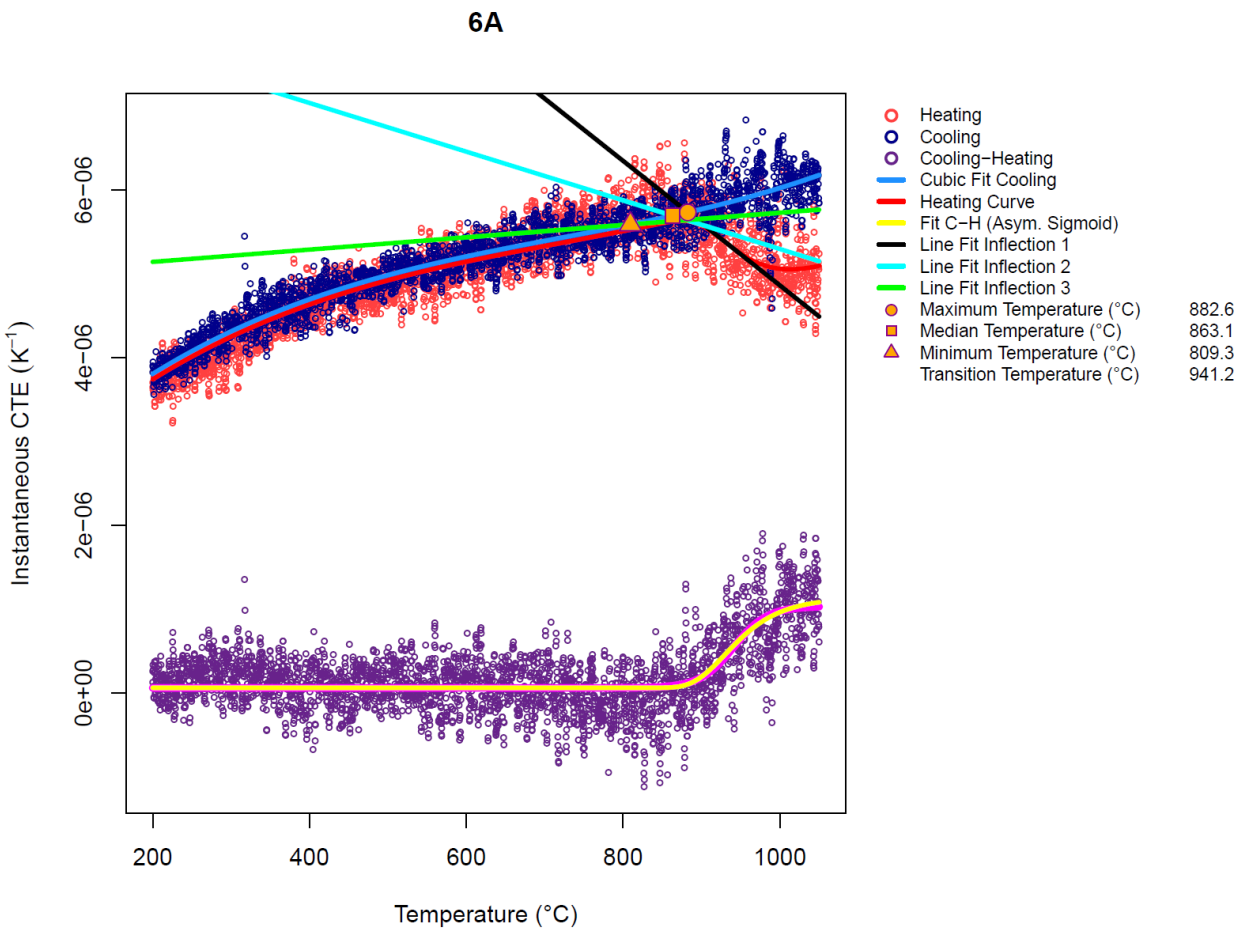

Figure 12 Analysis plot of temperature monitor 6A (HTV sub capsule 4)

Table 4 Summery table of indicated annealing temperatures from the SiC temperature monitors located in HTV sub capsules 2 and 4

TM #	Sub Capsule #	TEMPERATURE INDICATION °C		
		MAX	MEDIAN	MIN
2A	2	879.2	863.1	846.8
3A	2	894.9	883.8	872.4
5A	4	889.6	866.6	814.4
6A	4	882.6	863.1	809.3
	Mean of Med data		**869.15**	

4.1.2.2 Resistivity

The room temperature electrical resistivity and isochronal annealing temperature data are in Table 5 Table 8. The room temperature resistivity data are plotted for the SiC TMs as a function of isochronal annealing temperature in (Figure 13 to Figure 18). The resistivity data was

analyzed in EXCEL by linear regression to identify the inflection points for the data (Figure 13 to Figure 18). From these inflection points the actual irradiation temperatures were established for the T_{irr} = 1200 and 1500°C (Design) zones (Table 9). The straight line fit for the two data sets from each of the three SiC monitors had R2 values >0.8 at 1200°C(des) and >0.9 at 1500°C(des).

Table 5 RT electrical resistivity data as function of isochronal annealing temperature for the SiC TM's in the T_{irr}=1200°C (des) HTV sub-capsules

Type A 1600C SiC TMs from HTV			
sub cap	3	7	8
TM specimen number	4A	9A	10A
Ann. Temp, °C	Resistivity, Ωcm		
1000	780.2	1477.4	3552.1
1050	444.7	835.0	1781.4
1100	417.5	723.0	997.4
1150	258.4	360.1	481.7
1200	240.1	297.3	376.4
1250	115.0	122.5	143.0
1300	78.9	80.9	98.5
1350	73.1	67.9	83.5
1400	64.4	60.5	68.0
1500	52.2	51.4	56.7
1600	39.0	40.1	45.3

Table 6 RT electrical resistivity data as function of isochronal annealing temperature for the graphite TM's in the T_{irr}=1200°C (des) HTV sub-capsules

Type B 1600C GRAPHITE TMs from HTV			
sub cap	3	7	8
TM specimen number	8B	4B	1B
Ann. Temp, °C	Resistivity, μΩm		
1000	24.16	24.40	24.24
1050	24.46	24.55	24.37
1100	24.50	24.64	24.54
1150	24.34	24.56	24.51
1200	24.60	24.94	24.38
1250	24.62	24.73	24.55
1300	25.35	25.85	24.78
1350	24.02	24.10	23.40
1400	23.54	23.51	22.68
1500	21.87	21.60	20.59
1600	20.13	19.39	18.21

Table 7 RT electrical resistivity data as function of isochronal annealing temperature for the SiC TM's in the T_{irr}=1500°C (des) HTV sub-capsules

Type A 1800C SiC TMs from HTV			
sub cap	1	5	6
TM specimen number	1A	7A	8A
Ann. Temp, °C	Resistivity, Ωcm		
1200	141.7	325.2	222.8
1300	69.5	185.5	114.1
1400	59.2	161.9	95.3
1450	23.8	59.0	65.2
1500	38.7	92.9	53.0
1550	34.8	75.7	41.4
1600	32.0	68.2	35.1
1650	28.3	54.0	37.7
1700	24.7	50.3	24.4
1750	17.5	24.1	14.0

Table 8 RT electrical resistivity data as function of isochronal annealing temperature for the graphite TM's in the T_{irr}=1500°C (des) HTV sub-capsules

Type B 1800C Graphite TMs from HTV			
sub cap	1	5	6
TM specimen number	7B	5B	6B
Ann. Temp, °C	Resistivity, μΩm		
1200	18.83	16.74	15.94
1300	19.84	16.65	15.90
1400	18.36	16.32	16.00
1450	18.04	16.16	15.86
1500	18.02	16.17	15.85
1550	17.91	15.78	15.47
1600	17.72	15.88	15.71
1650	17.58	15.96	15.67
1700	17.44	15.85	15.57
1750	16.82	15.43	15.41

The uncertainty in actual graphite specimen irradiation temperature, as determined by isochronal annealing and measurement of the RT electrical resistivity, is assumed to be ±25°C.

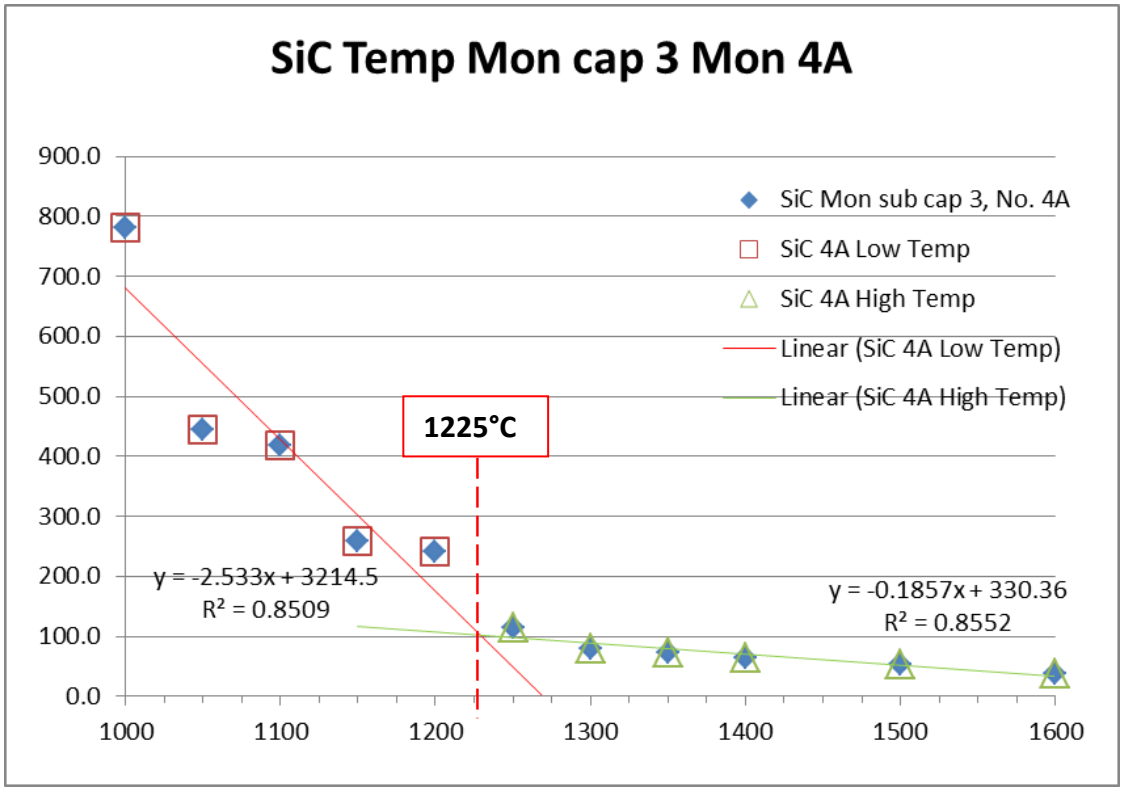

Figure 13 Isochronal annealing data for SiC monitor 4A from sub capsule 3, Tirr=1200°C (des)

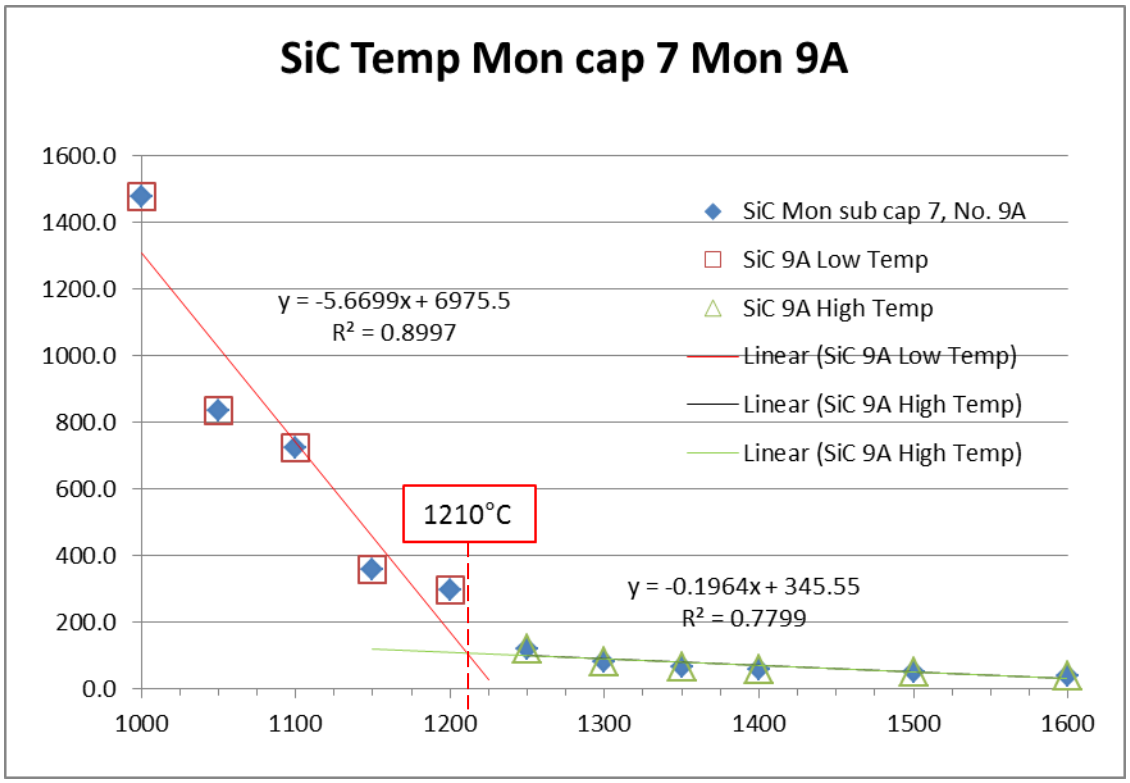

Figure 14 Isochronal annealing data for SiC monitor 9A from sub capsule 7, Tirr=1200°C (des)

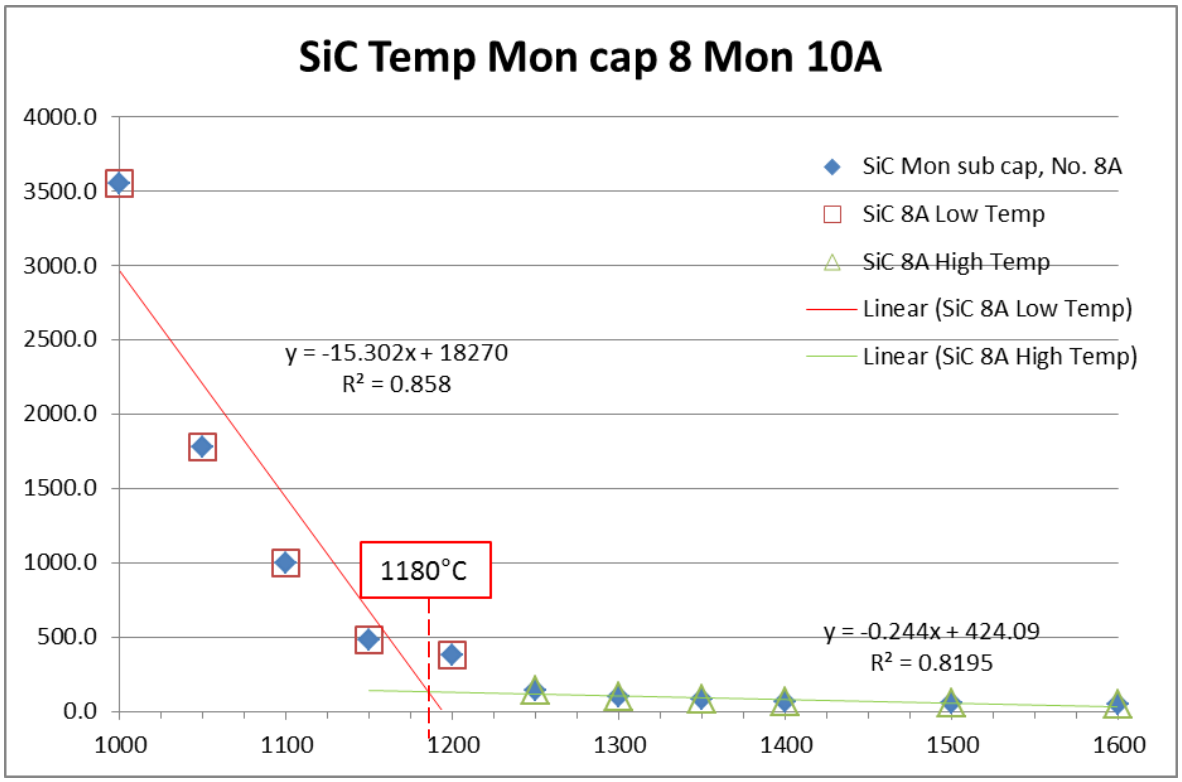

Figure 15 Isochronal annealing data for SiC monitor 10A from sub capsule 8, Tirr=1200°C (des)

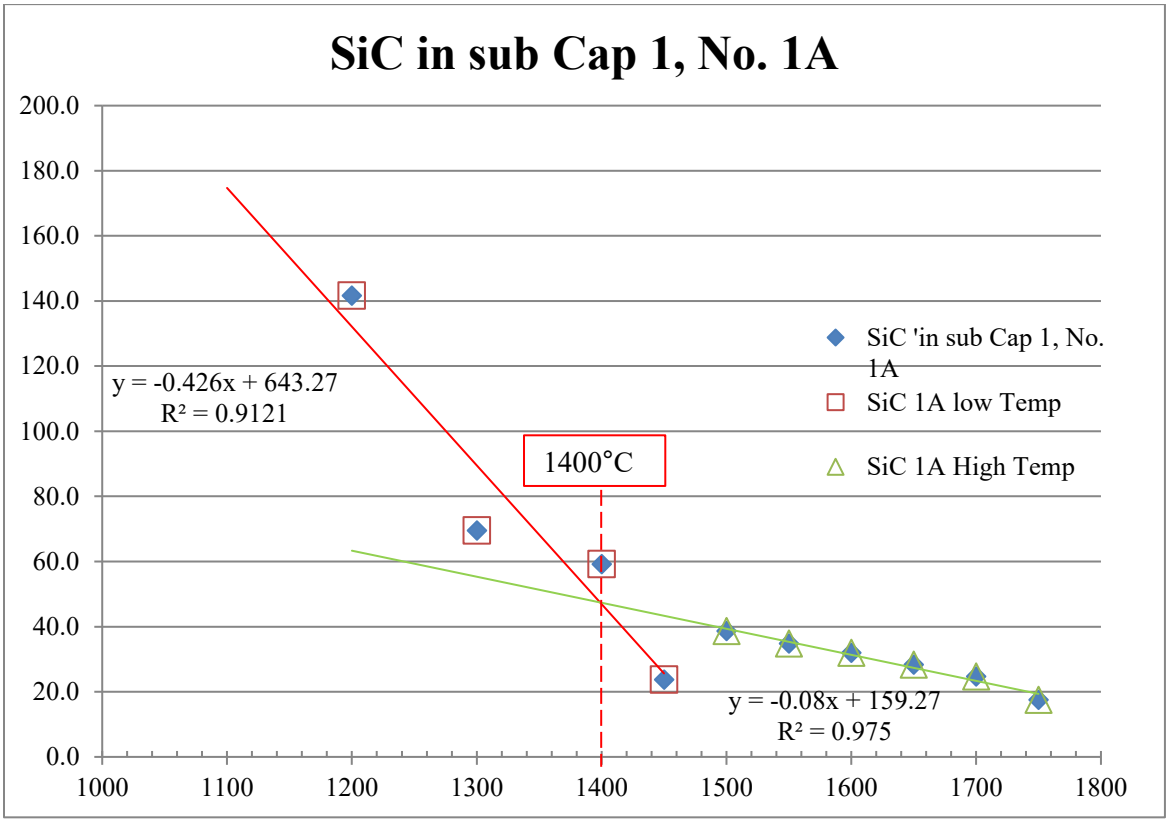

Figure 16 Isochronal annealing data for SiC monitor 1A from sub capsule 1, Tirr=1500°C (des)

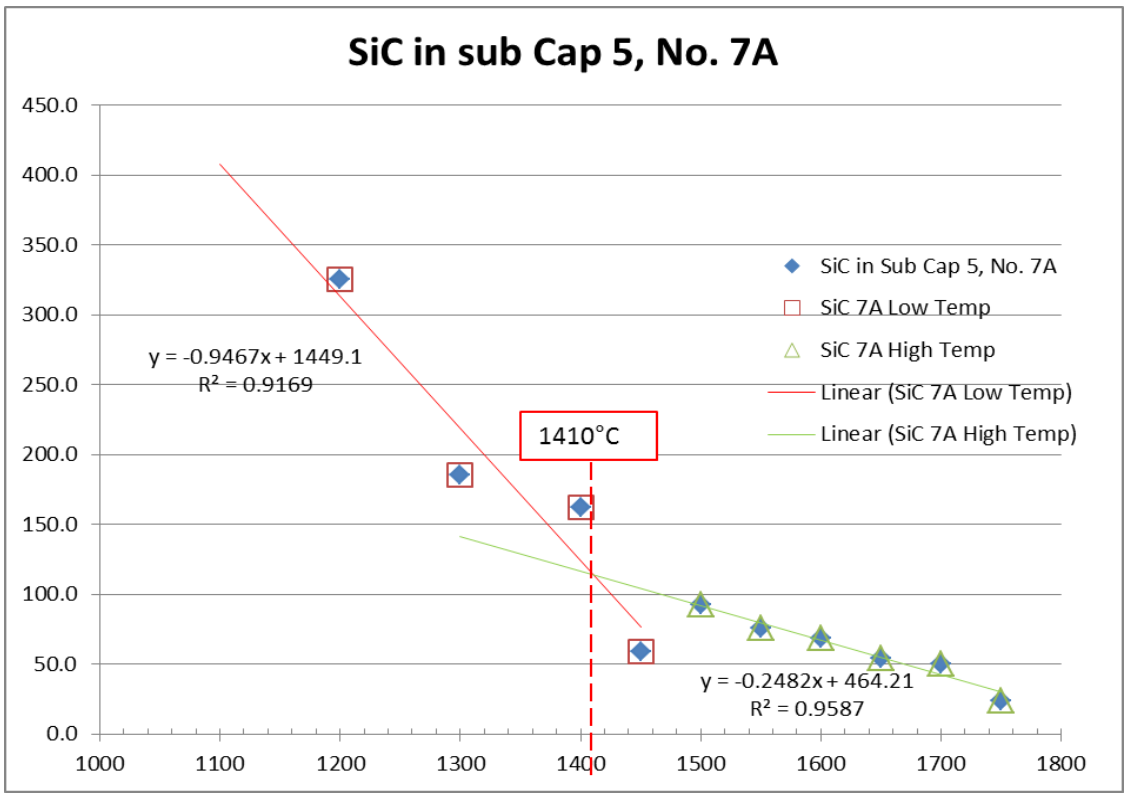

Figure 17 Isochronal annealing data for SiC monitor 7A from sub capsule 5, Tirr=1500°C (des)

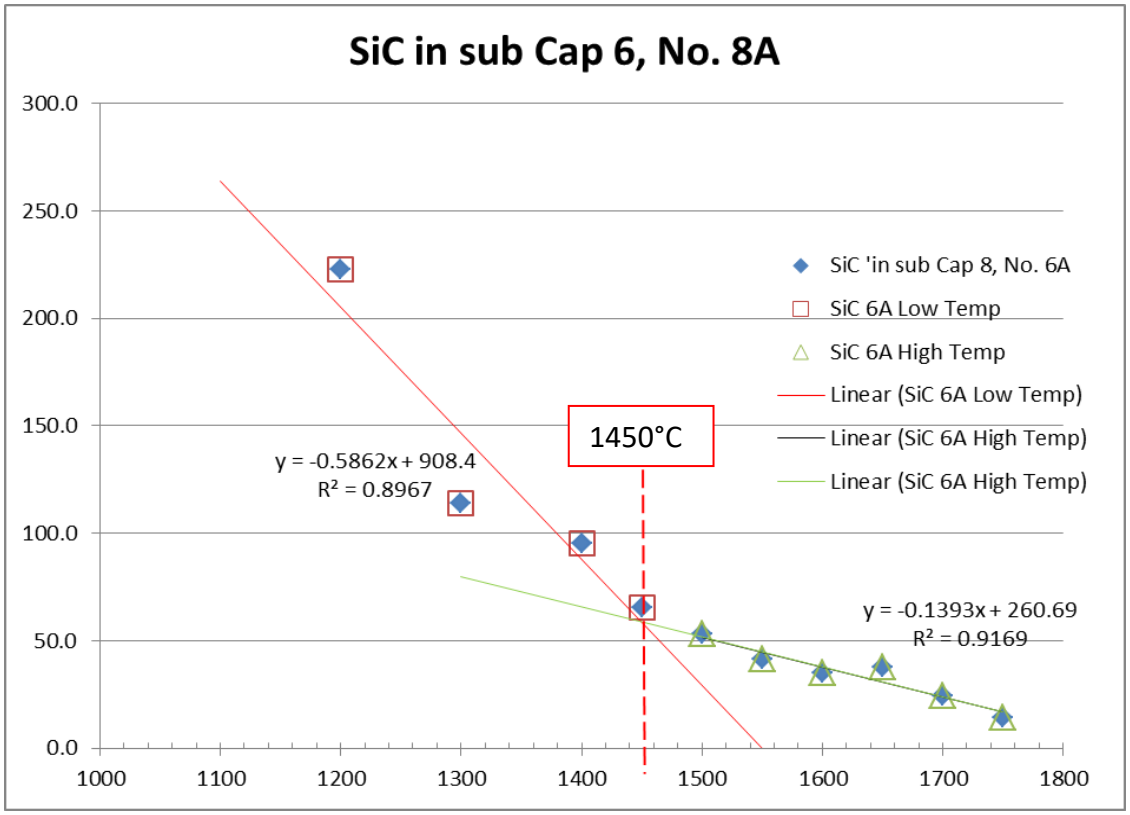

Figure 18 Isochronal annealing data for SiC monitor 8A from sub capsule 6, Tirr=1500°C (des)

Table 9 Summary of sub-capsule design temperature and estimated temperatures

HTV Temperatures											
			DAC: ANSY Model Values, °C						Prediced Temp Correction 'Spec(max)-TM(min)', °C	TM Exprimental Temperature, °C	Estimated Specimen Temperature, °C
			Specimens		TM's		Range or Differance, °C				
Capsule Zone	Temperature Monitor Material	Design Irradiatrion Temperature, °C	Max	Min	Max	Min	Specimen	TM			
3	SiC	1200	1204.9	1201.3	1227.4	1223.7	3.6	3.7	-18.8	1225.0	1206.2
7	SiC	1200	1201.3	1198.6	1221.6	1218.4	2.7	3.2	-17.1	1210.0	1192.9
8	SiC	1200	1202.8	1185.5	1219.6	1213.8	17.3	5.8	-11	1180.0	1169.0
1	SiC	1500	1503.7	1483.7	1517.5	1499.9	20	17.6	3.8	1400.0	1403.8
5	SiC	1500	1460.3	1457.6	1485.7	1476.8	2.7	8.9	-16.5	1410.0	1393.5
6	SiC	1500	1504.5	1502.7	1526.6	1515.7	1.8	10.9	-11.2	1450.0	1438.8

As shown in Table 9, the actual mean irradiation temperature of the graphite HTV specimens, as indicated by the SiC monitors and ANSYS sub-capsule analysis [18], in sub capsules 3, 7 and 8 [1200°C(design)] was 1196 ± 25°C(actual), and the actual graphite specimen irradiation temperature indicated for sub capsules 1, 5 and 6 [1500°C(design)] was 1412 ± 25C(actual) (Table 9). A summary of the graphite irradiation temperatures for all the sub-capsules in the HTV capsule can be found in Table 10.

Table 10 Summary of the actual specimen irradiation temperatures for the sub capsules in HTV

Sub Capsule No.	Temp Mon I.D.	Material	Specimen Irradiation Temperature (actual), °C [± 25°C]	
			Design	Actual
2	2A	SiC	900	840
2	3A	SiC	900	840
4	5A	SiC	900	840
4	6A	SiC	900	840
3	4A	SiC	1200	1189
7	9A	SiC	1200	1189
8	10A	SiC	1200	1189
1	1A	SiC	1500	1412
5	7A	SiC	1500	1412
6	8A	SiC	1500	1412

The TM data from the graphite monitors (added to the six high temperature sub capsules, to test the theory that graphite temperature monitors can be used at high temperature to replace SiC) are not discussed here but shall be the subject of another publication. Only the SiC data (Table 10) are used to indicate the graphite specimen's actual temperature of irradiation. The values quoted in the text as actual irradiation temperatures at 1200°C(design) and 1500°C(design) are the indicated (from SiC monitors) irradiation temperatures for each design temperature corrected for the expected difference (ANSYS analysis) [18] between the TMs and the graphite specimen (Table 10). The estimated error (from all sources) on the quoted "actual" graphite specimen irradiation temperature was taken as ±25°C.

4.2 DIMENSION AND VOLUME CHANGES

4.2.1 Specimen Diameter, Length and Volume

The PIE and Pre-IE Data for the dimensional and volume changes are in Table 12, Table 13 and Table 14 of appendix A. The data are grouped by grade, are presented in ascending dose, and the grain orientation is indicated. The experimental dimensional and volume change data are also presented graphically in Figure 19 to Figure 27. While the specimen length was always aligned with the forming direction and the dimeter was always perpendicular to the forming axis, the forming method varied from grade to grade. Consequently, for the isostatically pressed (IG-110, 2114) and vibrationally molded (NBG-17 and -18) the specimen length corresponds to the AG orientation and the diameter WG. Conversely, for the extruded grades (PCEA and H-451) the specimen length or forming direction corresponds to the WG orientation and the specimen diameter the AG orientation [10].

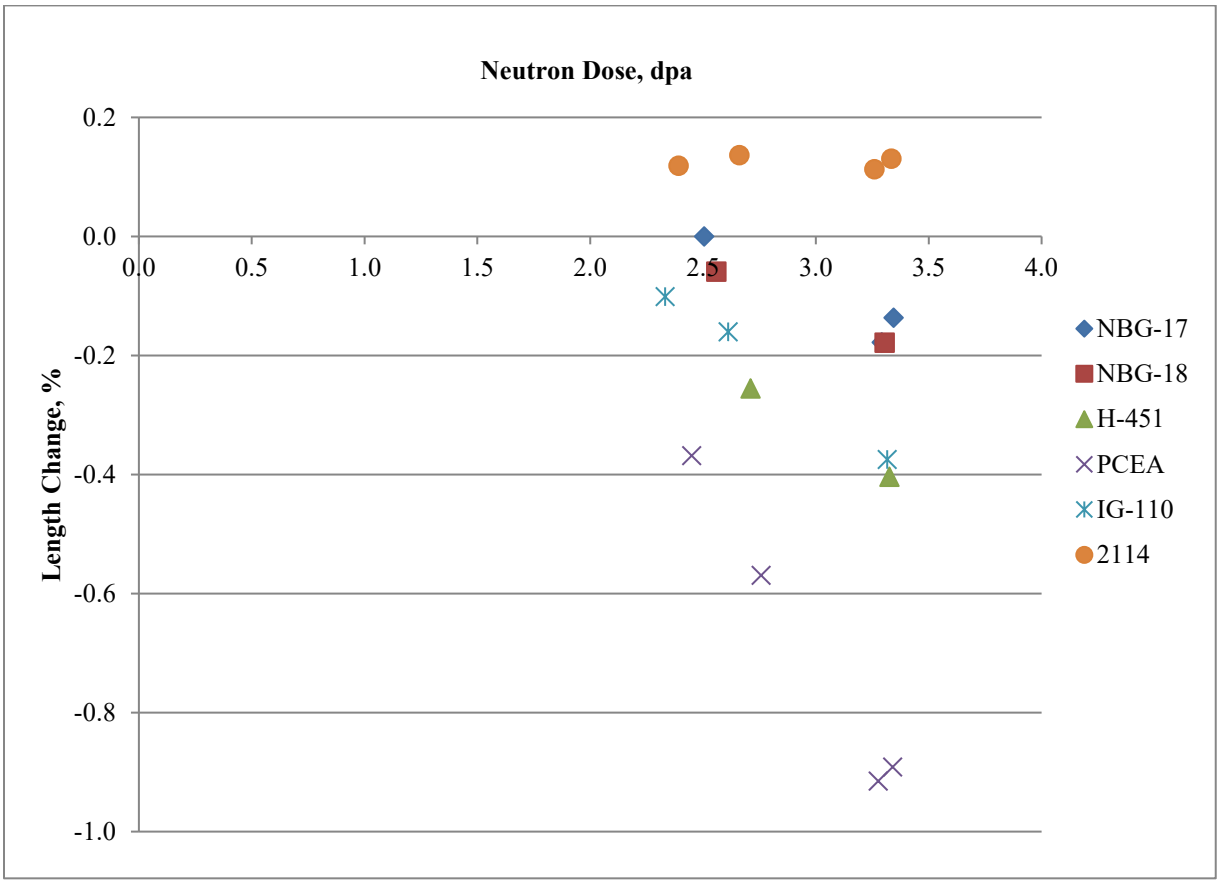

Figure 19 Fractional length change [ΔL/Lo] with neutron dose for the six graphite grades in capsule HTV at T_{irr} =900°C (design) 840°C (actual)

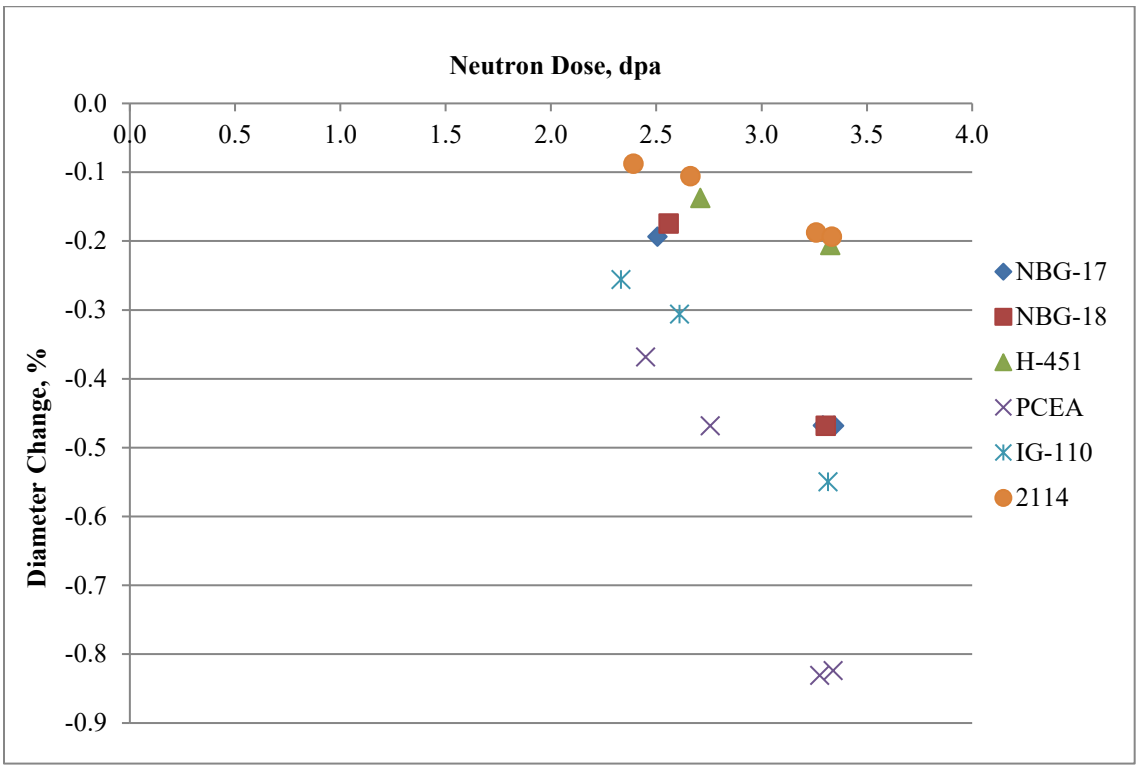

Figure 20 Fractional diameter change [ΔD/Do] with neutron dose for the six graphite grades in capsule HTV at T_{irr} =900°C (design) 840°C (actual)

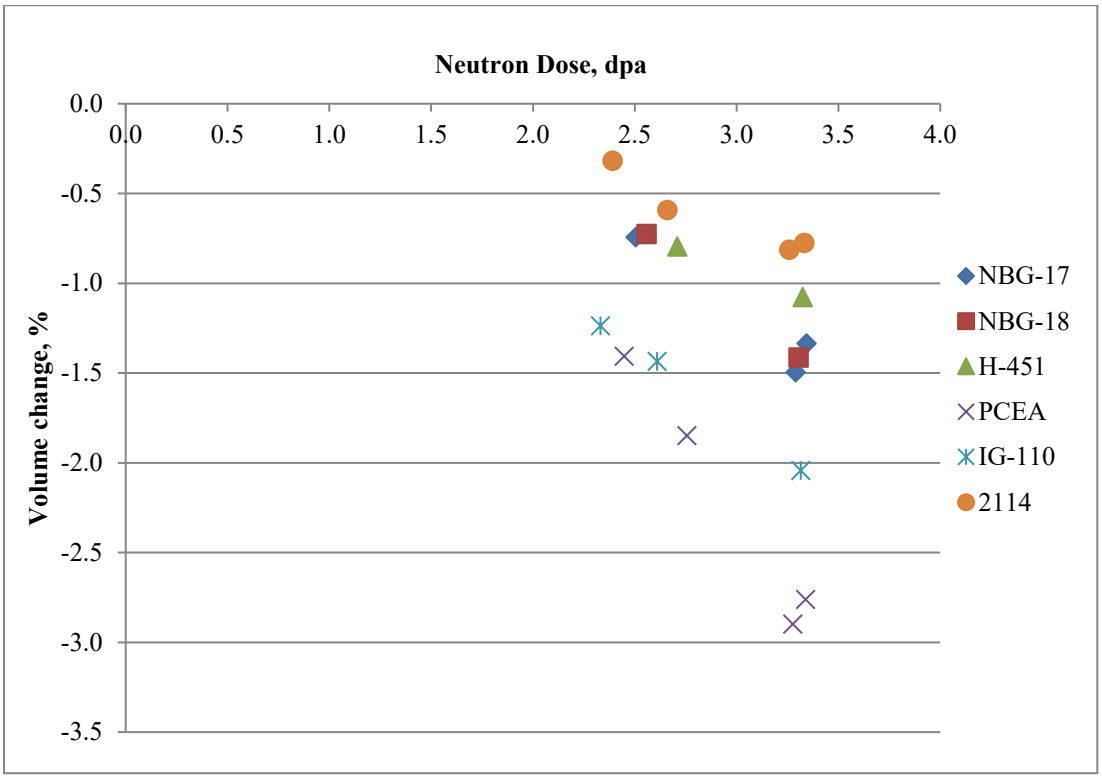

Figure 21 Fractional volume change [ΔV/Vo] with neutron dose for the six graphite grades in capsule HTV at T_{irr} =900°C (design) 840°C (actual)

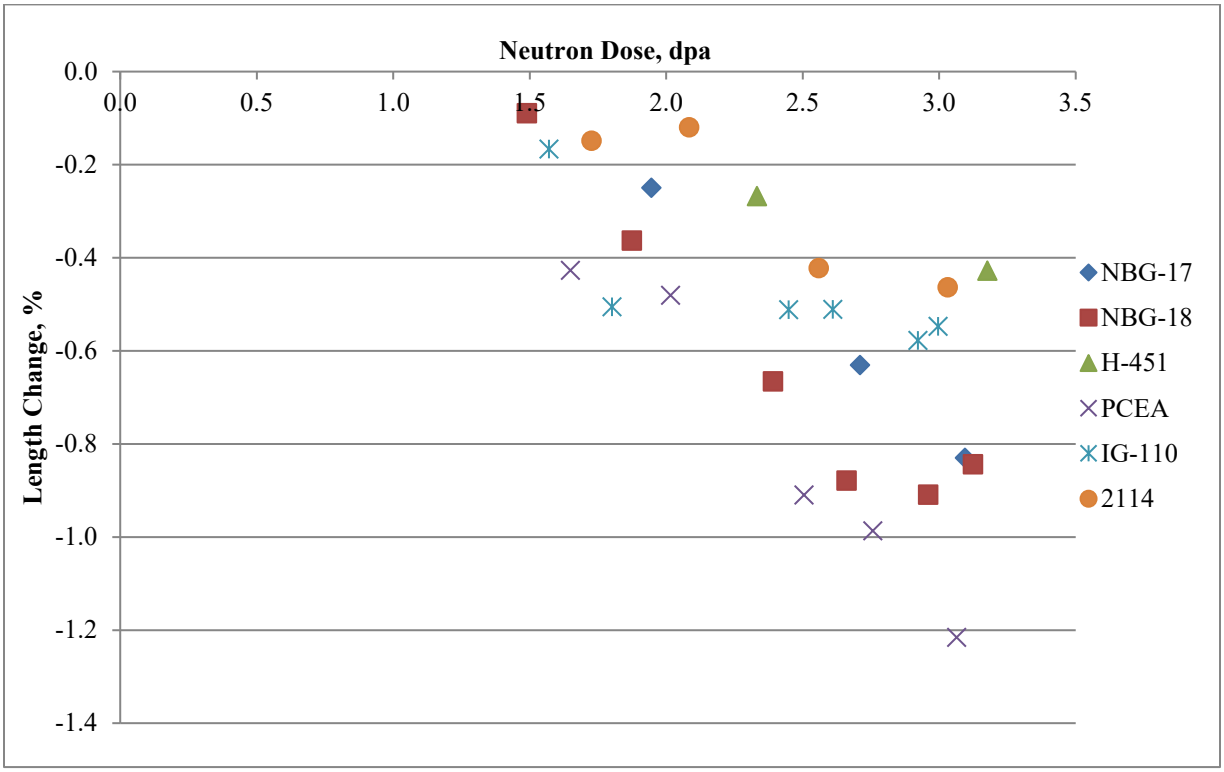

Figure 22 Fractional length change [ΔL/Lo] with neutron dose for the six graphite grades in capsule HTV at Tirr =1200°C (design) 1189°C (actual)

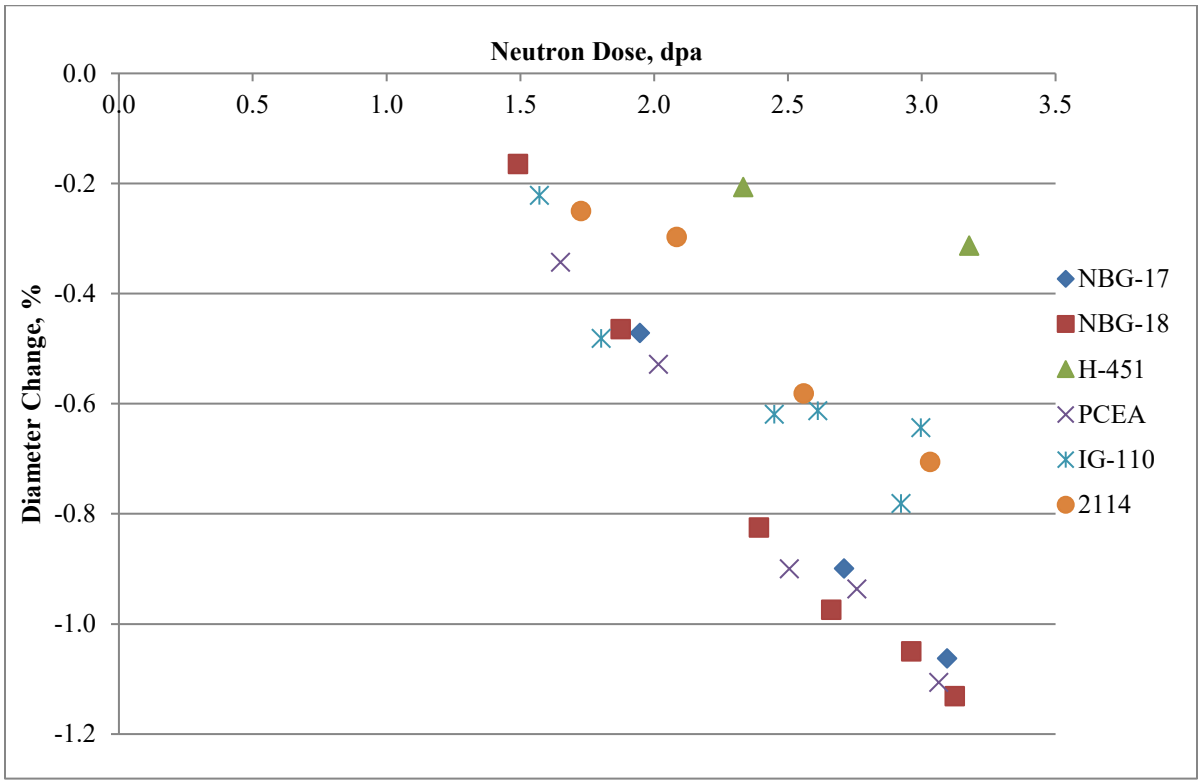

Figure 23 Fractional diameter change [ΔD/Do] with neutron dose for the six graphite grades in capsule HTV at Tirr =1200°C (design) 1189°C (actual)

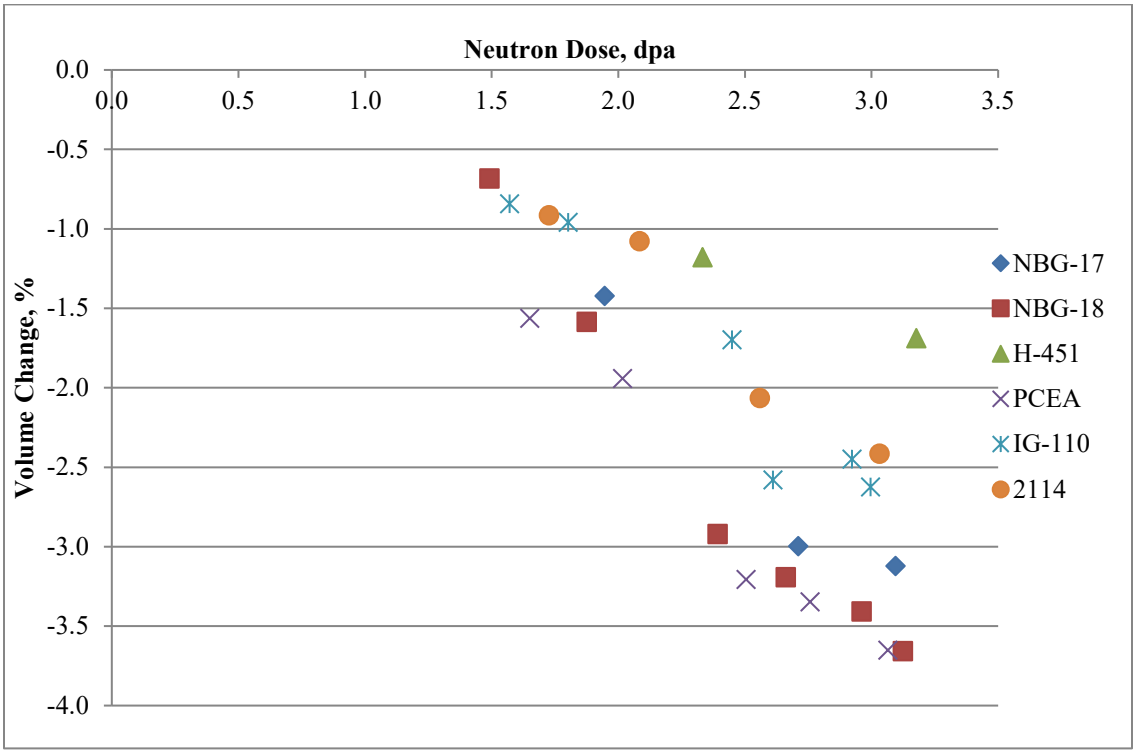

Figure 24 Fractional volume change [ΔV/Vo] with neutron dose for the six graphite grades in capsule HTV at Tirr =1200°C (design) 1189°C (actual)

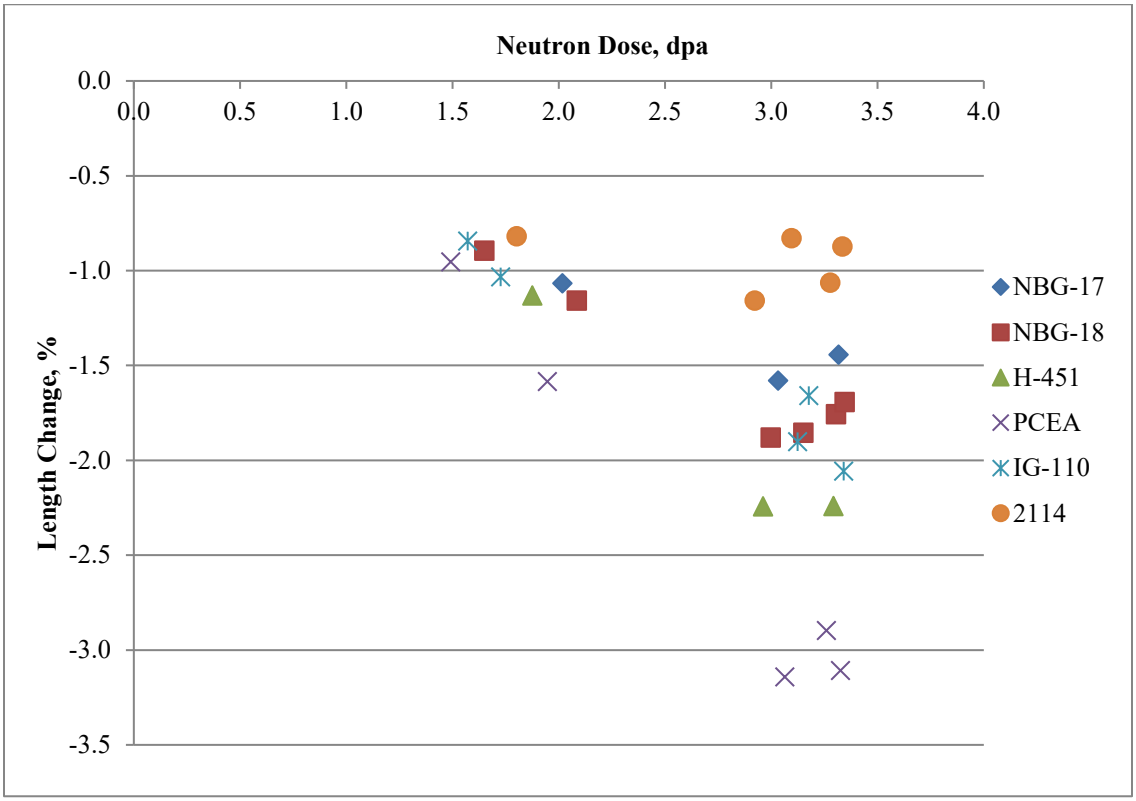

Figure 25 Fractional length change [ΔL/Lo] with neutron dose for the six graphite grades in capsule HTV at Tirr =1500°C (design) 1412°C (actual)

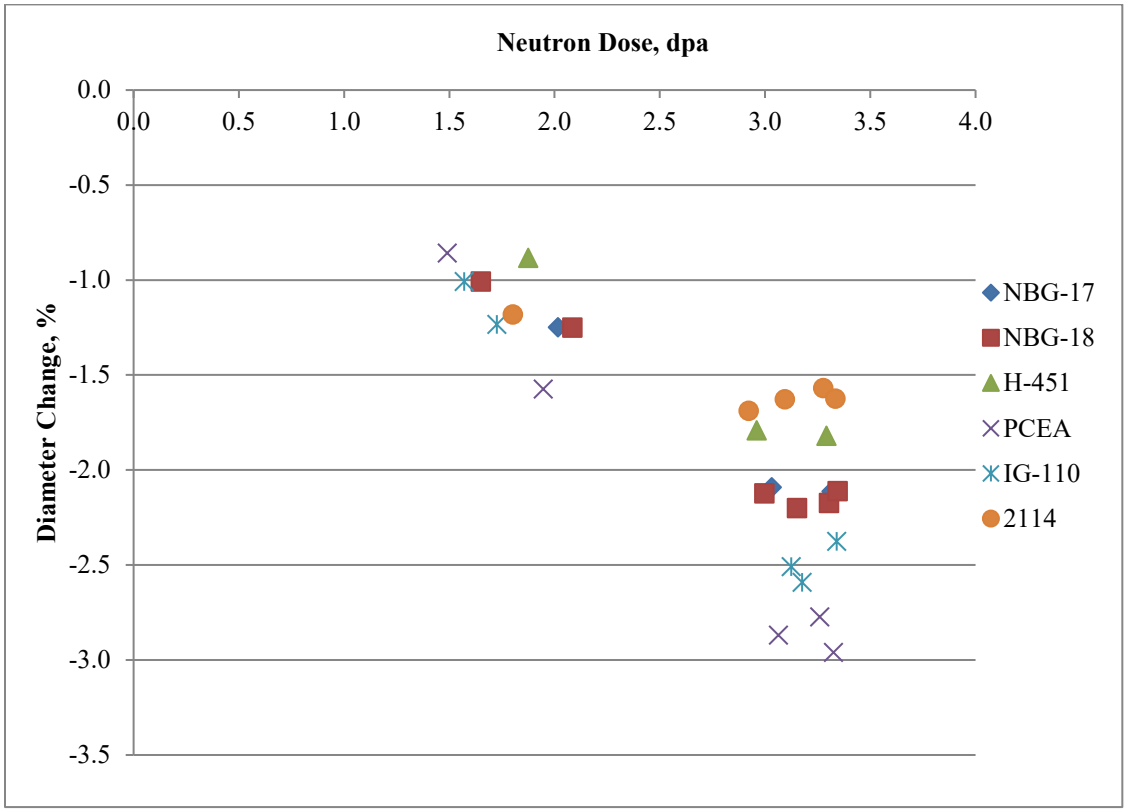

Figure 26 Fractional diameter change [ΔD/Do] with neutron dose for the six graphite grades in capsule HTV at Tirr =1500°C (design) 1412°C (actual)

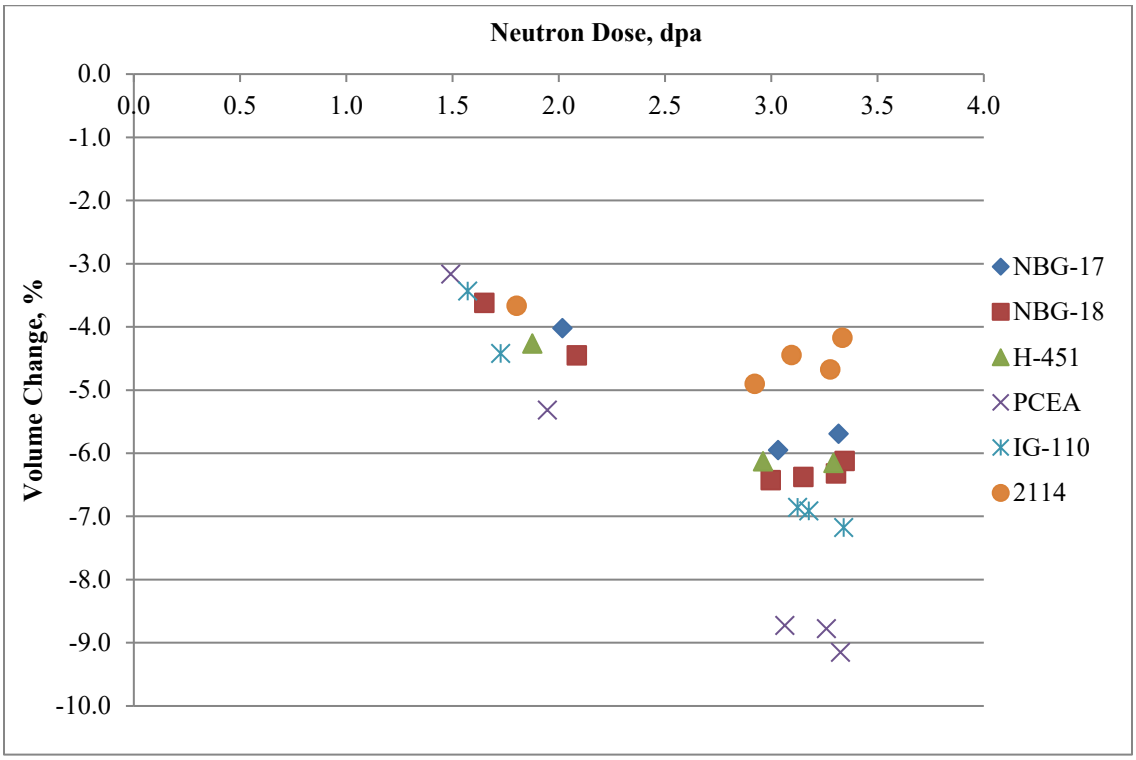

Figure 27 Fractional volume change [ΔV/Vo] with neutron dose for the six graphite grades in capsule HTV at Tirr =1500°C (design) 1412°C (actual)

4.2.2 Specimen Central Hole Diameter Changes

The results for diametral growth of the HTV specimen's inner hole diameter are in Table 15 - Table 17 and in Figure 28 - Figure 33. The data are grouped by specimen grade and are also ordered by ascending neutron dose. The data (HTV Specimen hole growth, %) are plotted according to the specimens inner hole diameter orientation (WG/AG).

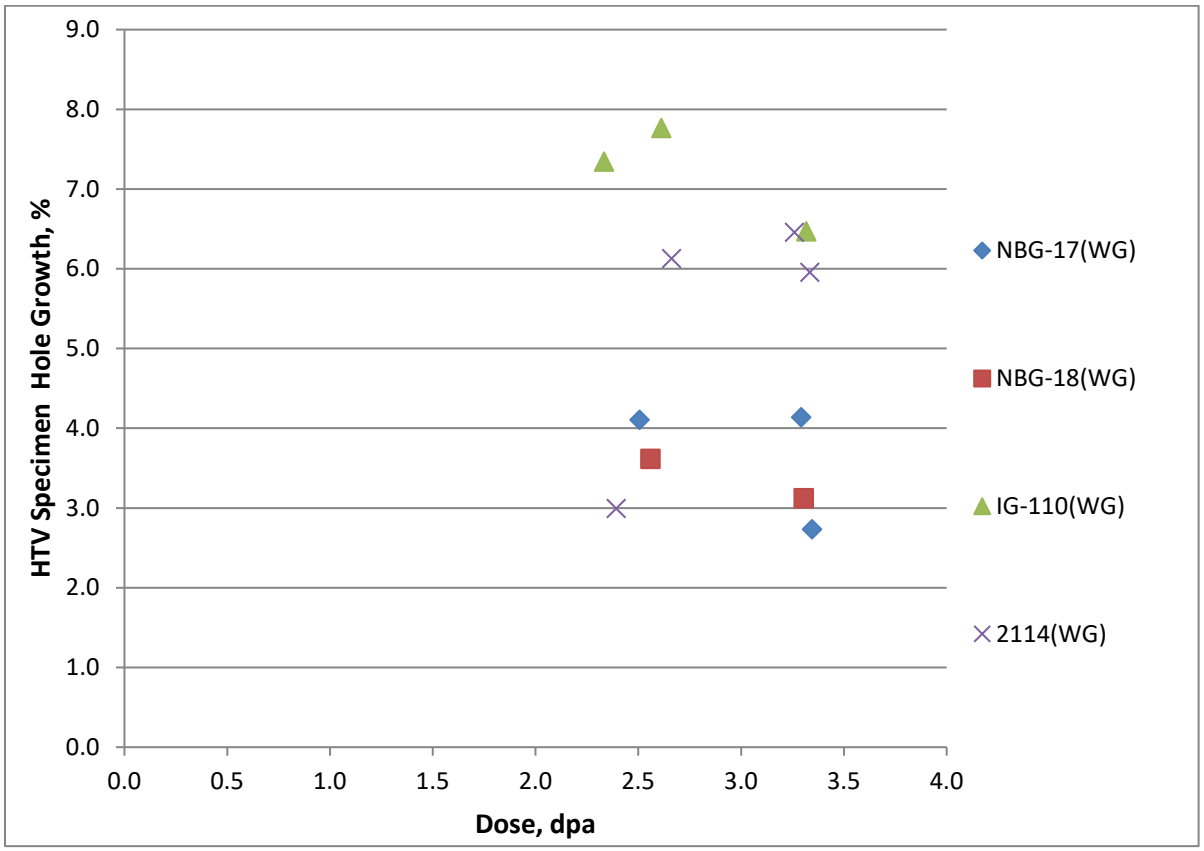

Figure 28 Fractional specimen central hole growth for HTV grades in which the central hole's diameter is aligned in a WG orientation at Tirr = 900°C (design) 840°C (actual)

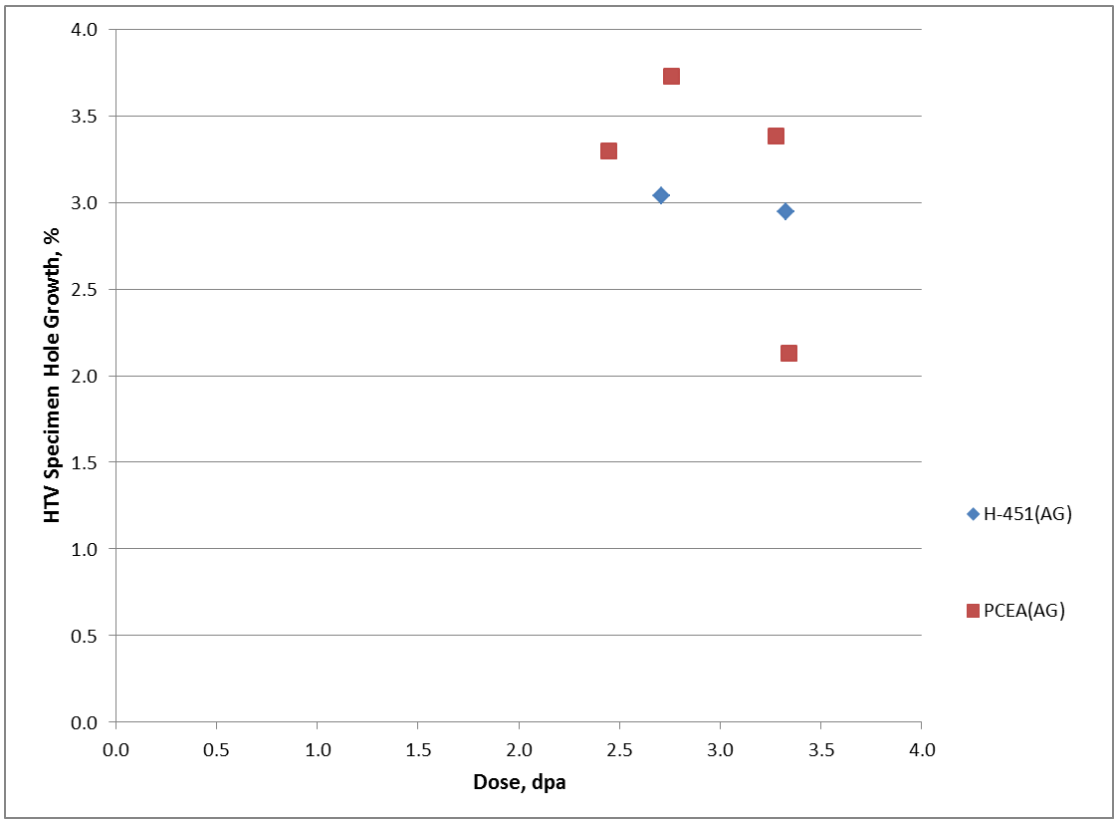

Figure 29 Fractional specimen central hole growth for HTV grades in which the central hole's diameter is aligned in an AG orientation at Tirr = 900°C (design) 840°C (actual)

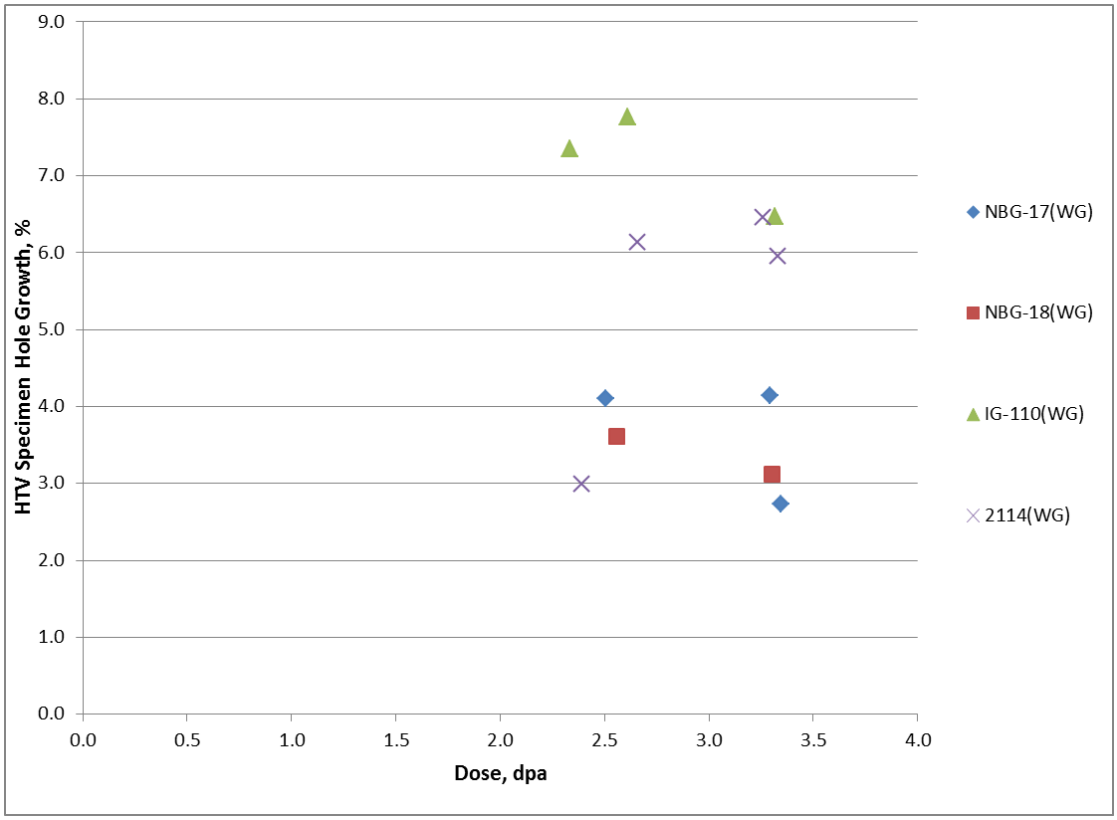

Figure 30 Fractional specimen central hole growth for HTV grades in which the central hole's diameter is aligned in a WG orientation at Tirr = 1200°C (design) 1189°C (actual)

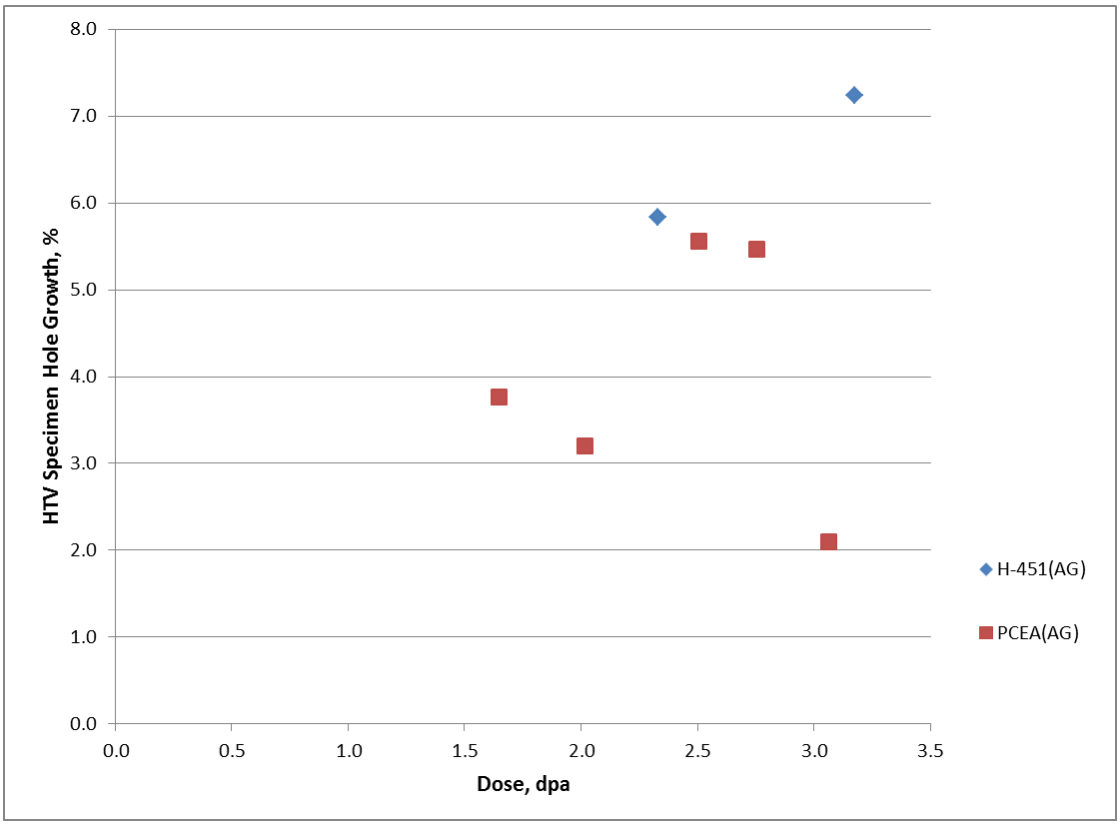

Figure 31 Fractional specimen central hole growth for HTV grades in which the central hole's diameter is aligned in an AG orientation at Tirr = 1200°C (design) 1189°C (actual)

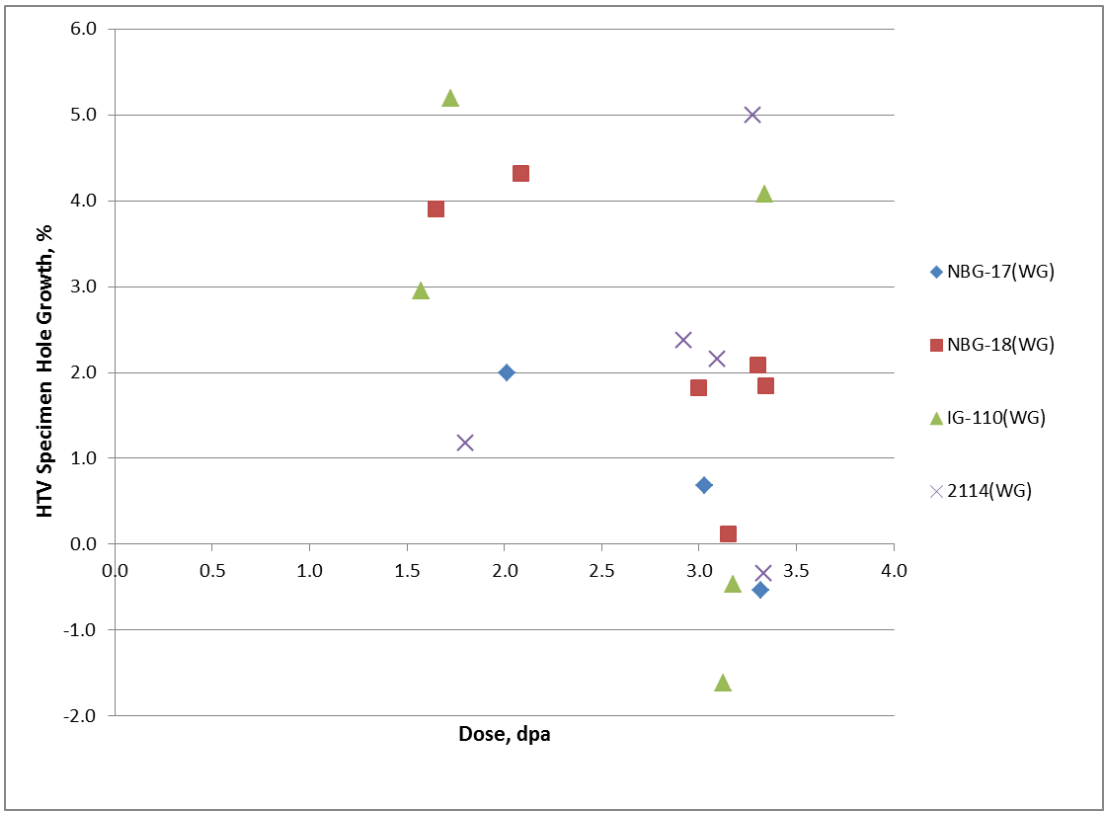

Figure 32 Fractional specimen central hole growth for HTV grades in which the central hole's diameter is aligned in a WG orientation at Tirr = 1500°C (design) 1412°C (actual)

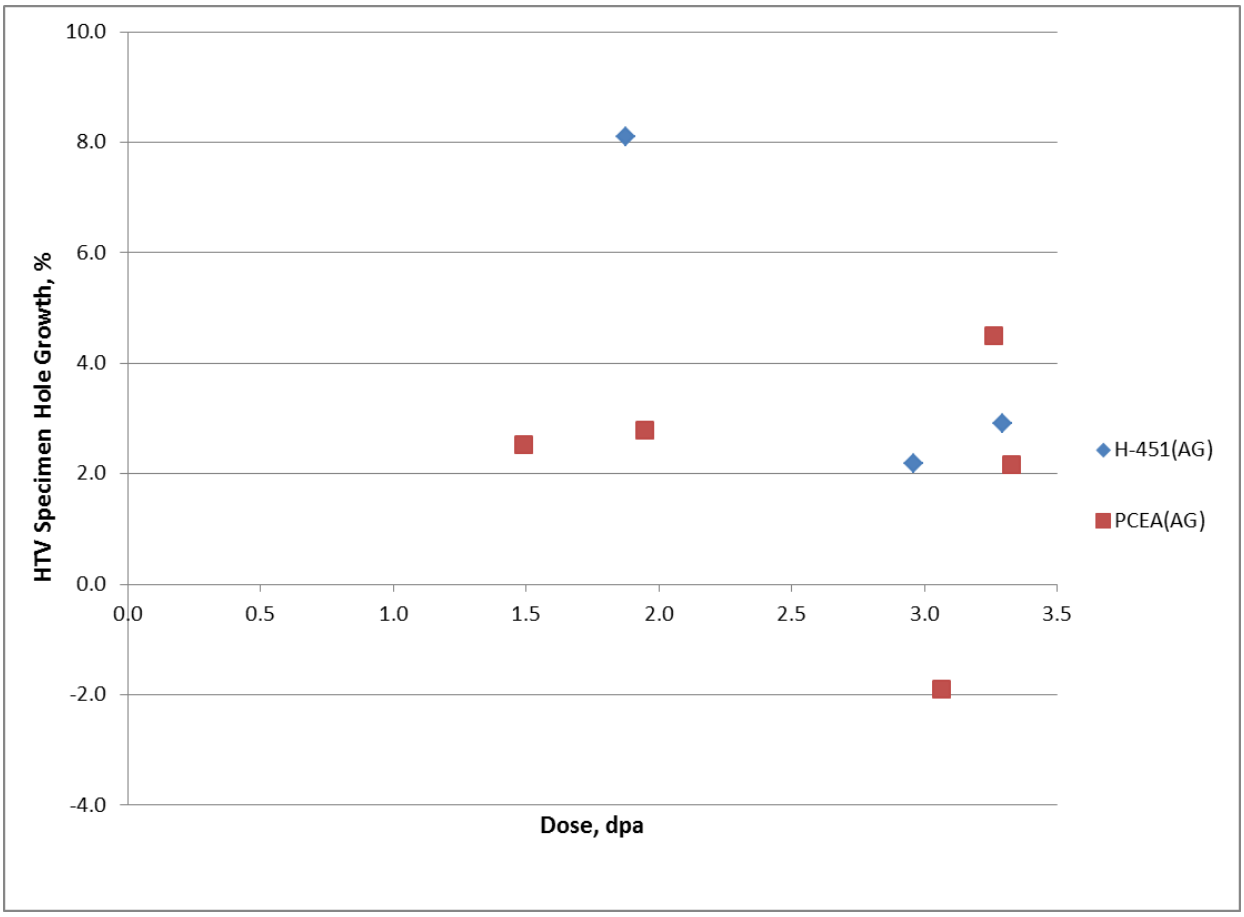

Figure 33 Fractional specimen central hole growth for HTV grades in which the central hole's diameter is aligned in an AG orientation at Tirr = 1500°C (design) 1412°C (actual)

4.3 YOUNG'S MODULUS CHANGE

The PIE Young's modulus data was determined in the same manner as the Pre-IE Young's Modulus (by measuring the Ultrasonic signal TOF, calculating the ultra-sounds velocity and hence the Young's Modulus) [10,12]. A typical ultrasonic signal trace for Mersen grade 2114 is shown in Figure 34.

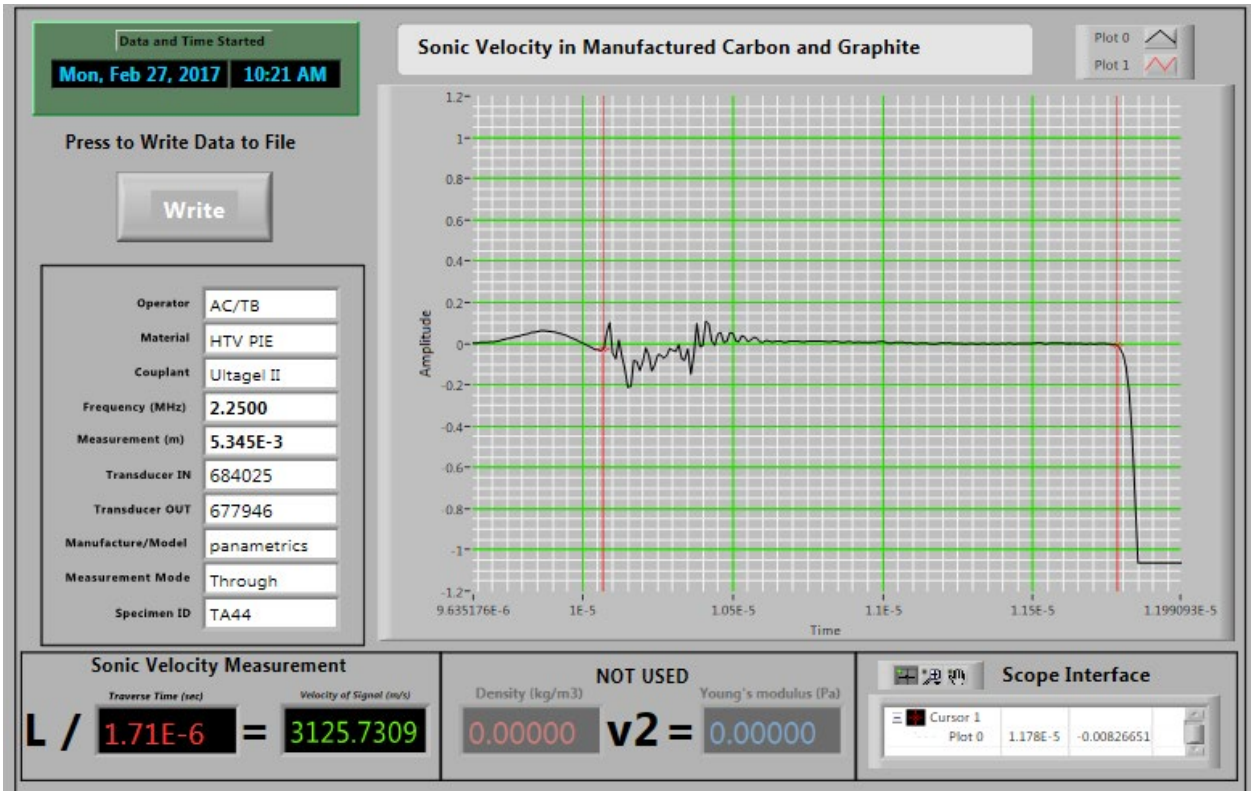

Figure 34 Typical signal trace for irradiated Mersen grade 2114, specimen TA-44, T_{irr}=900°C (design) 840°C (actual), dose=3.26 dpa

The velocity was measured along the length direction of the HTV specimen. While the specimen length was always aligned with the forming direction, the forming method varied from grade to grade. Consequently, for the isostatically pressed (IG-110, 2114) and vibrationally molded (NBG-17 and -18) the specimen length corresponds to the AG orientation. Conversely, for the extruded grades (PCEA and H-451) the specimen length or forming direction corresponds to the WG orientation [10].

The modulus data are given in Appendix B, Table 18 to Table 20, where they are separated into their different irradiation temperatures and are sorted by grade. The orientation (WG/AG) is also indicated. Figure 35 to Figure 40 additionally show graphically the Modulus data for each irradiation temperature, sorted by grade and orientation.

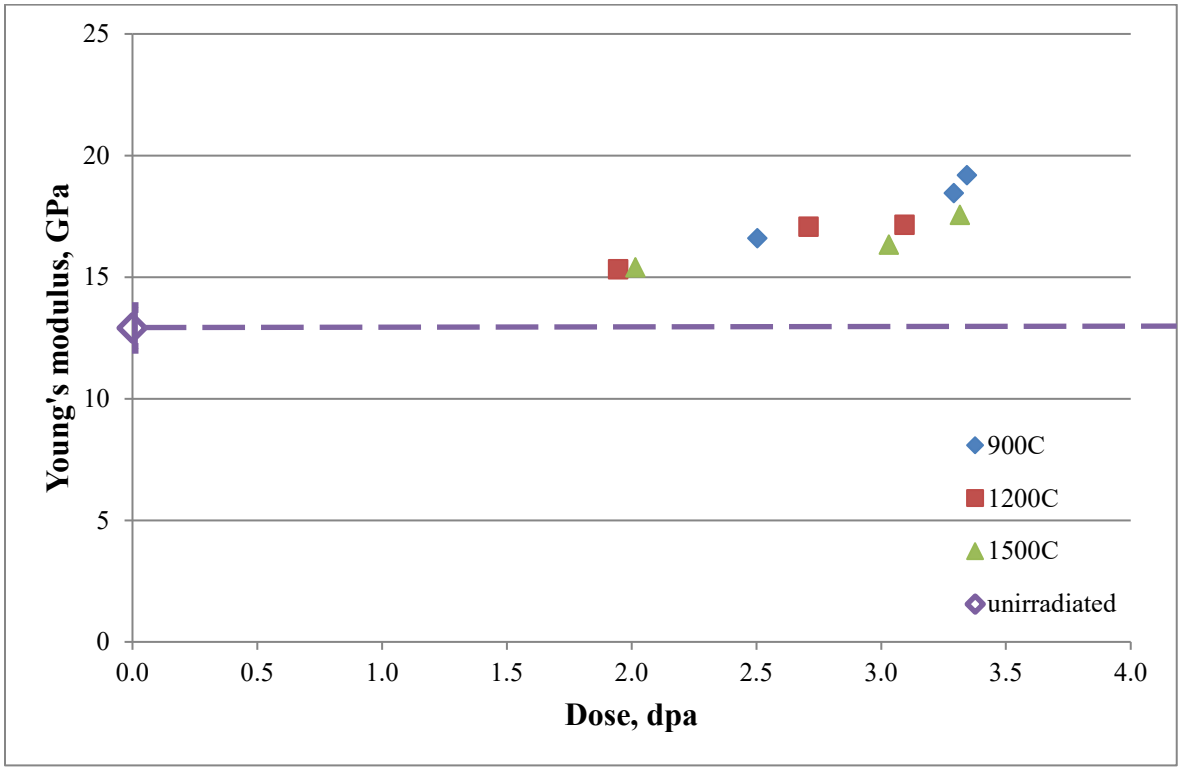

Figure 35 Increase of Young's modulus with dose for vibrationally molded graphite grade NBG-17 (WG)

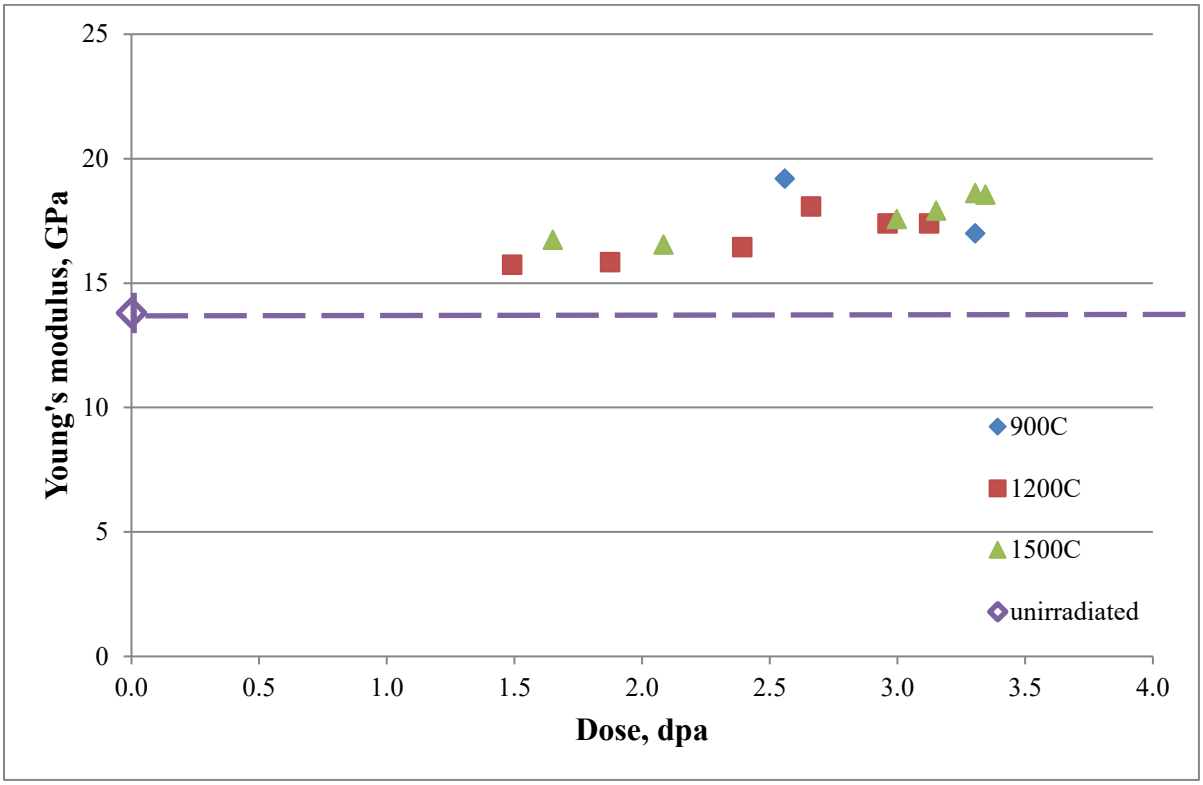

Figure 36 Increase of Young's modulus with dose for vibrationally molded graphite grade NBG-18 (WG)

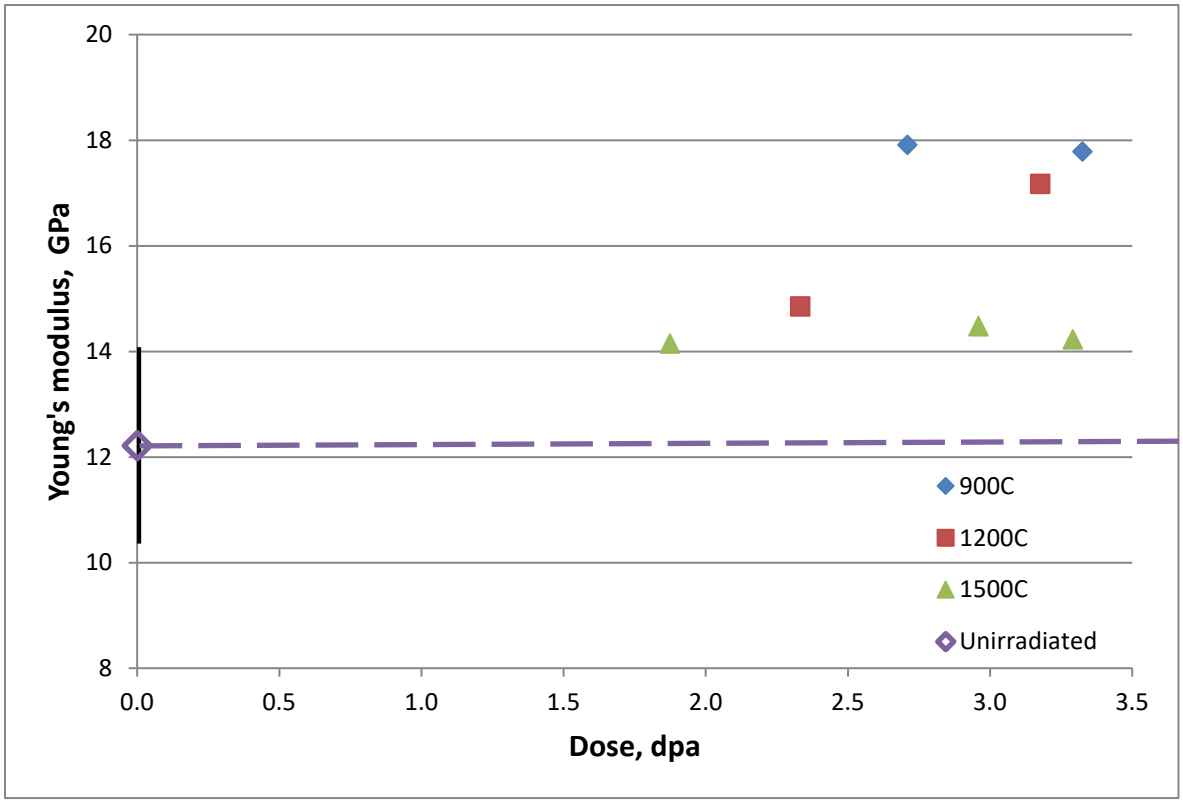

Figure 37 Increase of Young's modulus with dose for extruded graphite grade H-451 (WG)

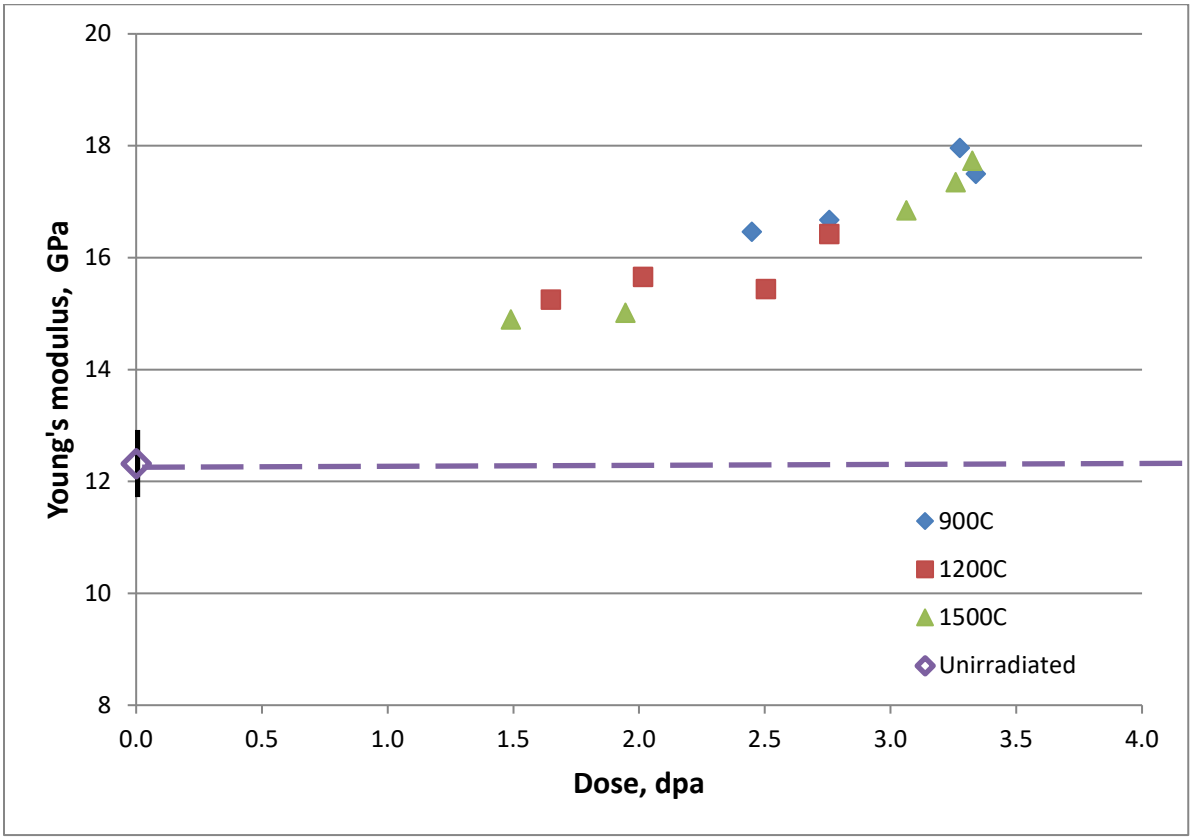

Figure 38 Increase of Young's modulus with dose for extruded graphite grade PCEA (WG)

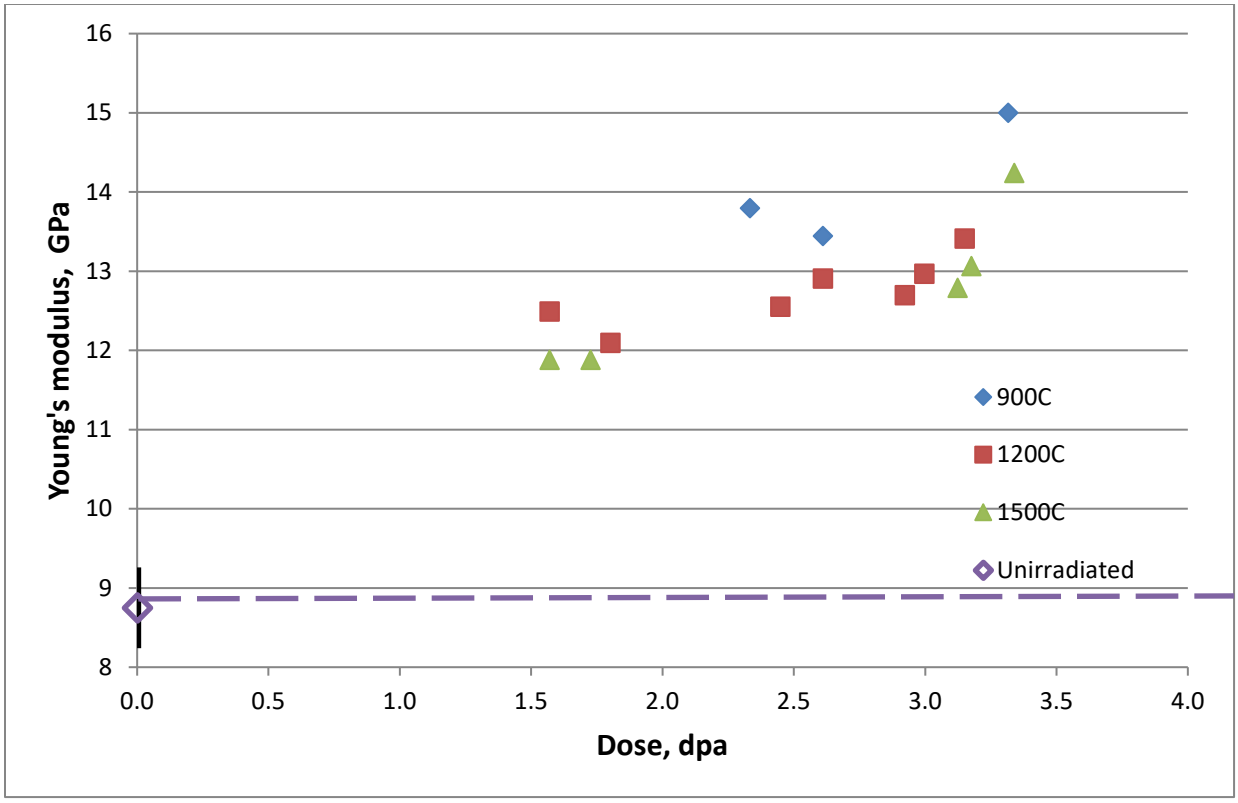

Figure 39 Increase of Young's modulus with dose for isostatically pressed graphite grade IG-110 (AG)

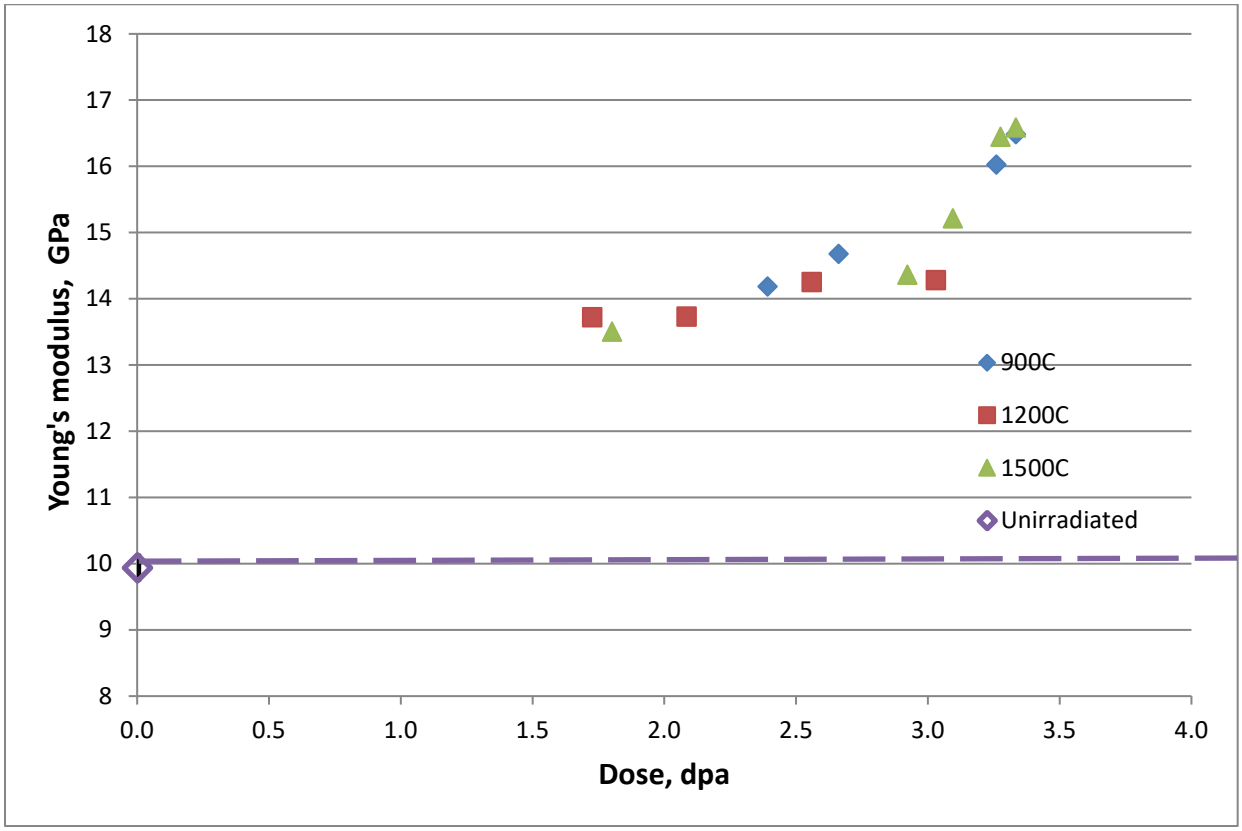

Figure 40 Increase of Young's modulus with dose for isostatically pressed graphite grade 2114 (AG)

5. DISCUSSION

5.1 DIMENSIONAL AND VOLUME CHANGES

5.1.1 Response of Different Grades

A useful way of presenting the dimensional change data is to group by specimen orientation, i.e., WG or AG. While the specimen length (thickness) was always aligned with the billet forming axis (Figure 41), because of the different forming methods the WG/AG orientations were not constant. Table 11 gives the specimen orientation with respect to the grain orientation.

Table 11 HTV-1 specimen manufacture and orientation

Supplier/Graphite Grade	Forming method	Specimen Orientation	
		Length	Diameter
SGL NBG-17	Vibrational Molding	AG	WG
SGL NBG-18	Vibrational Molding	AG	WG
SGL H-451 (not in production)	Extrusion	WG	AG
GrafTech PCEA	Extrusion	WG	AG
Toyo Tanso IG-110	Isostatically Pressed	AG	WG
Mersen 2114	Isostatically Pressed	AG	WG

The dimensional changes data from HTV are shown in Figure 42 to Figure 47 sorted by design irradiation temperature, specimen orientation, and grade. The dimensional anisotropy with grain orientation is very apparent. The preferential alignment of the crystallographic <a> and <c> axis within the filler coke and the filler cokes alignment during forming are largely responsible for this anisotropy. The long axis of filler coke particle tends to align parallel to the forming direction in an extruded grade, and the long axis of the filler coke particles tend to align perpendicular to the forming direction in a vibrationally molded or isostatically pressed grade. The preferential alignment of a certain class of pores and crack (thermal cracks that form on cooling from graphitization temperatures due to anisotropic crystal thermal contraction) that occur between the basal plane (<a>-planes) also complicates the dimensional irradiation response since this class of pores/cracks initially "accommodates" the <c>-axis crystal growth. The behavior of the extruded grade PCEA and the isostatically pressed Mersen 2114 at T_{irr} (design) = 900°C (840°C actual) clearly shows the result of this texture (Figure 42 and Figure 43). The 2114 displayed AG and WG fractional dimensional changes of ~+0.13% and -0.2% respectively at ~3.3 dpa. The extruded PCEA had WG and AG fractional dimensional changes ~-0.8% and ~-0.9%, respectively.

The anisotropy of the grades is exemplified by in Figure 48 to Figure 53 by the behavior of the two grades, PCEA and 2114. Ignoring temperature effects for the moment and just focusing on

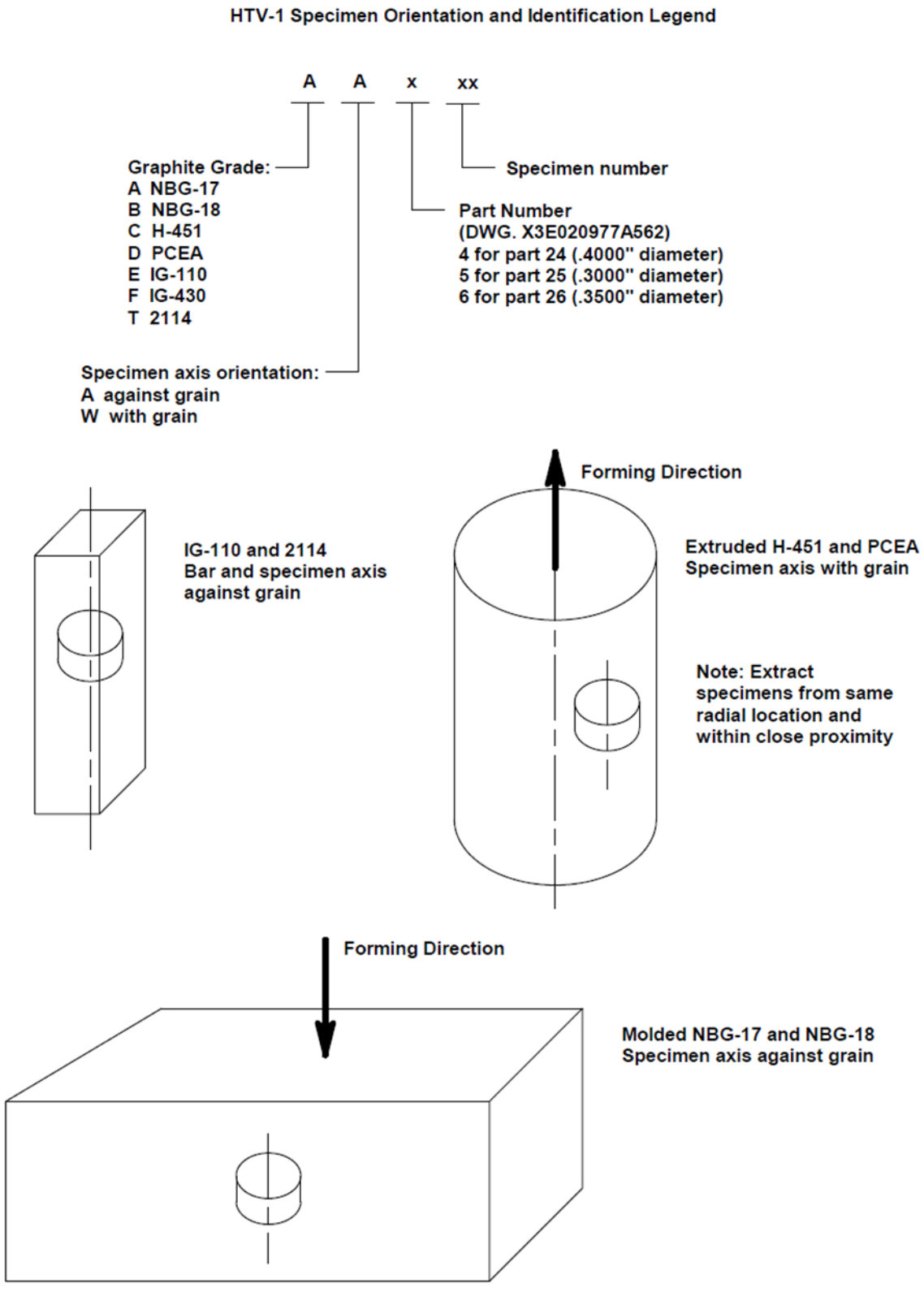

Figure 41 HTV-1 specimen orientation and identification legend

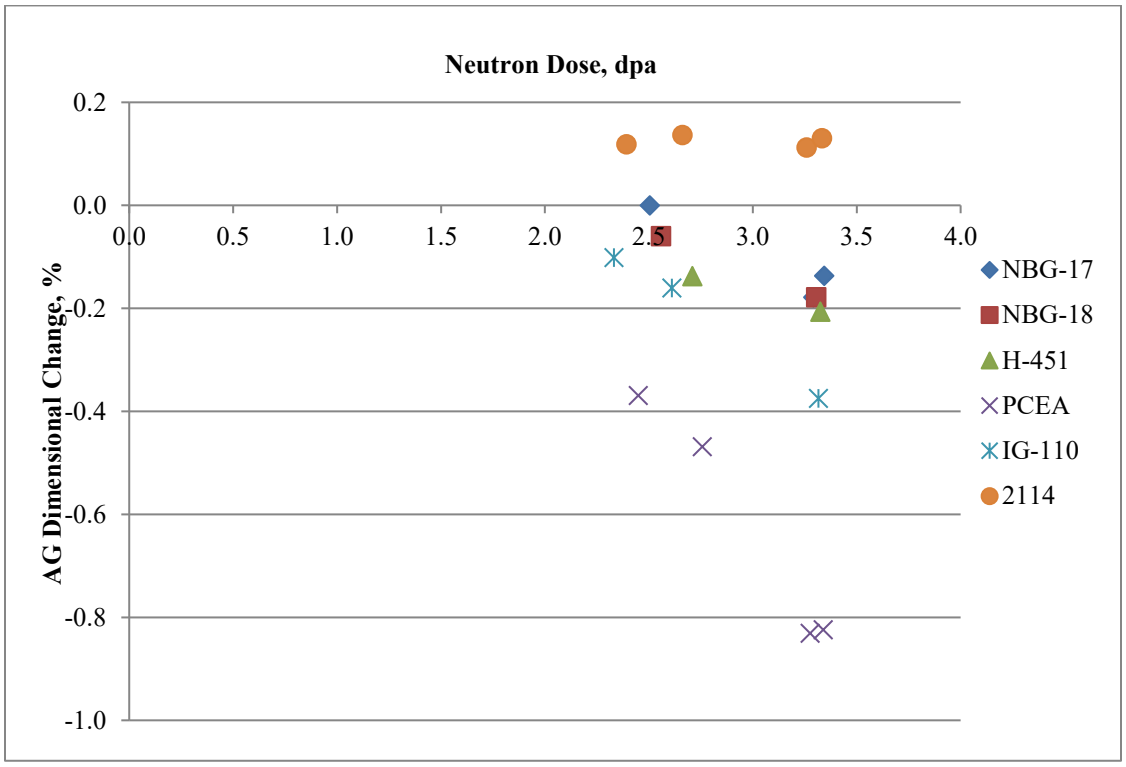

Figure 42 Fractional dimensional change in the AG orientation with neutron dose for the six graphite grades in capsule HTV at T_{irr} =900°C (design) 840°C (actual)

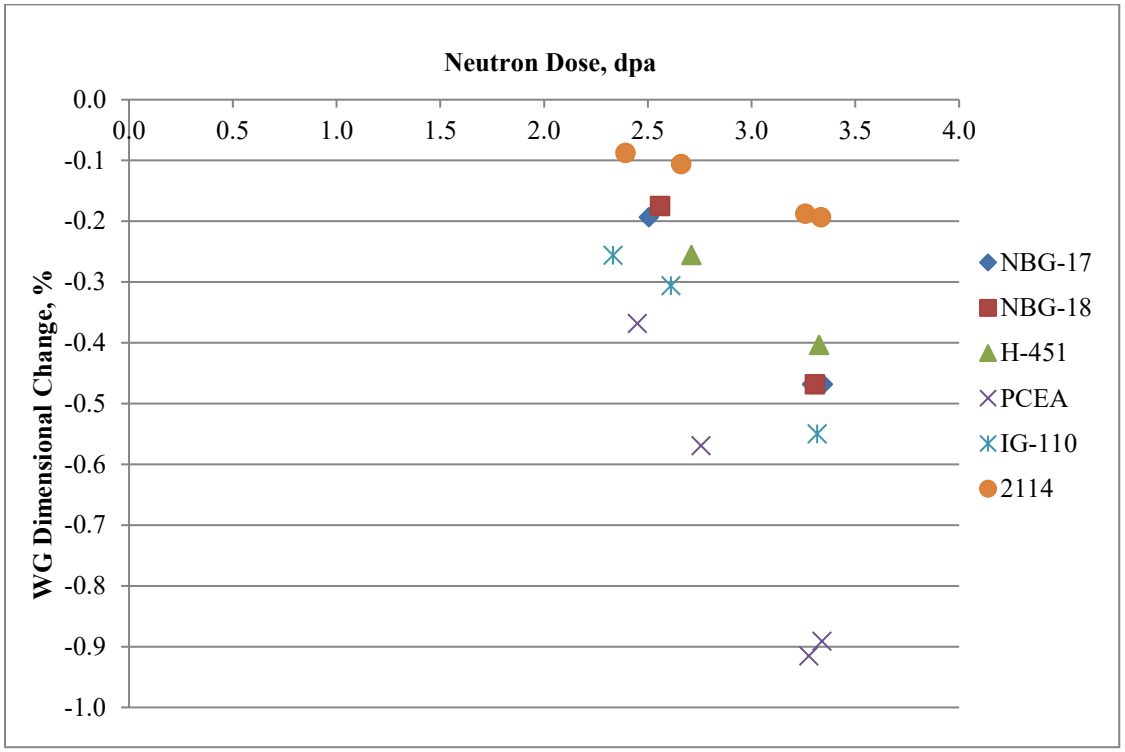

Figure 43 Fractional dimensional change in the WG orientation with neutron dose for the six graphite grades in capsule HTV at T_{irr} =900°C (design) 840°C (actual)

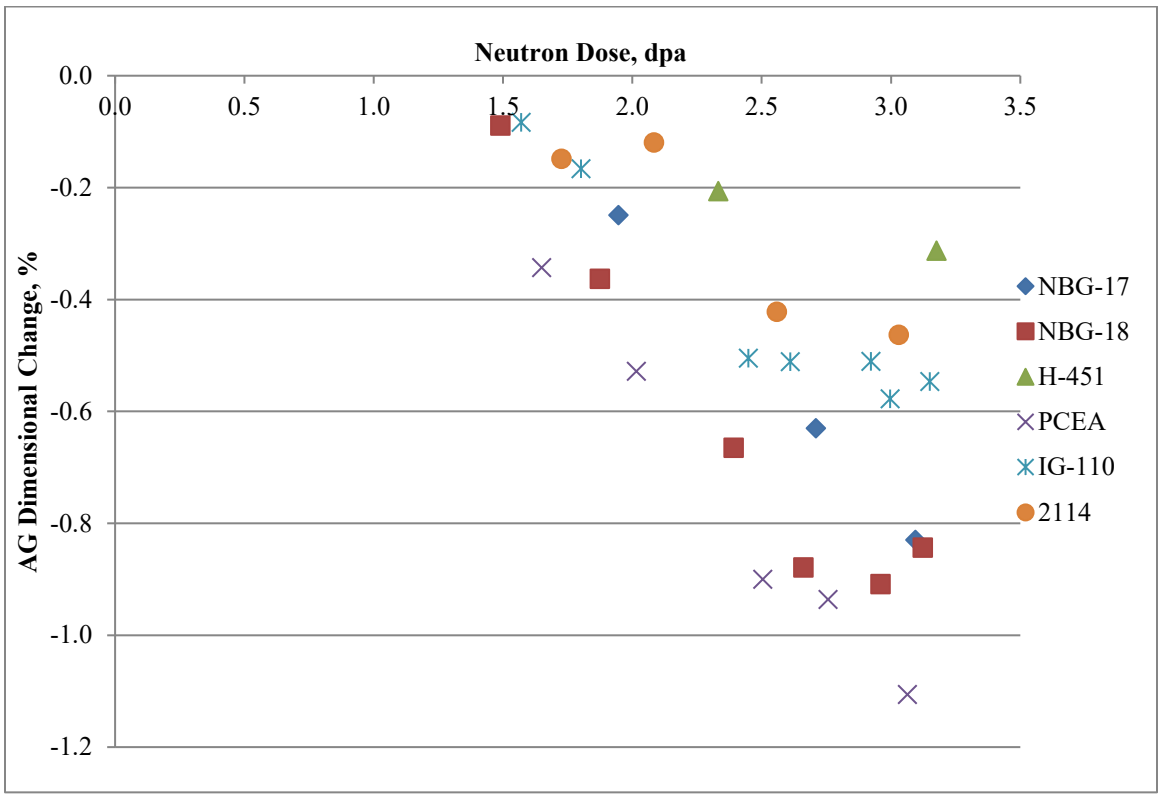

Figure 44 Fractional dimensional change in the AG orientation with neutron dose for the six graphite grades in capsule HTV at Tirr =1200°C (design) 1189°C (actual)

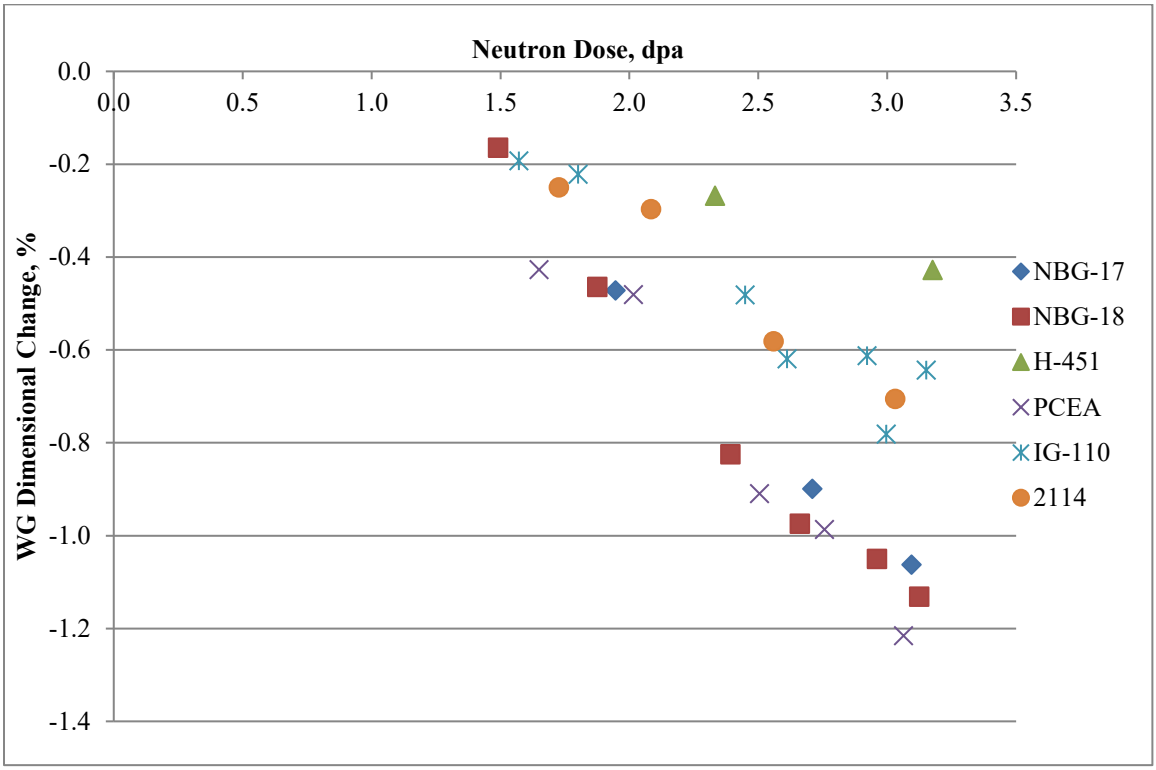

Figure 45 Fractional Dimensional change in the WG orientation with neutron dose for the six graphite grades in capsule HTV at T_{irr} =1200°C (design) 1189°C (actual)

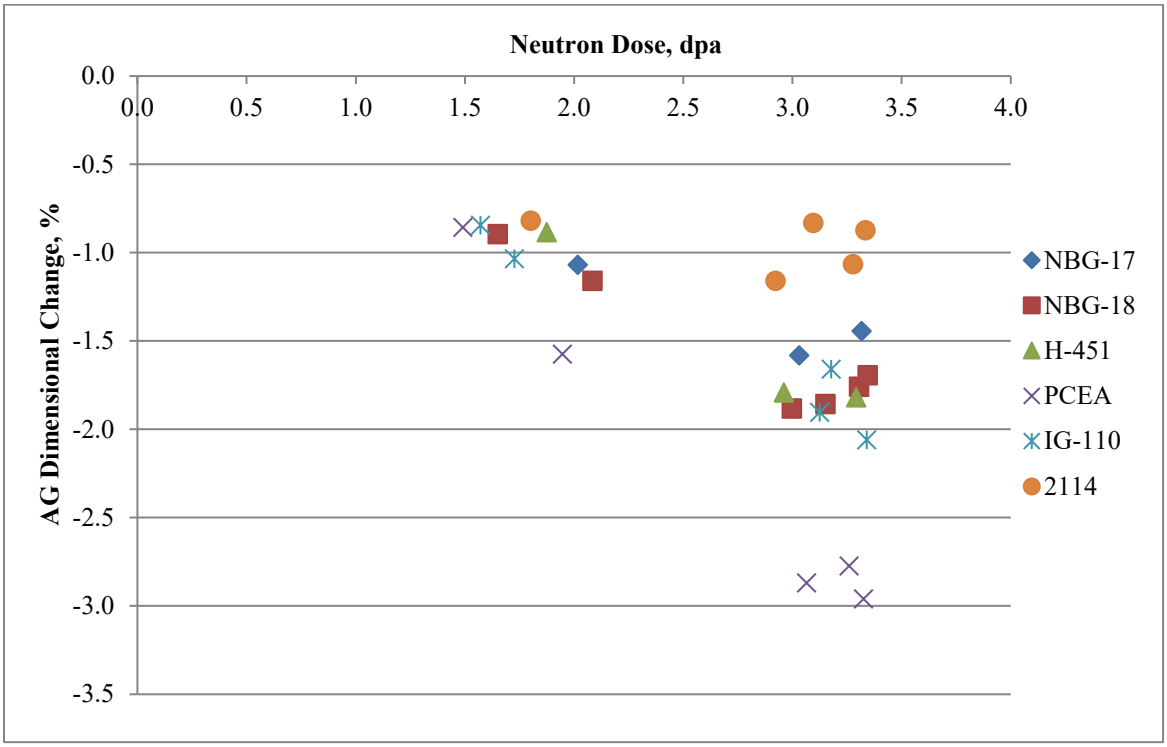

Figure 46 Fractional dimensional change in the AG orientation with neutron dose for the six graphite grades in capsule HTV at T_{irr}=1500°C (design) 1412°C (actual)

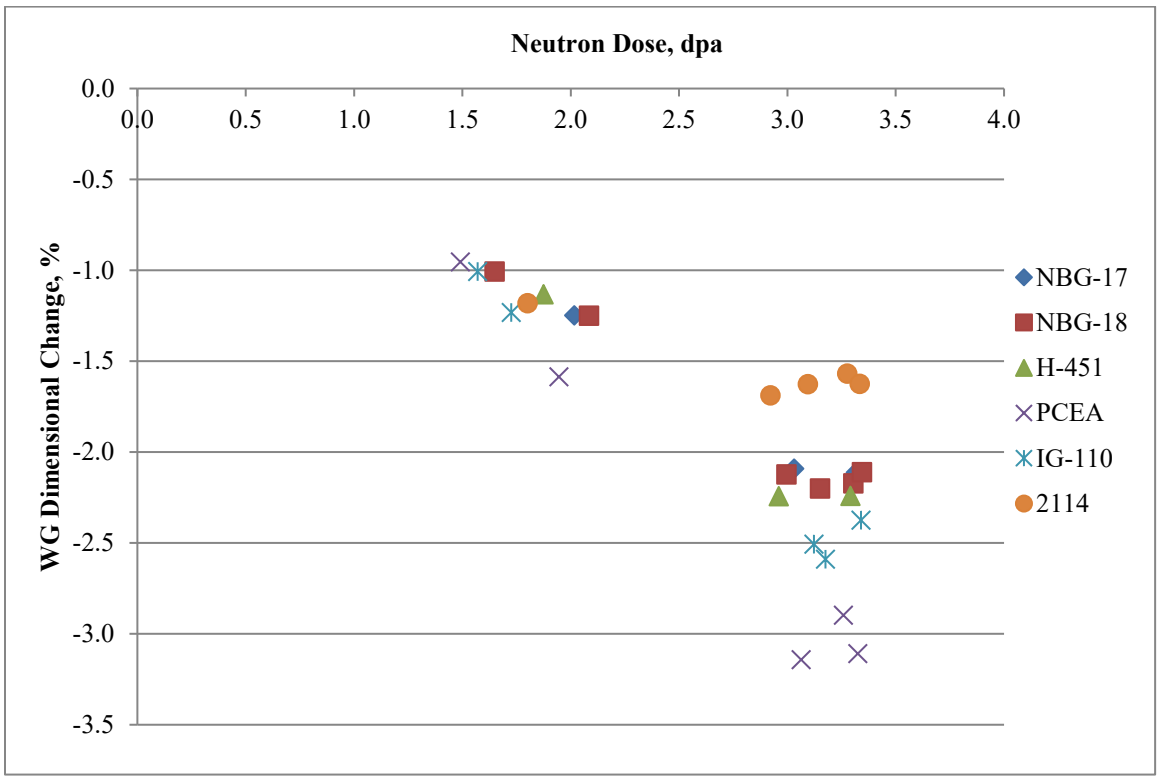

Figure 47 Fractional Dimensional change in the WG orientation with neutron dose for the six graphite grades in capsule HTV at T_{irr}=1500°C (design) 1412°C (actual)

isotropy, it is seen that in all cases the WG dimensional shrinkage exceeds the AG orientation dimensional shrinkage. This effect is largely attributable to the preferred orientation of the filler particles and the preferred orientation if the crystallographic axes within those filler particles. As illustrated in Figure 1 the graphite crystal expand along the <c>-axis and shrinks along the <a>-axis. Thus the preferential alignment of the graphite crystal by the forming process assures the AG dimensional change exhibits a greater fraction of c-axis growth (i.e., it displays more growth) and the WG direction exhibits a greater fraction of a-planes and thus shrinks more than the AG orientation. Thus we should expect the WG shrinkage to always exceed the AG shrinkage. The two grades plotted in Figure 48 to Figure 53, i.e., PCEA and 2114, display differing degrees of dimensional anisotropy. Whereas the extruded PCEA show very little anisotropy (WG≈AG) the isostatically pressed 2114 clearly displayed anisotropic dimensional behavior (WG[shrink] > AG[shrink]). These differences are probably attributable to the degree of crystallinity of the cokes used in the graphite grade's manufacture.

In addition to the anisotropy of the AG/WG orientations the magnitude of the fractional dimensional changes between the grades is worthy of comment. Fractional dimensional change in the AG orientation with neutron dose for the six graphite grades in capsule HTV, at T_{irr} =900°C (design) 840°C (actual) (Figure 42), the fractional dimensional change varied from + 0.13% at 3.3 dpa for grade 2114, to -.82% at 3.3dpa for grade PCEA. Similarly, in the WG direction, at T_{irr} =900°C (design) 840°C (actual) (Figure 43), the fractional dimensional change varied from - 0.19% at 3.3 dpa for grade 2114, to -.82% at 3.3 dpa for grade PCEA.

The fractional volume changes are shown in Figure 21, Figure 24 and Figure 27 for the six grades examined, at Tirr=900°C (des), Tirr=1200 (des) and Tirr=1500 (des), respectively. The volume changes ranged from ~ -1% (2114 at T_{irr}=900°C(design)) to ~-9% (PCEA at Tirr=1500°C (design)). The order of the grades was fairly constant irrespective of the irradiation temperature. The isostatically pressed, fine grained grade 2114 often shows the least volume shrinkage of the six grades examined. The largest volume shrinkages occurred in the extruded grade PCEA. Temperature effects are further discussed in a subsequent section.

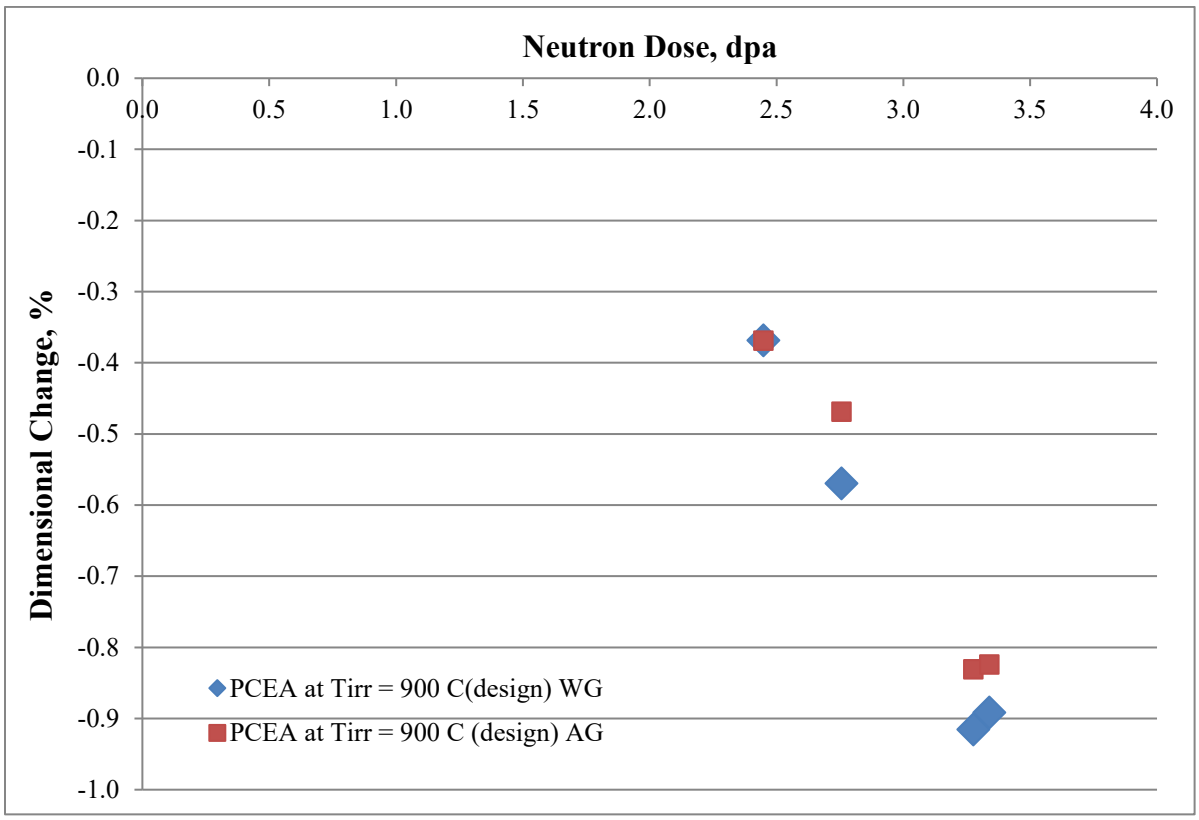

Figure 48 A comparison of the WG and AG fractional dimensional changes for PCEA at Tirr=840°C (actual)

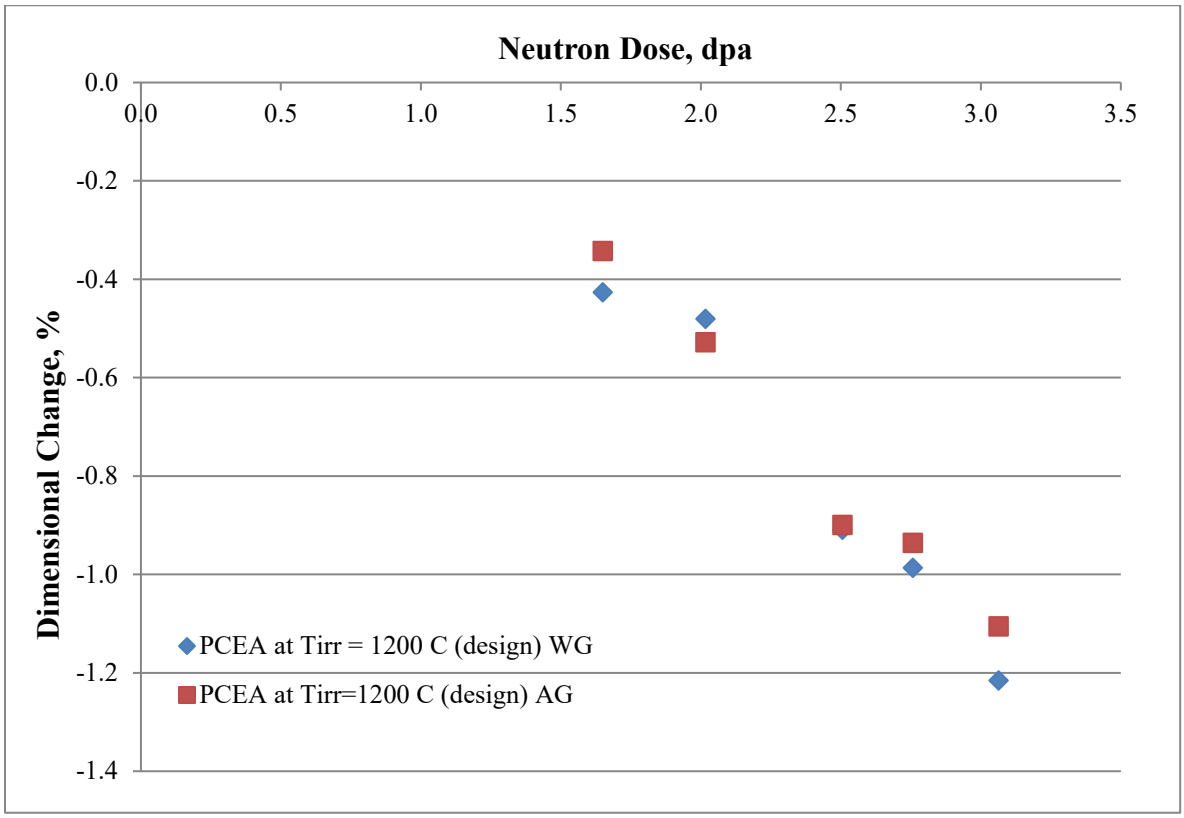

Figure 49 A comparison of the WG and AG fractional dimensional changes for PCEA at Tirr=1189°C (actual)

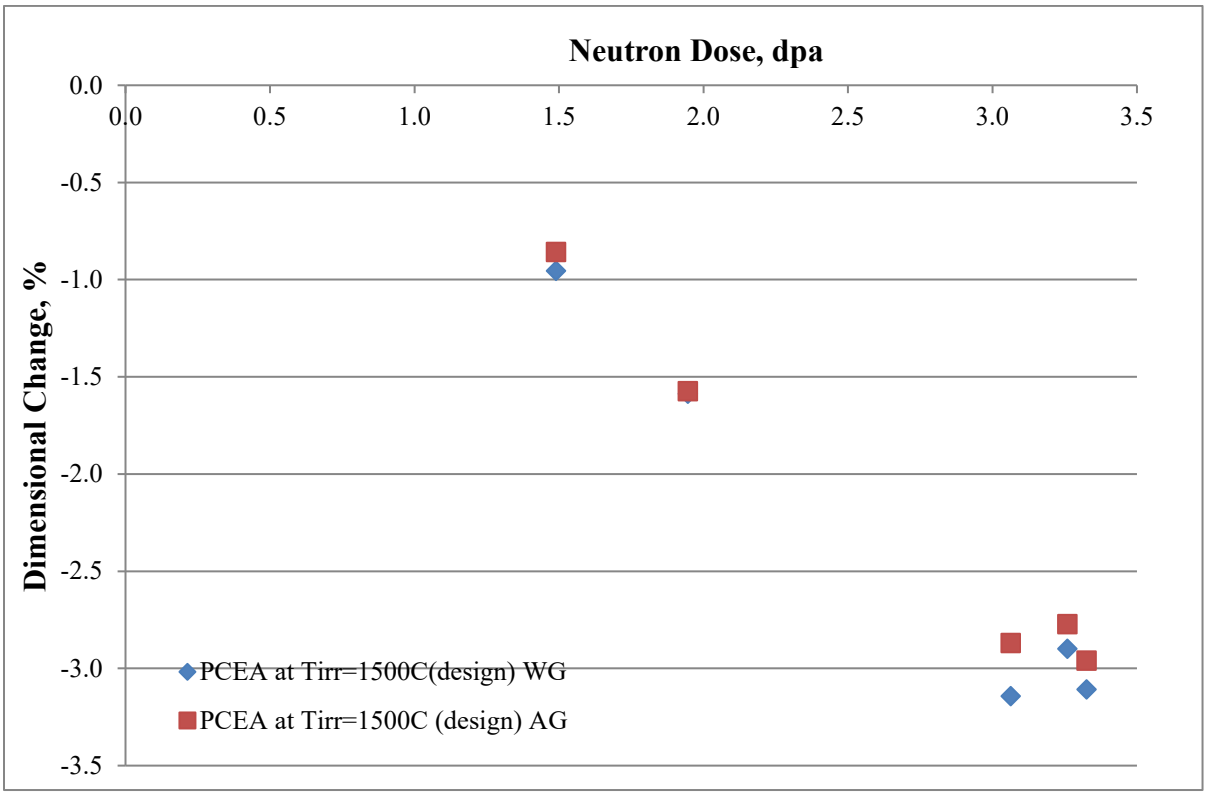

Figure 50 A comparison of the WG and AG fractional dimensional changes for PCEA at Tirr= 1412°C(actual)

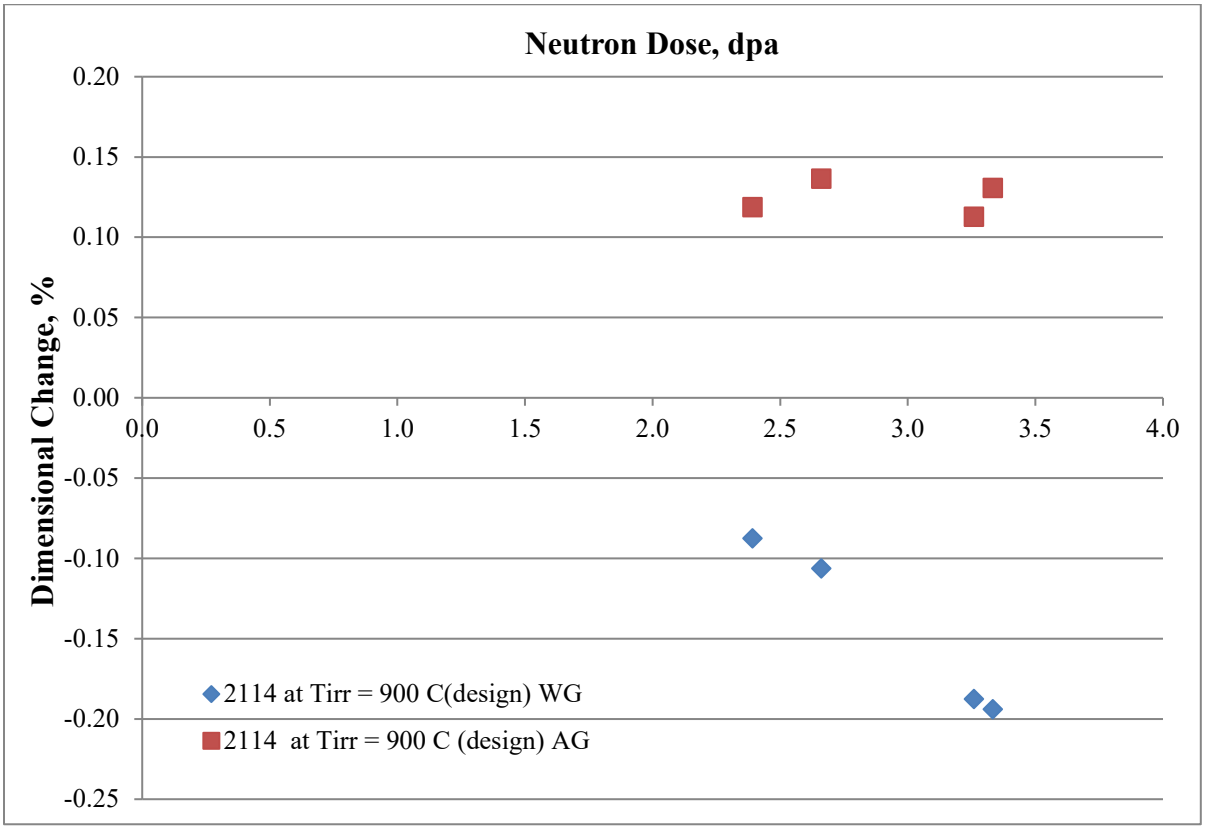

Figure 51 A comparison of the WG and AG fractional dimensional changes for 2114 at Tirr=840°C(actual)

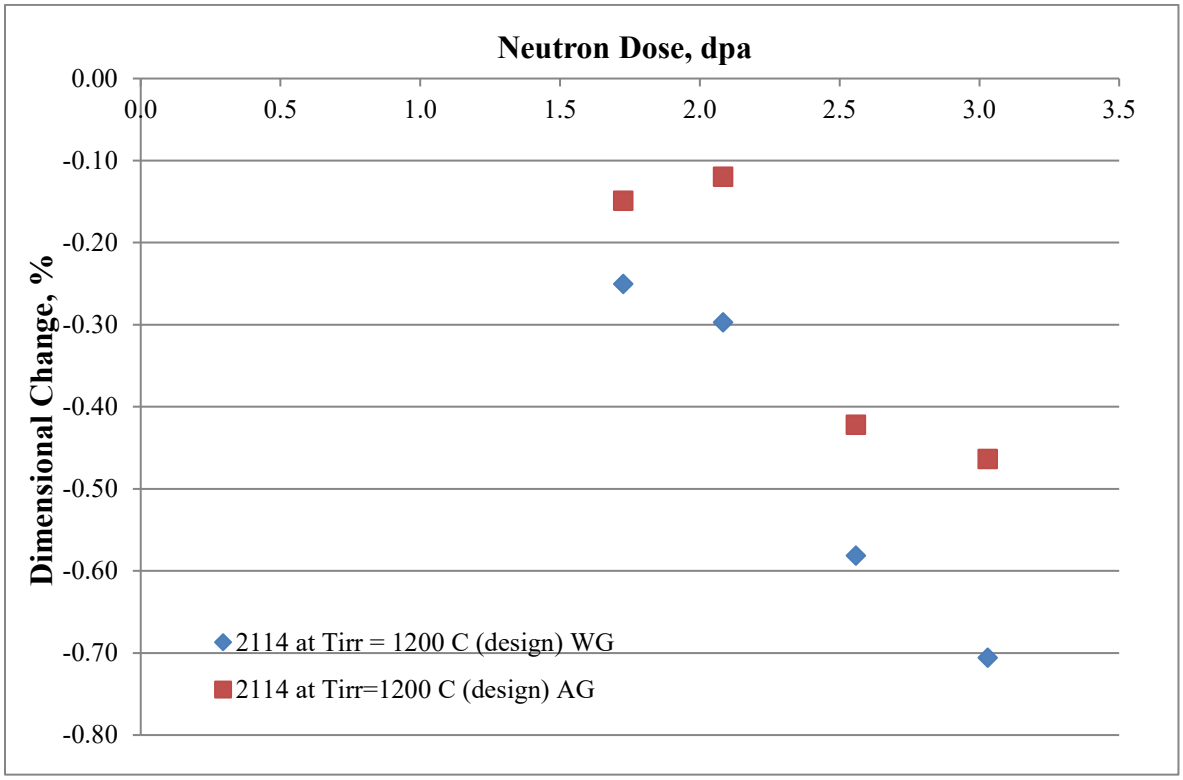

Figure 52 A comparison of the WG and AG fractional dimensional changes for 2114 at Tirr=1189°C(actual)

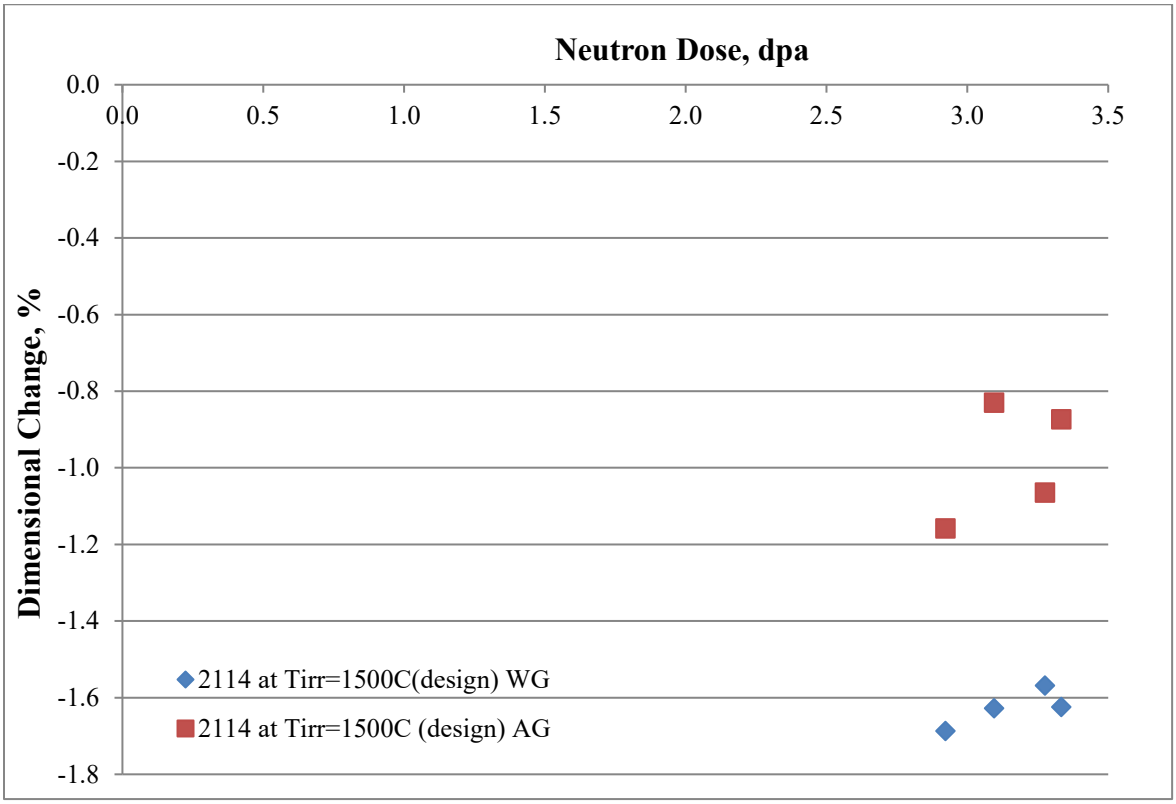

Figure 53 A comparison of the WG and AG fractional dimensional changes for 2114 at Tirr=1412°C(actual)

5.1.2 Comparison of Dimensional Change Data with Previously Published Data

To assist with establishing the irradiation temperature and to provide some degree of confidence in the HTV data, the HTV dimensional change data were compared to some previously published H-451dimensional change data [19-21]. A body of PCEA irradiation dimensional change data at Tirr= 900°C (design) 896°C (actual) was available from prior work on the effect of irradiation on the fracture toughness of PCEA [19,20]. Although the dose range of the HTV capsule was lower, the HTV graphite dimensional shrinkage data was clearly of the correct order (Figure 54) and is in reasonable agreement with prior PCEA data.

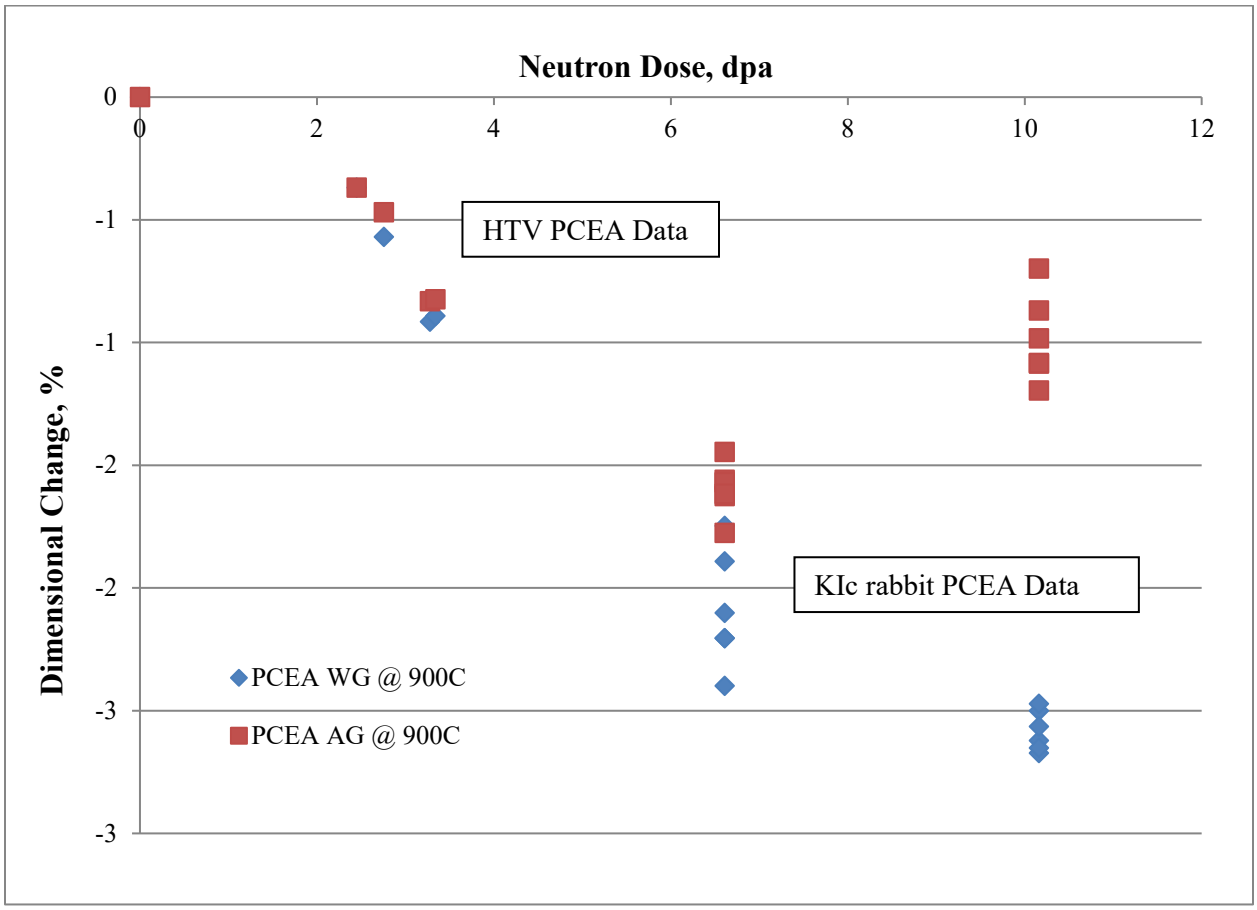

Figure 54 A comparison of grade PCEA dimensional change data from HTV Tirr=900°C (design) 840°C (actual) and PCEA data from previously published work at Tirr=900°C (design) 896°C (actual)

A second set of high temperature data for H-451 at Tirr~1200°C was available for comparison [21] with the HTV data for H-451 at Tirr~1200°C. The older data was at Tirr=1150-1249°C (both WG and AG dimensional changes) and at Tirr=1100-1149°C (AG only). These data are shown in Figure 55 along with the H-451 data from the HTV capsule. The dimensional change data compare less favorably for H451 at Tirr~1200°C than they did for the PCEA at Tirr~900°C. Comparing the HTV H-451 (WG) data for Tirr=1200 (des)) with older H-451 (WG) data (Figure 55) it is seen that the lower temperature range 1100-1149 cf. 1150-1249°C is a more satisfactory

match to the HTV dimensional change data, suggesting that the HTV sub capsule's 3,7 & 8 actual irradiation temperature was indeed less than 1200°C.

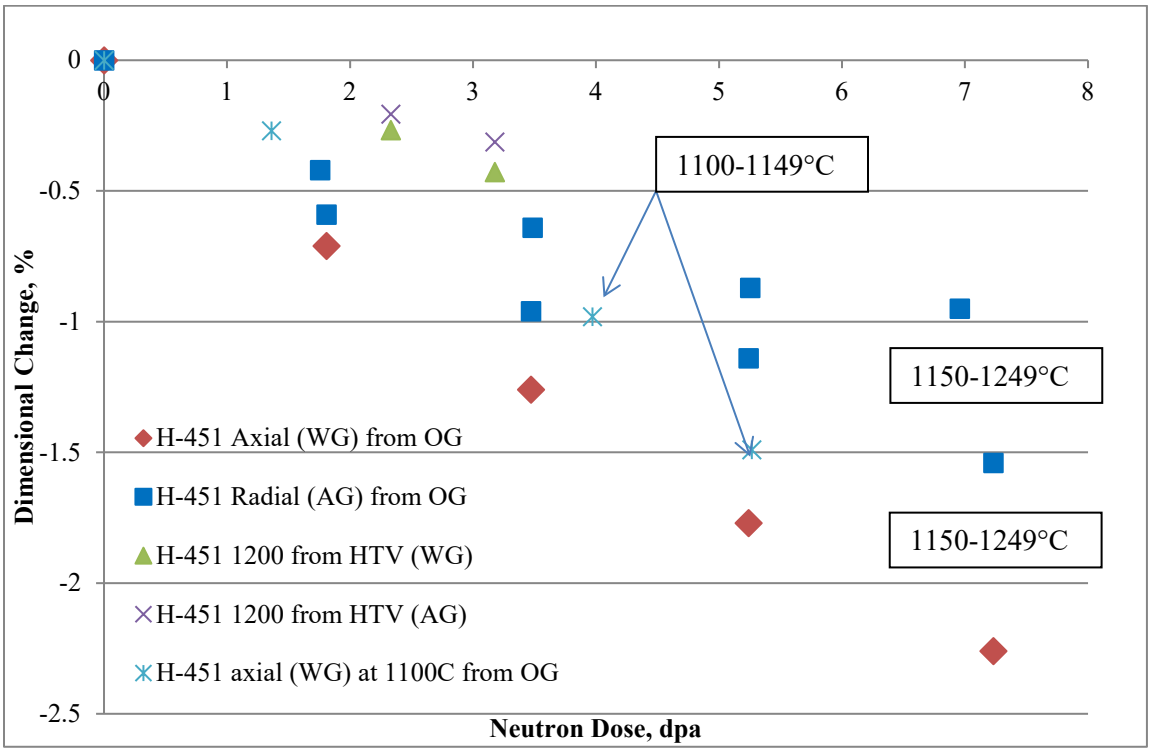

Figure 55 A comparison of grade H-451 dimensional change data from HTV Tirr=1200°C (design) and H--451 data from previously published work at Tirr=1100-1149°C and Tirr=1100-1150°C

5.1.3 Effect of Irradiation Temperature

Two factors are particularly influential in controlling the irradiation temperature response of graphite. As the irradiation temperature increases over the range 900-1500°C these factors are increasingly important:

- The crystal growth rate increases, as shown in Figure 2. Thus we can expect the magnitude of the volume changes to be greater at higher temperatures.
- The available accommodating volumes of fine cracks and pores between the basal planes will reduce as larger fractions of the "accommodation porosity" are filled by the increased internal thermal expansion of the graphite at higher temperatures. This accommodation porosity masks the c-axis expansion and thus the volume change is dominated by the a-axis shrinkage. Thus, the expected volume turn-around from shrinkage to growth to occur at lower doses for higher temperature irradiations.

The behavior of grade 2114 (Figure 56) and PCEA (Figure 57) show the effect described above.

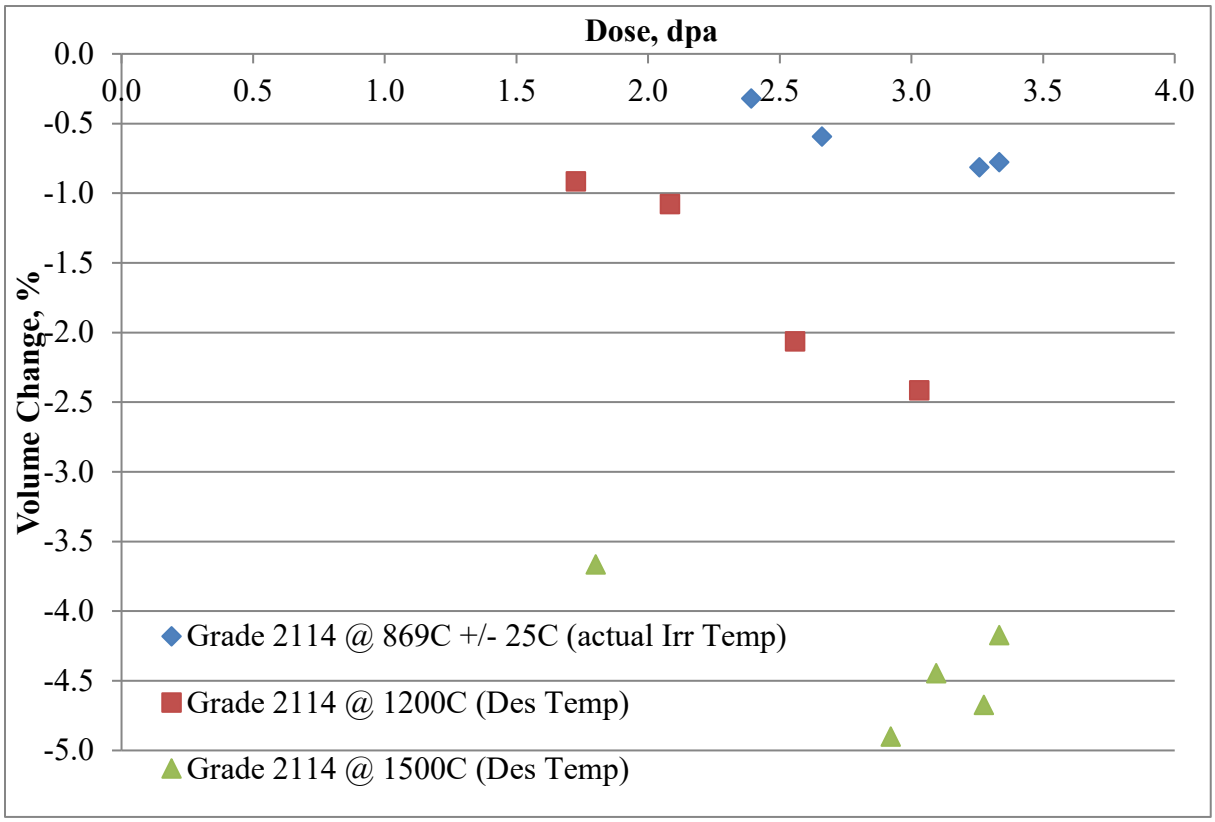

Figure 56 Irradiation temperature effects on irradiation induced volume changes in grade 2114 graphite

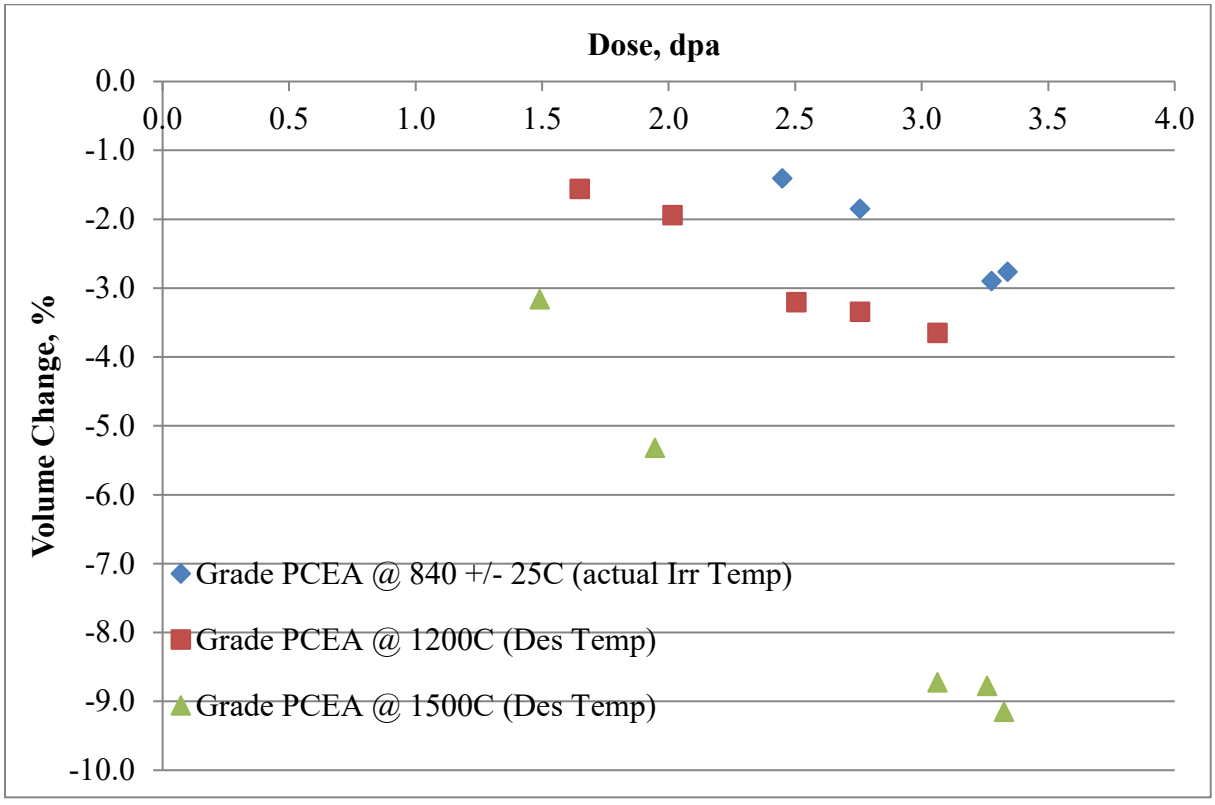

Figure 57 Irradiation temperature effects on irradiation induced volume changes in grade PCEA graphite

In both cases the magnitude of the volume shrinkage increases as the irradiation temperature increases. For isostatically pressed grade 2114 (Figure 56) reaching ~ -5% at Tirr=1500°C (des) and for and extruded grade PCEA (Figure 57) the volume shrinkage reached ~-10% at Tirr=1500°C (des).

Although the volume change data in Figure 56 and Figure 57 does not clearly define the volume turn-around, the volume turn-around (from shrinkage to growth) is expected to occur at lower doses for higher temperature irradiations.

5.1.4 Specimen Central Hole Diameter Change

The data for the HTV specimen's central hole diameter change is less clear than other HTV dimensional change data probably due to the difficulty in making the measurements. The largest dimensional changes were seen for the grade IG-110 with ~+8 to +10% diametral swelling in the in the WG inside diameter orientation at design irradiation temperature of 900-1200°C. The grades where the specimens were aligned such that the diameter was in the AG direction, i.e. PCEA and H-451(Figure 29, Figure 31 and Figure 33), showed a lesser hole (ID) growth than the grade which had their hole diameters in the WG orientation (Figure 28, Figure 30 and Figure 32) In the former case (i.e. H-451 and PCEA), both extruded grades, there is a tendency to develop a radial texture(<c>-axis preferentially aligned radially in the billet). Hence, there will be some <c>-axis alignment with the hole's diameter. Thus, there would be less <a>-axis shrinkage and more <c>-axis growth in this orientation within the graphite, causing more graphite net growth. If the graphite shrinks less in the diametral AG orientation the hole diameter must also increase less.

At 900°C (design) and 1200°C (design) irradiation temperatures the central specimen's hole diameter increased with increasing dose. At 1500°C (Des) irradiation temperature Grades PCEA (AG) (Figure 58), IG-110 (WG) (Figure 59), NBG-17 (WG) and 2114 (Figure 61) showed signs they had entering into diametral shrinkage (of the hole) potentially producing a dimensional interference of the creep specimens in their creep channels (for AGC-5/6 specimens). An irradiation temperature effect is expected since an increasing fraction of the accommodation porosity is closed at higher temperature, thus we expect to see more a-axis shrinkage at higher temperatures. Moreover, the crystal growth rate (Figure 2) substantially increases over the HTV experimental temperature range.

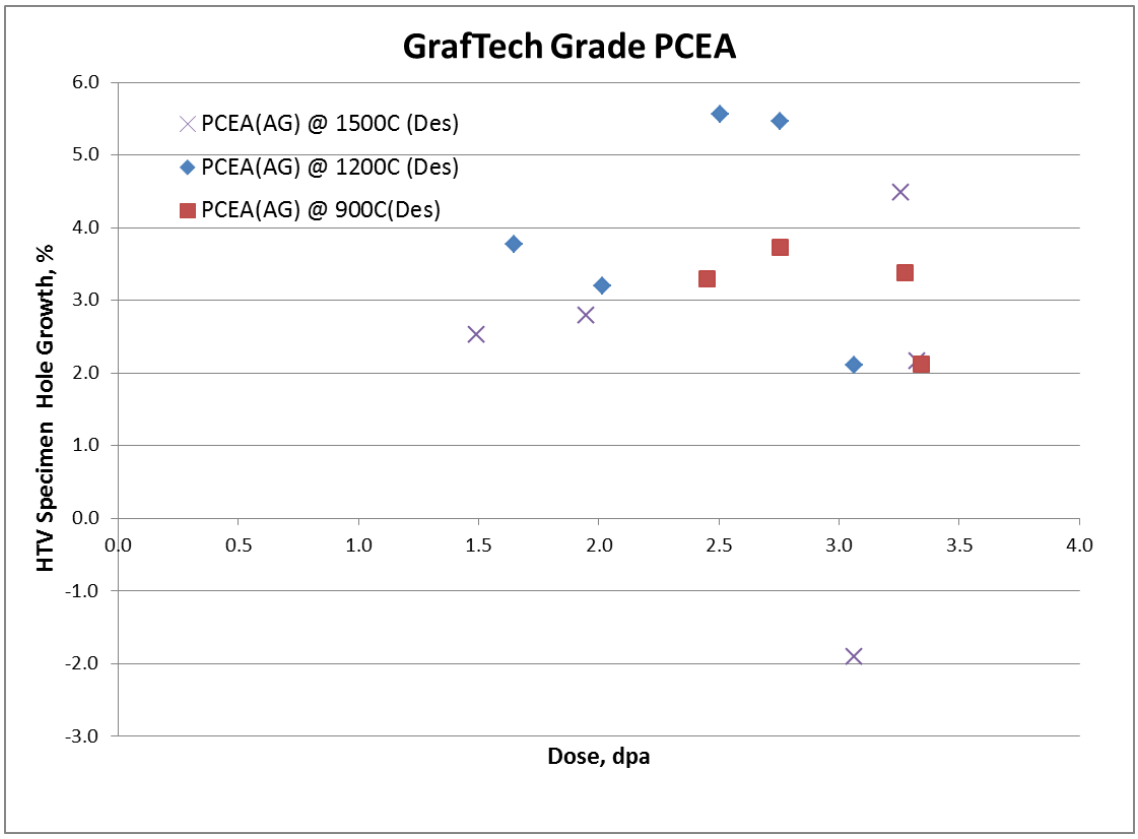

Figure 58 HTV central hole diameter changes for grade PCEA (AG) at various temperatures

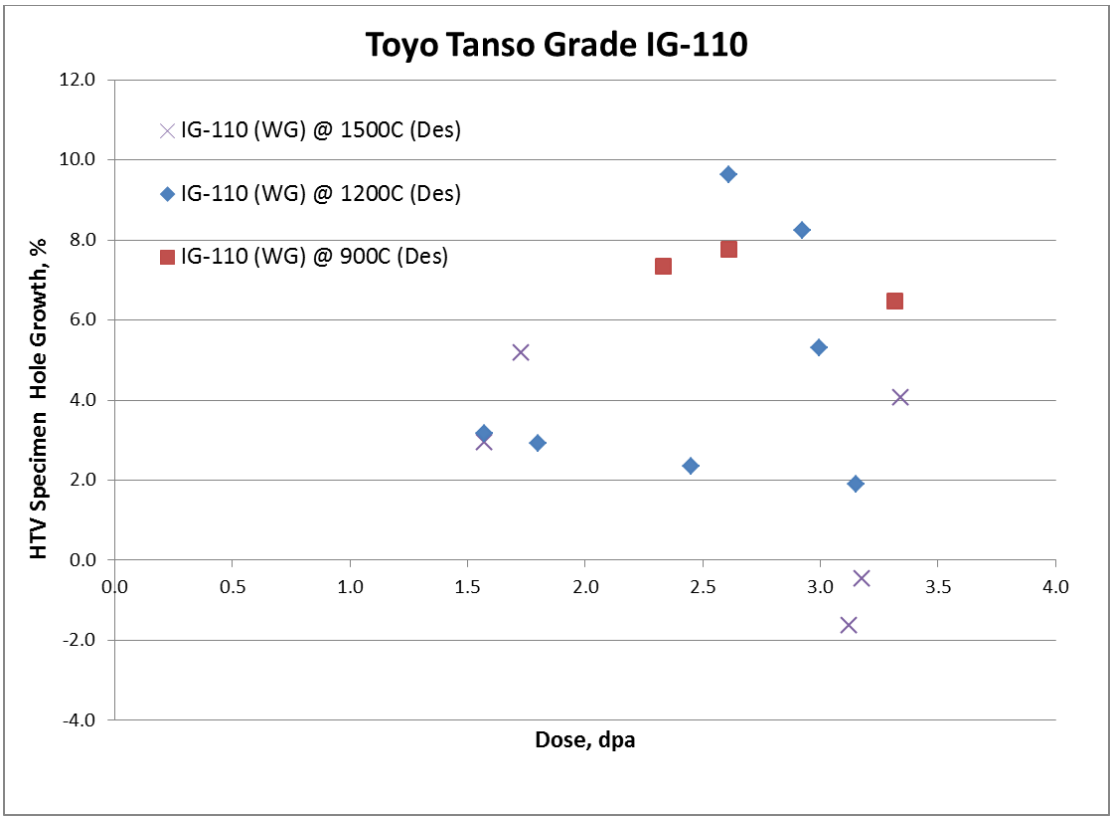

Figure 59 HTV central hole diameter changes for grade IG-110 (WG) at various temperatures

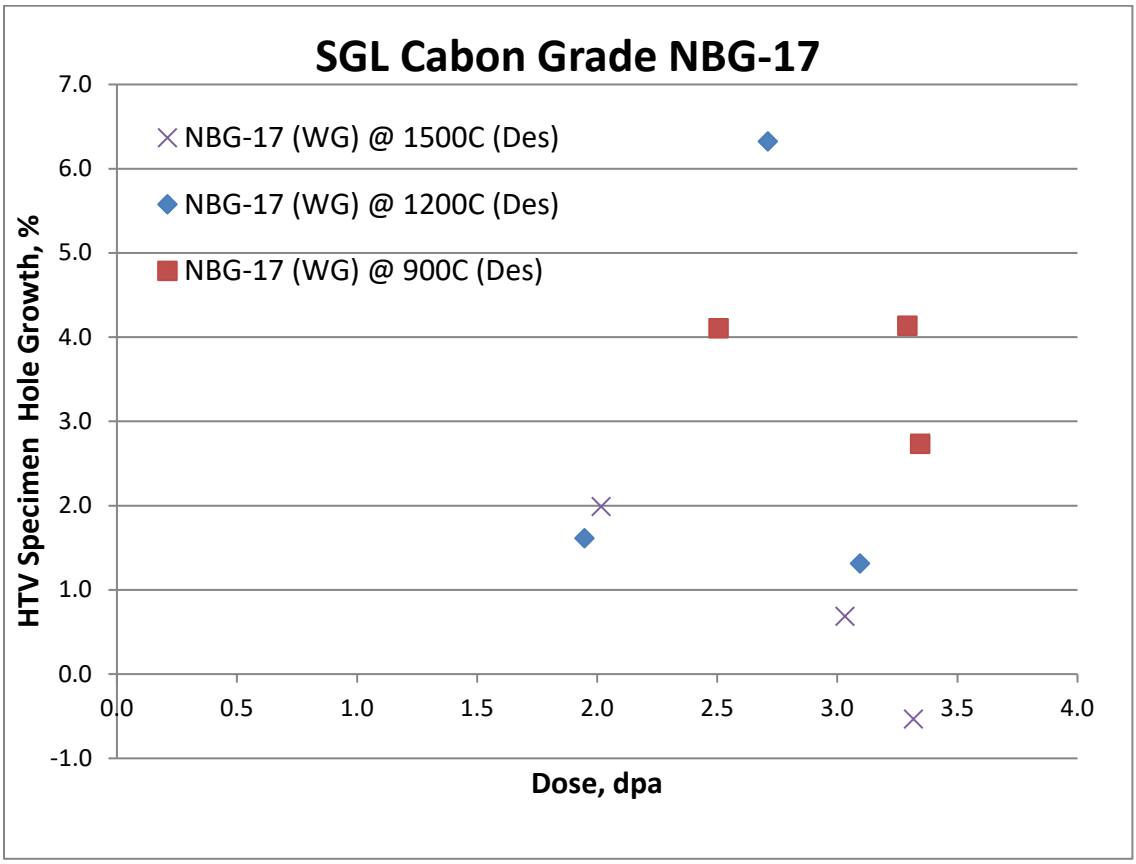

Figure 60 HTV central hole diameter changes for grade NBG-17 (WG) at various temperatures

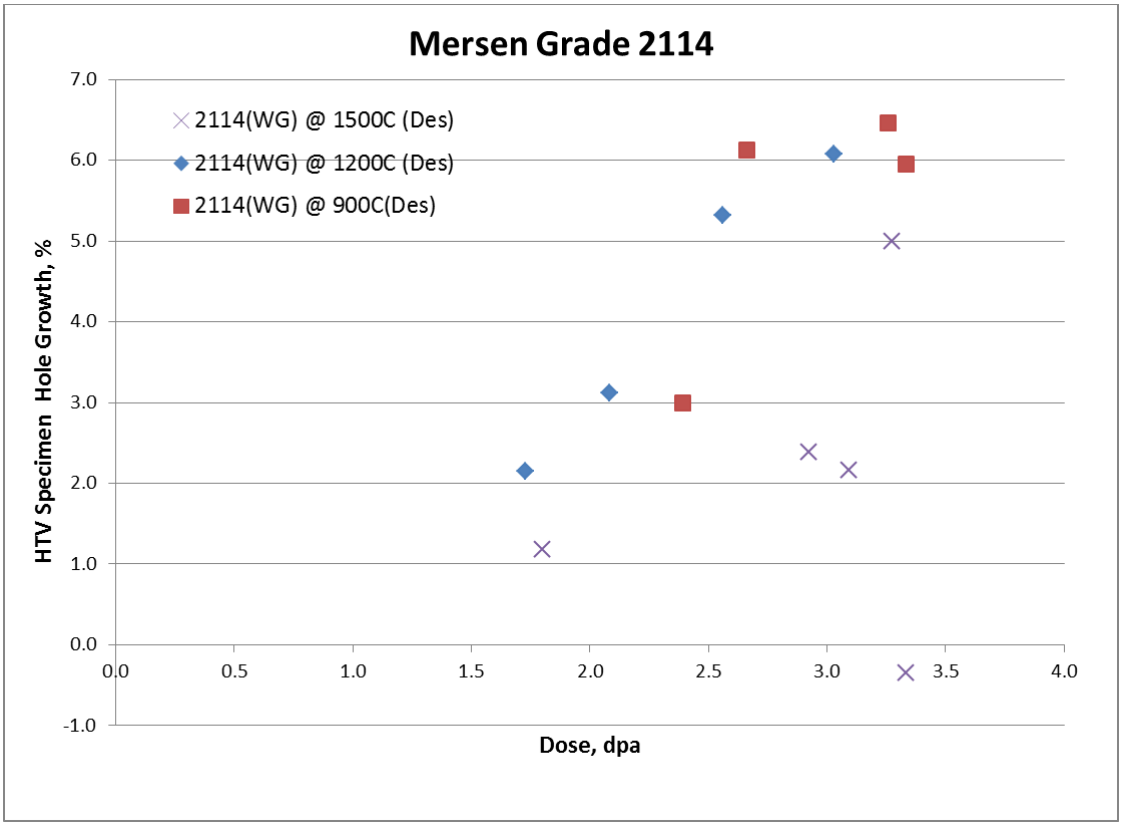

Figure 61 HTV central hole diameter changes for grade 2114 (WG) at various temperatures

5.1.5 Dose Limits at Elevated Temperature

Unfortunately, the data from HTV does not allow identification of dose limits for the grades examined. However, based on these data, some guidance can be offered. It is undesirable for the specimen's dimensions to exceed their original dimension i.e., a positive fractional dimensional change potentially producing a dimensional interference. Moreover, it is unreasonable to apply the viscoelastic creep model to creep strains evaluated from beyond turn-around dimensional data. Grade 2114(AG), Tirr = 900°C (design) (Figure 51) exhibits positive dimensional fractional change above ~1.0-1.5 dpa. Grade 2114 does not show any positive dimensional change in the WG orientation, where a-axis shrinkage dominates as a result of texture introduced during forming. However the anisotropy of grade 2114, supposedly isotropic graphite, is alarming. A significant anisotropy in grade 2114 is also apparent in the T_{irr} = 1500°C (design) (Figure 53). The apparent irradiation induced anisotropy of Grade 2114, a fine grained, relatively high density, isotropic graphite grade, is a concern. Thus it is probably prudent to keep the doses low (3dpa) at elevated temperature (>1200°C), especially for any high density grades.

5.2 ELASTIC (YOUNG'S) MODULUS CHANGES

5.2.1 Response of Different Grades

The effects of irradiation on the Young's Modulus of the grades in HTV are shown in Table 18 to Table 20 and in Figure 35 to Figure 40. The fractional changes in elastic modulus have been calculated and are shown in Table 18 to Table 20 and in Figure 62 to Figure 67. All of the graphite grades experienced an increase in Young's Modulus with irradiation dose. The maximum post irradiation Young's modulus value occurred for grade NBG-17 at Tirr (design) = 900°C and dose of 3-3.5 dpa (Figure 35), with a value of ~19 GPa. The smallest post irradiation Young's modulus value occurred for IG-110 at Tirr (design) = 900°C and at a comparable dose of 3-3.5 dpa (Figure 39), with a value of ~15 GPa. The fractional change on irradiation of these two grades (NBG-17 & IG-110) was approximately 0.4 for NBG-17 and 0.6 for IG-110 (Figure 62).

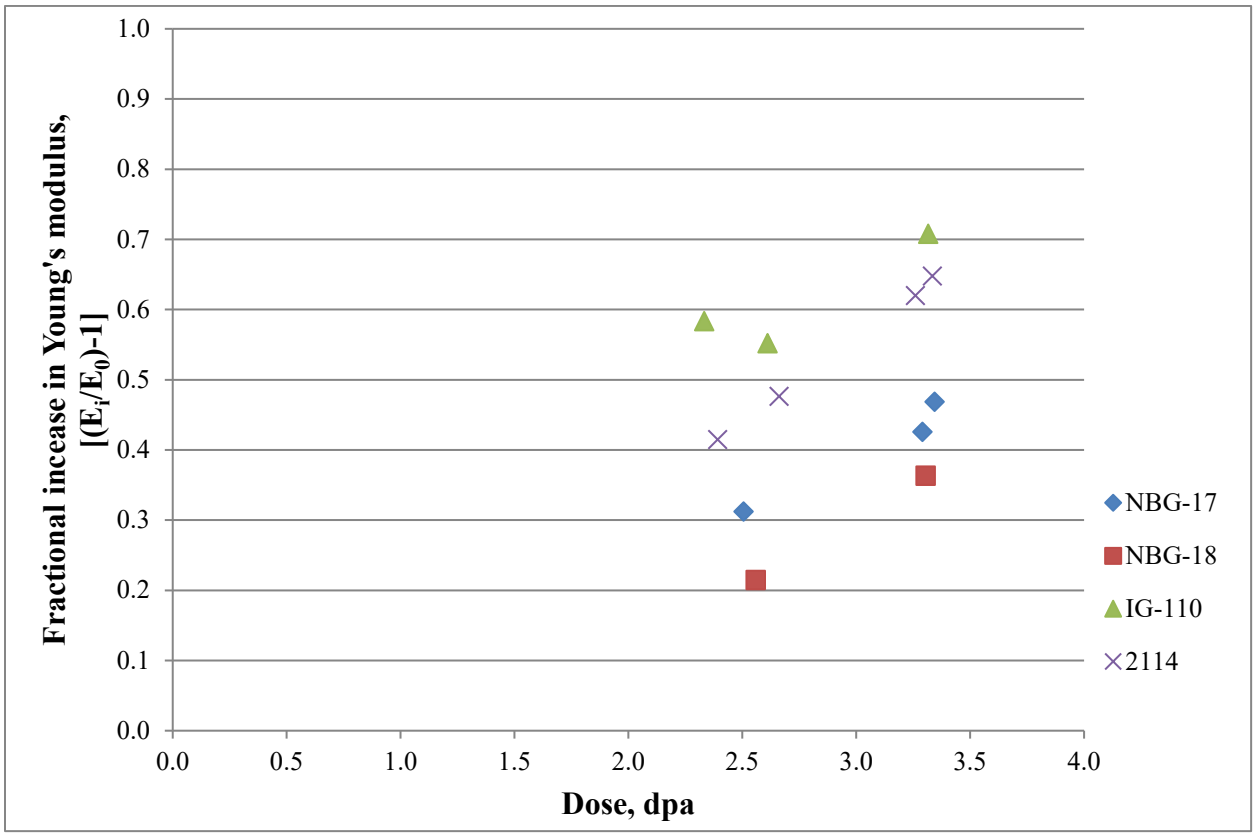

Figure 62 Fractional increase of Young's modulus with irradiation for several grades in the AG orientation in capsule HTV at T_{irr} =900°C (design) 840°C (actual)

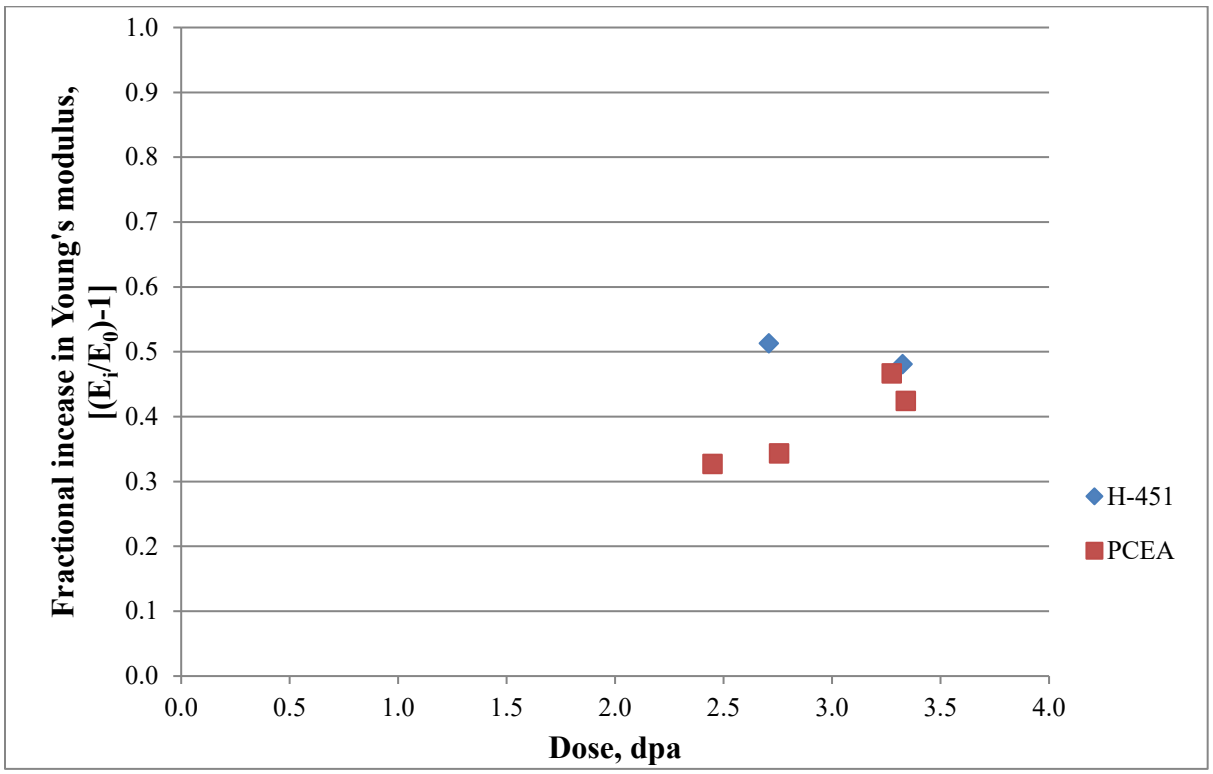

Figure 63 Fractional increase of Young's modulus with irradiation for two grades in the WG orientation in capsule HTV at T_{irr} =900°C (design) 840°C (actual)

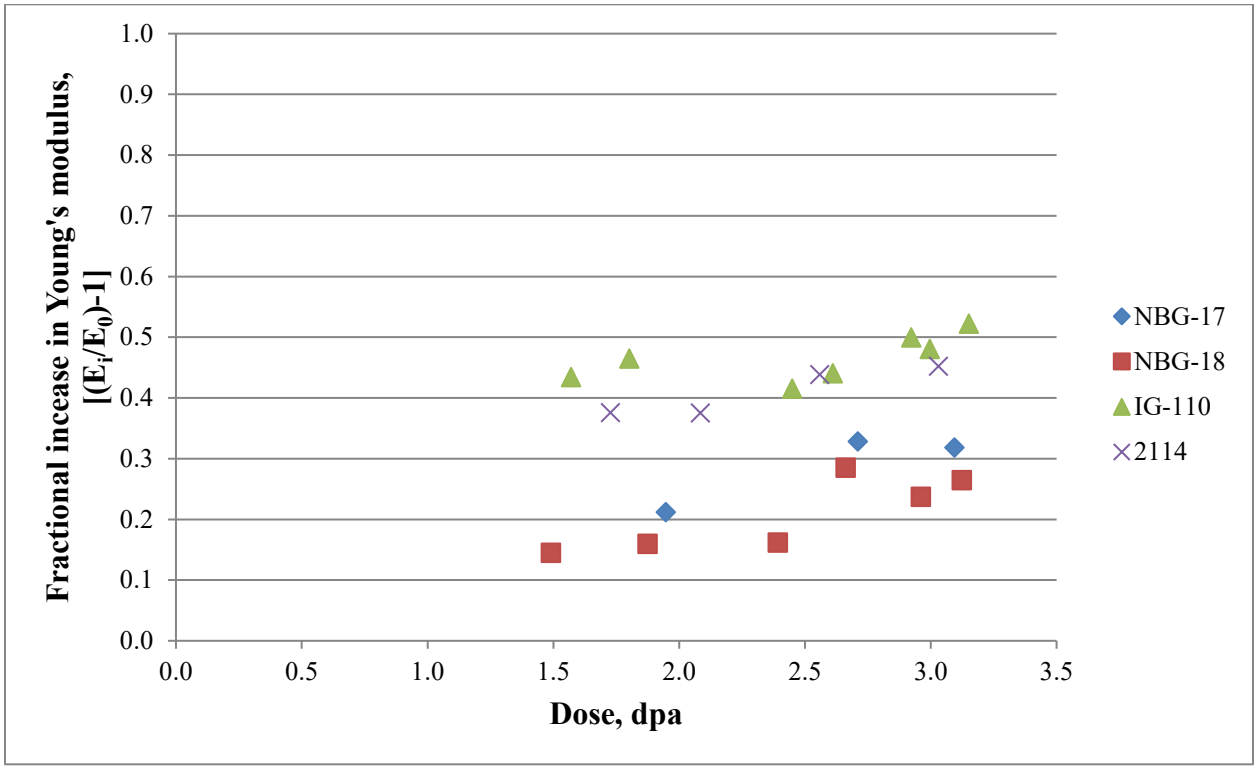

Figure 64 Fractional increase of Young's modulus with irradiation for several grades in the AG orientation in capsule HTV at Tirr =1200°C (design) 1189 °C (actual)

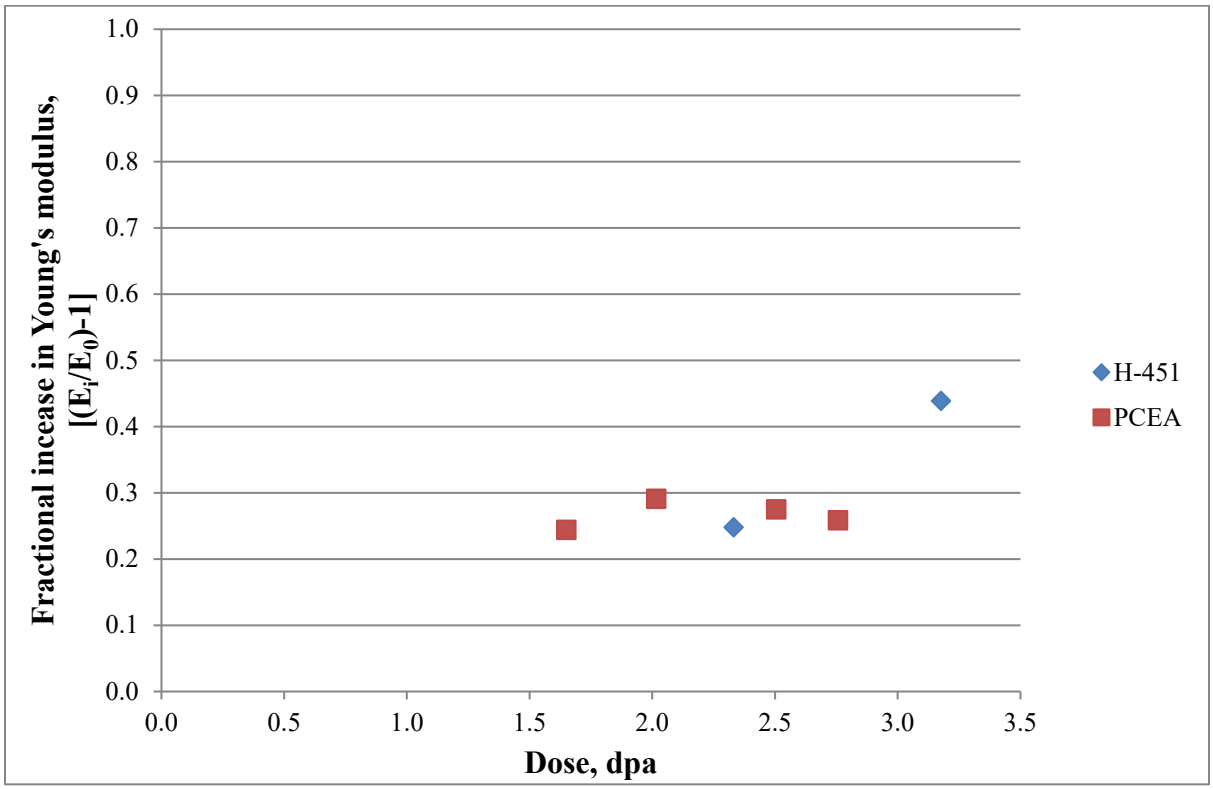

Figure 65 Fractional increase of Young's modulus with irradiation for two grades in the WG orientation in capsule HTV at Tirr =1200°C (design) 1189 C (actual)

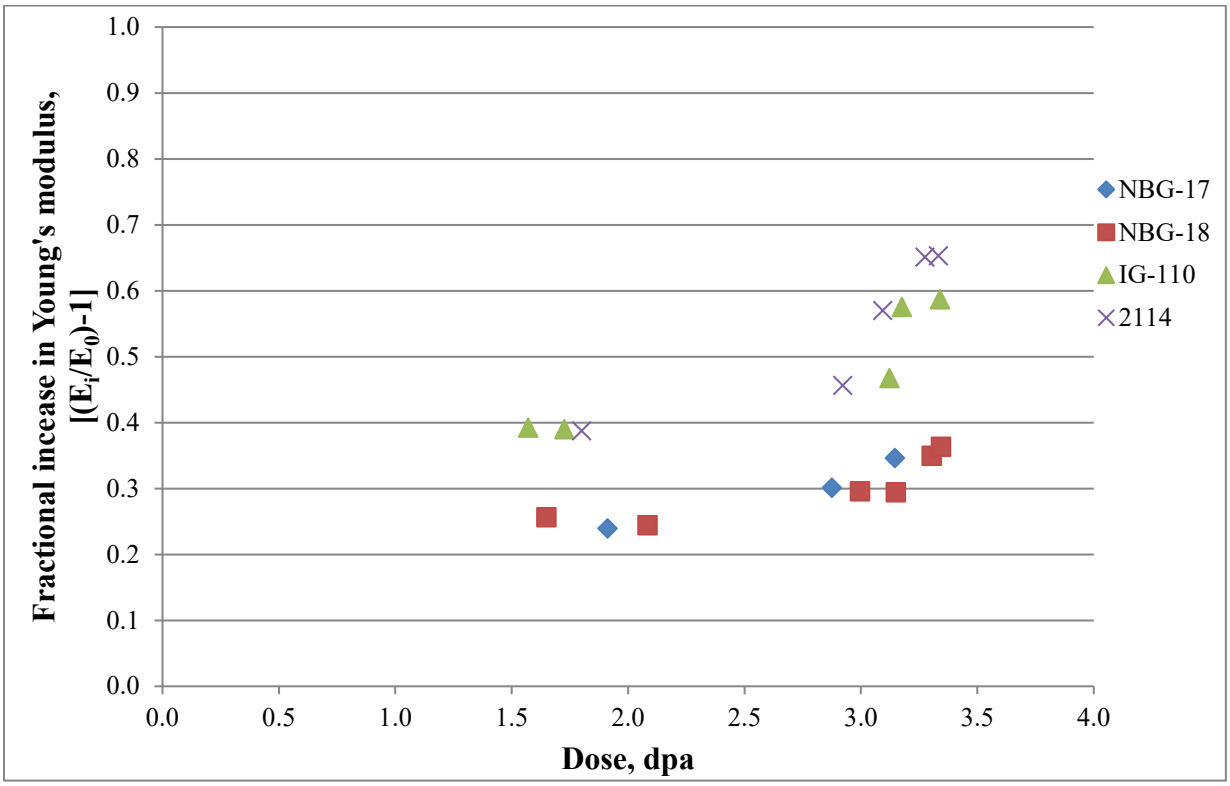

Figure 66 Fractional increase of Young's modulus with irradiation for several grades in the AG orientation in capsule HTV at T_{irr} =1500°C (design) 1412°C (actual)

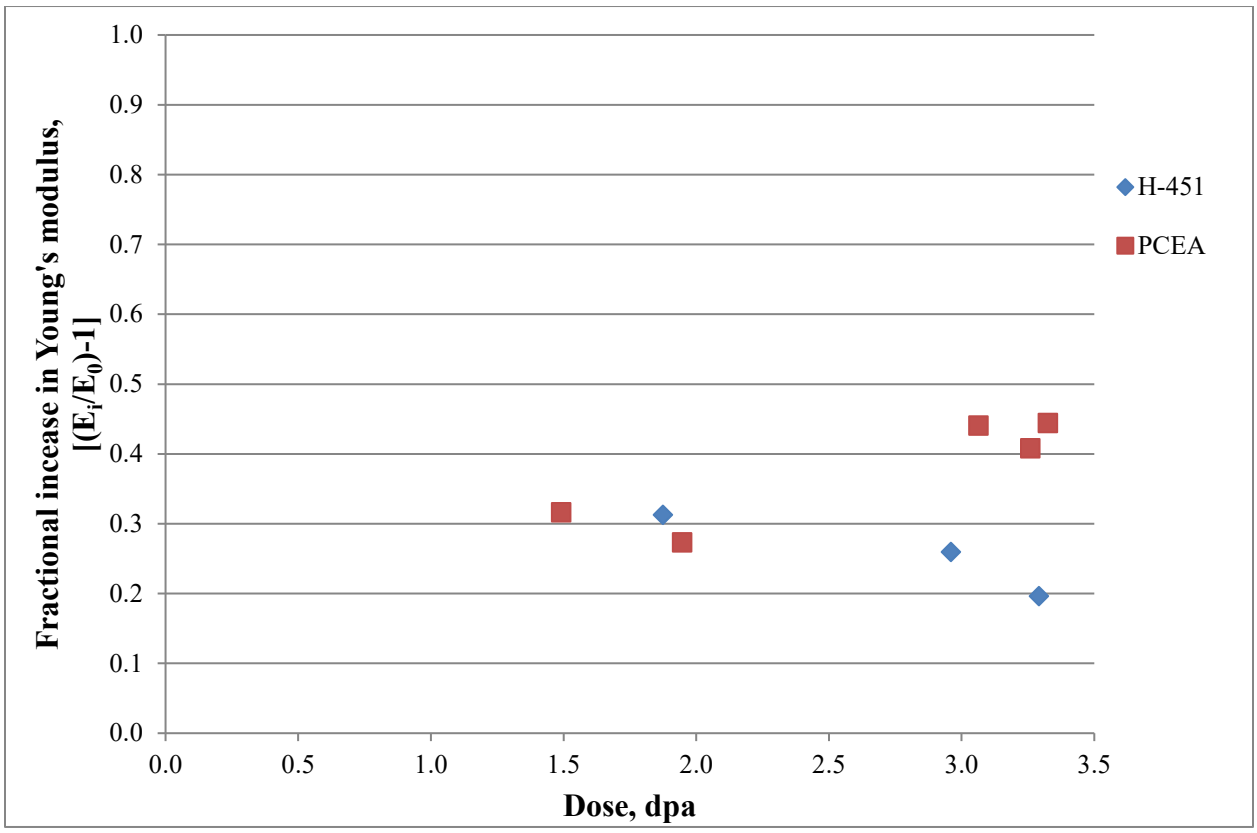

Figure 67 Fractional increase of Young's modulus with irradiation for two grades in the WG orientation in capsule HTV at T_{irr} =1500°C (design) 1412°C (actual)

5.2.2 Effect of Irradiation Temperature

A plot of the fractional change in elastic modulus of H-451 graphite is shown in Figure 68. The data is taken from the IAEA database for irradiated graphites [21] and shows that the magnitude of the fractional changes increase with irradiation temperature. HTV data for the fractional change in elastic modulus of H-451 graphite is shown in Figure 69. Three observations are in agreement with the literature data:

1. The magnitude of the H-45 fractional changes obtained here are in good agreement with the literature data [21] (at higher temperatures).
2. The trend for the fractional change to be smaller at higher irradiation temperatures is seen in both data sets.
3. The fractional change in Young's Modulus increases as irradiation dose increases at a constant irradiation temperature prior to irradiation induced structural changes (turn-around)

A similar result is obtained for PCEA (Figure 70), although the trends are not as obvious. The fractional change in modulus is seen to increase (prior to turnaround) as the dose increases. This is clearly indicated by the ~900°C data (Figure 62). N.B. Modulus data are from this and prior work [19, 20].

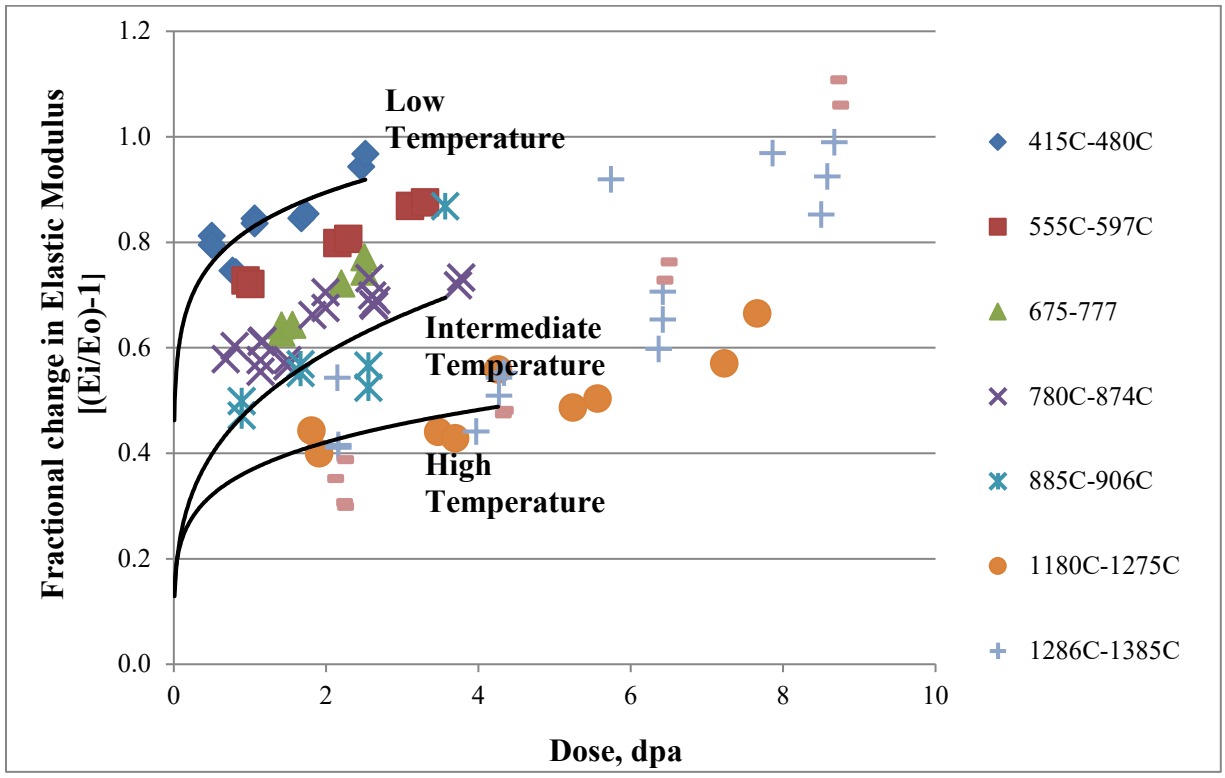

Figure 68 Fractional elastic modulus change for H-451 (Axial) as a function of dose and irradiation temperature from a HFR irradiation series [21]

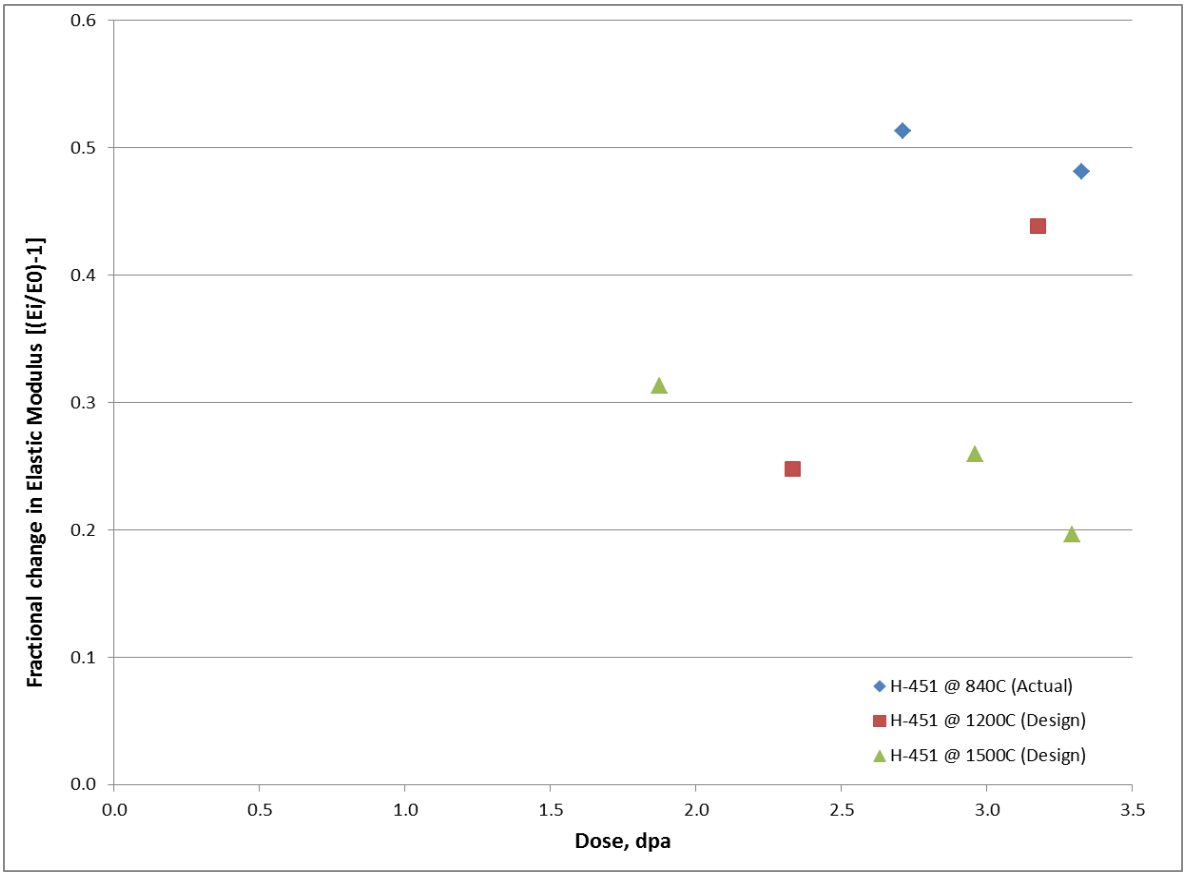

Figure 69 Fractional elastic modulus Change for H-451 (Axial) as a function of dose and irradiation temperature (current irradiation)

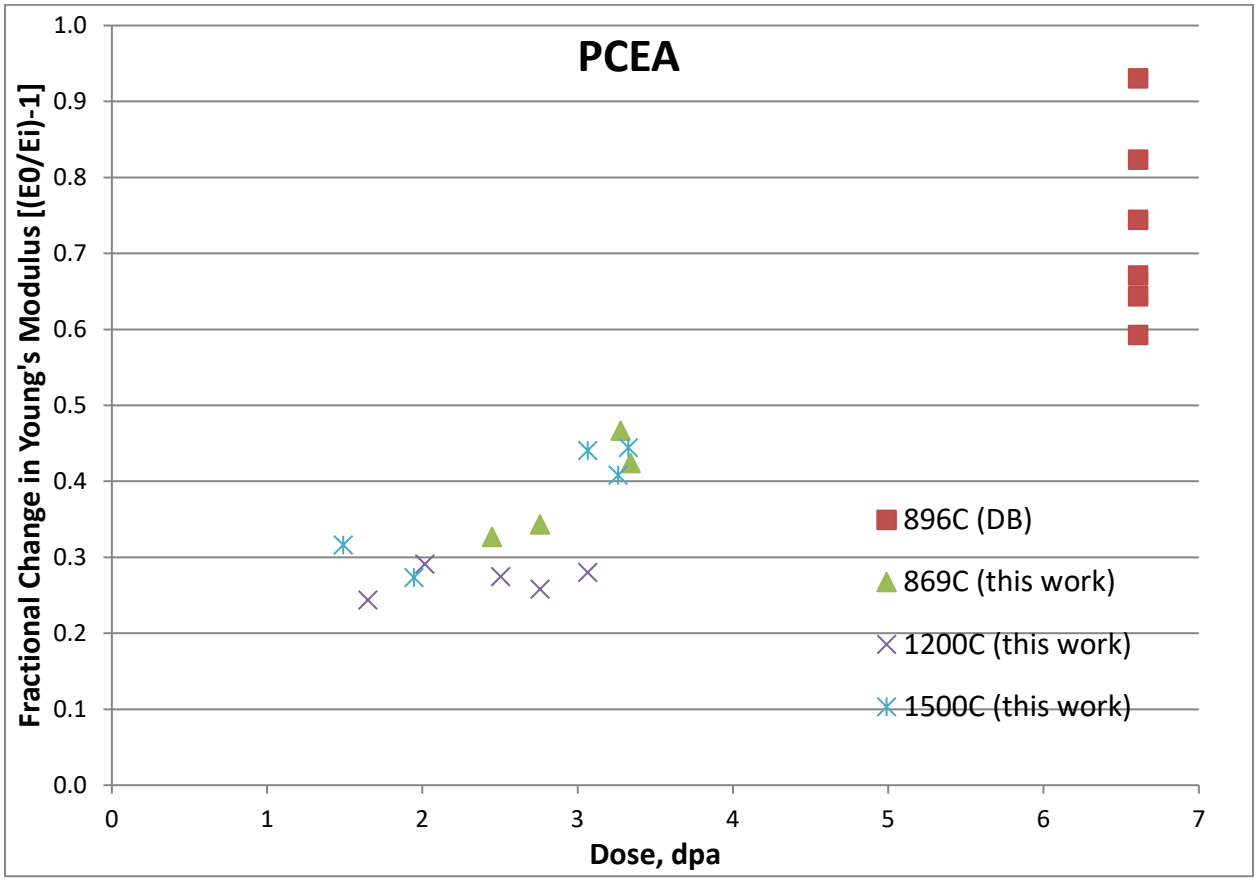

Figure 70 Comparisons of the fractional elastic modulus changes for PCEA (Axial) as a function of dose and irradiation temperature from DOE Deep Burn Program and the current irradiation

Moreover, the magnitude of the change in Young's Modulus at ~900°C is correct given that the ~900°C (des) HTV data are at different doses (N.B. Modulus data are from this and prior work [19, 20]). At the higher irradiation temperatures [Tirr=1200°C(design), and = 1500°C (design)] the graphite may of transitioned into dimensional turnaround. The variation of the modulus as a function of the irradiation temperature is clear as in the previously considered grade H-451.

5.3 APPLICABILITY OF THE CREEP STRAIN CORRECTION

Comparisons or calculations of creep strains are sometimes made at the irradiation temperature, but can be made at room temperature (as was the case for the previous AGC experiments), i.e., the temperature that dimensions, and some physical and mechanical property determinations are made. If a comparison of the strains at the irradiation temperature is desired, two effects must be corrected for: the effect of creep irradiation on the thermal expansion coefficient and on the elastic strain during testing of the specimen caused by the applied stress. Firstly, the effect of creep irradiation on the thermal expansion behavior must be determined. The specimen will experience a thermal strain (expansion) when the specimen is heated to the irradiation temperature and subsequently cooled (shrinkage) to the measurement (ambient) temperature after irradiation and creep. The extent of thermal expansion depends upon the value of the specimen

coefficient of thermal expansion (CTE) which is altered by irradiation and creep; typically CTE increases at low neutron irradiation doses but is seen to fall at higher neutron irradiation doses due to irradiation alone. Compressive and tensile creep strains have been demonstrated to influence the thermal behavior in different directions, with compressive creep increasing the CTE and tensile creep reducing the CTE. The thermal strain correction is largely negated since it is made to both creep and control specimens and the irradiation creep strain is defined as the difference in dimensional change strain between the creep and control specimens. Since both creep and control specimens are irradiated to similar levels there in only minimal differences from the thermal strain correction. Secondly, there will be an elastic strain caused by the applied creep stress. The magnitude and sign of the strain depends upon the applied creep stress (i.e., compressive or tensile). Moreover, the irradiated and crept Young's modulus, E', is significantly increased (except at very large neutron doses and can be expected to be greater than E_0 (zero dose Young's Modulus). Moreover, the HTV data demonstrates the initial rise in E will be smaller at greater irradiation temperatures. The elastic strain correction only applies to the stressed specimen in the creep pair and is expected to be more significant (although no correction was applied in earlier lower temperature AGC experiments).

Example corrections are shown schematically in Figure 71 and Figure 72 for the creep specimens in tensile or compressive creep experiments, respectively. The measured room temperature creep strain is corrected to give the creep strain at the irradiation temperature by subtracting the **thermal strain** caused by (i) heating before creep irradiation and (ii) cooling after creep irradiation. Then the strain in the stressed specimen is further corrected by subtracting the **elastic strain** caused by applying the creep load.

When making the corrections special attention must be paid to the sign of the strain. The magnitude of the correction in comparison to the magnitude of the creep strain is significant. This is demonstrated by the creep strain (defined as the stressed specimens length change minus the unstressed specimens length change) being often a few percent of change whereas the value of the thermal strain correction is often an order of magnitude lower. Similarly, the elastic modulus correction due to irradiation and creep induced changes in elastic stiffness is very small in magnitude compared with the creep strain. For example, if the unirradiated modulus is ~10 GPa and the applied creep stress level is 10 MPa the induced elastic strain would be σ_c/E = 0.001. Upon irradiation at high temperature and to moderate dose (1-5 dpa) the elastic modulus may increase by up to a factor of 0.5 If we assume a factor of 50% increase in modulus due to irradiation damage and creep the net elastic modulus change would (~15 GPa) and the associated elastic strain correction for a 10 x MPa creep load would be [correction = $\sigma_c/ (E'-E_0)$]or (10 MPa/5 GPa), yielding a strain correction of 0.002 compared to a creep strain typically measured at 1-5 % change (creep strain typically = 0.01-0.05). Thus, the correction values are an order of magnitude less than the typical creep strain value and can be considered insignificant unless the creep strain is very small.

Moreover, making corrections from the room temperature measured strain and relating this measurement to creep strain at the irradiation temperature is further complicated by insufficient knowledge of the elevated temperature behavior of the elastic modulus. Typically the elastic modulus measured at room temperature is assumed to apply, but in reality the irradiation temperature modulus will not be the same as the room temperature modulus. Similarly, the mean CTE used to make the thermal strain correction to the creep strain is, of necessity, over a temperature interval in which the maximum temperature is less than the irradiation temperature (to avoid any thermal annealing of irradiation damage). This will introduce a potential error in the creep strain correction.

For these reasons a creep correction is often **not** applied to room temperature dimensional strain data and comparisons/analysis are performed on room temperature creep strain data. Therefore no creep strain correction is required in the high temperature creep capsules (AGC 5 & 6). However, all creep data sets should be reported with a clear statement as to whether the creep strain data are corrected for temperature and modulus effects.

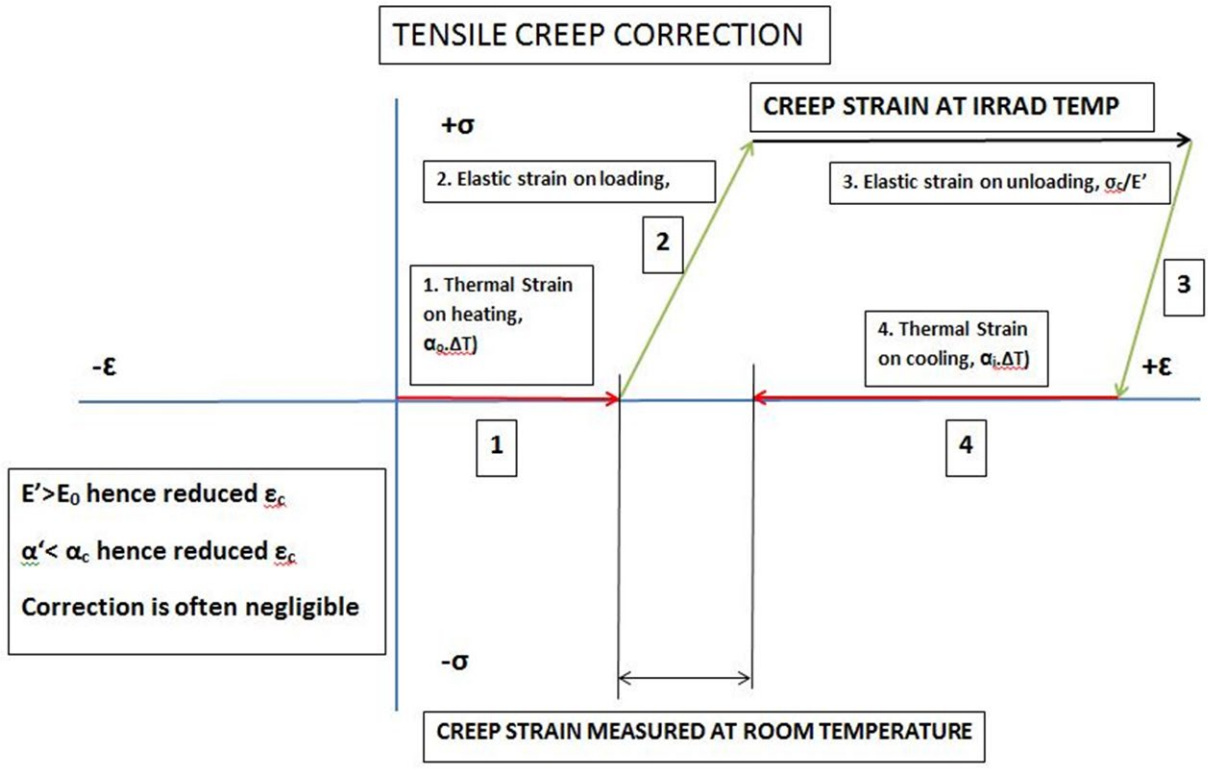

Figure 71 Schematic diagram of the creep stain corrections for a tensile creep experiment

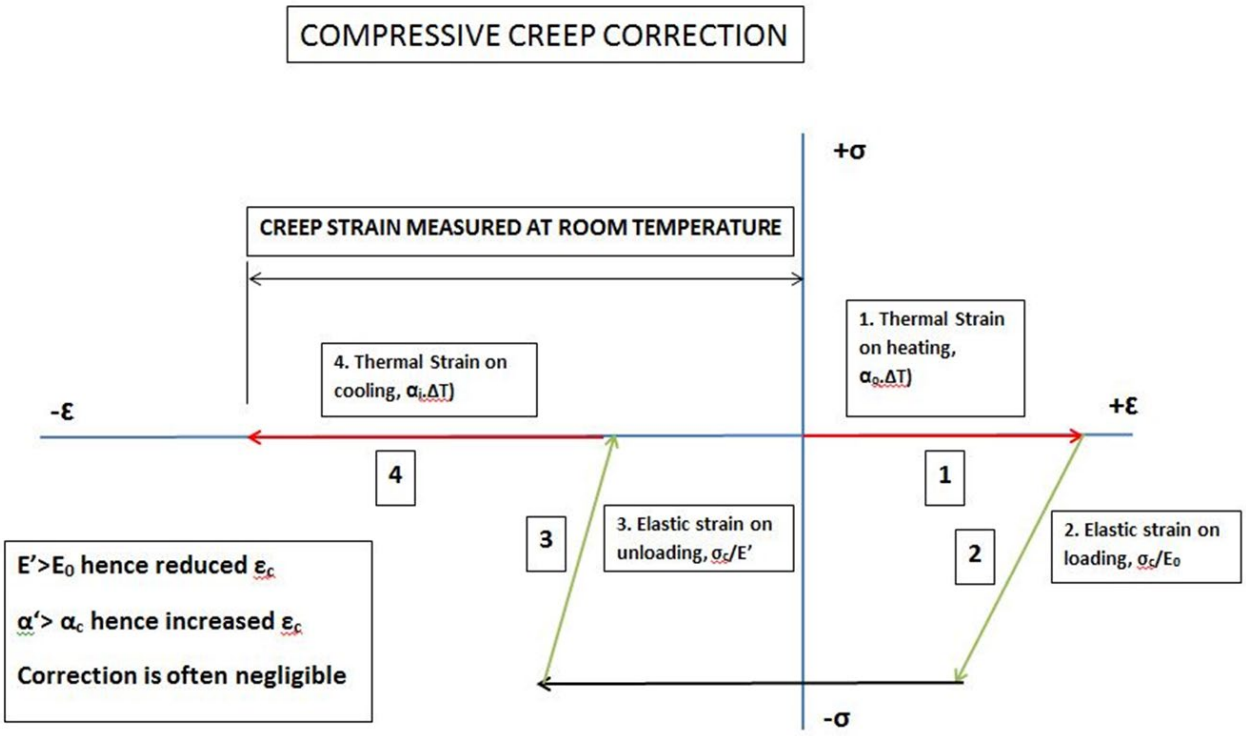

Figure 72 Schematic diagram of the creep stain corrections for a compressive creep experiment

6. CONCLUSIONS

The HTV irradiation experiment was very successful. All of the goals listed in Section 1 OBJECTIVES were met.

Firstly, six graphite grades used in the AGC graphite creep experiment were irradiated at high temperature in the HTV capsule. Indication from the temperature monitor analysis suggested that the three zones, whose design temperatures were 900, 1200 and 1500°C, actually ran at 840, 1189 and 1412°C. Although the actual irradiation temperatures were lower than the design irradiation temperatures (i.e., the graphite samples in the HTV capsule were a little cooler than anticipated (Table 10)) the range of the irradiation temperatures was sufficient to encompass the expected upper irradiation temperatures seen in the AGC experiment and thus meet the experimental objectives. The maximum dose obtained in the capsule 3.17 dpa with a capsule dose range from 1.49 to 3.17 dpa.

None of the grades examined here entered into a condition of net volume swelling at the temperatures and doses in the HTV capsule. However, grade 2114 WG at T_{irr} = 840°C (actual) did exhibit dimensional swelling. i.e., the graphite entered net positive dimensional growth (Figure 19 and Figure 43). Thus at T_{irr}=840°C (actual) depending upon the orientation of the grade 2114 specimen and the channel clearance (including potential net dimensional shrinkage of the channel bore diameter in the AGC graphite holder) could well cause dimensional interaction. Interference fits between the graphite specimen and graphite holder would at best complicate capsule disassembly and could cause fracture of the specimens or graphite body during irradiation.

The linear (Visco-Elastic) creep law should be applicable since the volume swelling is predominantly pre turn-around (signs of turn-around were only seen in certain grades at the highest irradiation temperatures). Hence the pore generation mechanism of higher dose (post turnaround) is not dominant.

Finally, the Young's modulus creep strain correction was explained and it was concluded that it is very small and is negligible at the dose and irradiation temperatures experienced in the AGC high temperature capsule(s).

Perhaps the most startling result was the behavior of grade 2114 (WG) at T_{irr}= 840°C (Actual). The turnaround into dimensional growth was explainable with our current understanding of graphite behavior, but was perhaps not expected at this relatively low dose (2.5-3.0 dpa). Some of the other grades showed evidence of dimensional turn-around but did not cross into positive net dimensional growth. The specimen hole generally grew dimensionally (inside diameter increases). Thus, applying the HTV specimen hole data to the AGC capsules it is expected that

the graphite body channel diameter to increase up to a dose of at least ~3 dpa. Similarly, the specimen's diameter will be in dimensional shrinkage up to at least ~3 dpa (with the possible exception of grade 2114). Hence the control specimens are unlikely to jam in the graphite body. The creep specimens (i.e., those specimens under a compressive stress) are however likely to exhibit larger dimensional changes due to the barreling (Poisson's stress) effect of loading and thus attaining a dimensional interference is much more likely. Close attention must be paid to the sizing of the gap between the specimen and the graphite body channels.

In addition to dimensional and volume changes the HTV capsule yielded data on high temperature irradiation effects on Young's modulus. The significant conclusions from the modulus data were:

1. The observed Young's Modulus data was agreement with previous data.
2. The magnitude of the Young's modulus change was greatest for the extruded grade H-451 and PCEA, but the largest fractional changes occurred in the isostatically pressed grades IG-110 and 2114 (fractional changed >60%).
3. At all of the temperatures examined the Young's modulus increased with neutron dose.
4. The increase in Young's modulus with neutron dose was smaller at higher irradiation temperatures.

7. DISTRIBUTION

Internal

Anne Campbell
Cristian Contescu
Keith Leonard
Weiju Ren
William Matisiak,

External

Mike Davenport
Larry Hull
William Windes

Sam Sham, ANL

Alice Caponiti DOE NE
William Corwin DOE NE

8. ACKNOWLEDGMENTS

This work is sponsored by the U.S. Department of Energy, Office of Nuclear Energy Science and Technology under contact DE-AC05-00OR22725 with Oak Ridge National Laboratories managed by UT-Battelle, LLC. This research [or, A portion of this research] at ORNL's High Flux Isotope Reactor was sponsored by the Scientific User Facilities Division, Office of Basic Energy Sciences, US Department of Energy. The author wishes to acknowledge the technical assistance of Ashli Clark.

APPENDIX A. DIMENSIONAL, VOLUME & DESITY DATA

Table 12 HTV capsule summary and pre- and post-irradiation examination mass, dimension and density data for design temperature, T_{irr}=900°C

HTV Capsule Summary and Pre- and Post-Irradiation Examination Mass, Dimensions and Density Data																														
HTV Capsule Summary												Pre-IE Data Summary							PIE Summary								(Irr-Unirr)/Unirr			
	Distance from HMP		Est. flux ratio[1]	Graphite grade	Irr. Temp		Spec. No.	Irr. Dose		Nominal Specimen OD		Graphite Grade	Spec. No.	Spec. Pre-IE Dims		Mass	Volume	Bulk Density g/cm³	Graphite Grade	Specimen Number	Mass	Volume	Bulk Density, g/cm3	Spec PIE Dims		ΔL/Lo	ΔD/Do	ΔDEN/DEN	ΔV/Vo
Position	in.	cm			Design Temp., °C	Actual Temp., °C		Est. dose[2] dpa	Actual dose[3], dpa	in.	mm			Mean Dia, m	Mean Length, m	g	cm³				g	cm³		Mean Length, m	Mean Dia, m	%	%	%	%
2-13	6.46	16.4084	0.75	NBG-17	900	840	AA41	2.38	2.50	0.4	10.16	NBG-17	AA41	0.010165	0.005356	0.77128	0.4177	1.847	NBG-17	AA41	0.7704	0.4145	1.858	0.005356	0.010145	0.000	-0.194	0.634	-0.744
4-30	1.67	4.2418	0.98	NBG-17	900	840	AA43	3.12	3.29	0.4	10.16	NBG-17	AA43	0.010173	0.00535	0.77074	0.4176	1.846	NBG-17	AA43	0.7700	0.4114	1.872	0.00534	0.010126	-0.178	-0.468	1.422	-1.497
4-36	0.41	1.0414	1.00	NBG-17	900	840	AA44	3.17	3.34	0.4	10.16	NBG-17	AA44	0.010167	0.005345	0.77285	0.4168	1.854	NBG-17	AA44	0.7716	0.4112	1.876	0.005337	0.010119	-0.137	-0.468	1.190	-1.336
2-14	6.25	15.875	0.76	NBG-18	900	840	BA41	2.43	2.56	0.4	10.16	NBG-18	BA41	0.010165	0.005343	0.77387	0.4165	1.858	NBG-18	BA41	0.7734	0.4134	1.871	0.005339	0.010147	-0.059	-0.175	0.670	-0.726
4-31	1.46	3.7084	0.99	NBG-18	900	840	BA44	3.14	3.30	0.4	10.16	NBG-18	BA44	0.010167	0.005338	0.76827	0.4161	1.847	NBG-18	BA44	0.7669	0.4102	1.870	0.005329	0.010119	-0.178	-0.468	1.253	-1.414
2-17	5.62	14.2748	0.81	H-451	900	840	CW41	2.57	2.71	0.4	10.16	H-451	CW41	0.010167	0.00534	0.71518	0.4163	1.718	H-451	CW41	0.7141	0.4130	1.729	0.005326	0.010153	-0.256	-0.137	0.650	-0.796
4-33	1.04	2.6416	0.99	H-451	900	840	CW43	3.16	3.33	0.4	10.16	H-451	CW43	0.010171	0.005349	0.70975	0.4173	1.701	H-451	CW43	0.7086	0.4128	1.716	0.005327	0.01015	-0.404	-0.206	0.924	-1.077
2-12	6.67	16.9418	0.73	PCEA	900	840	DW41	2.32	2.45	0.4	10.16	PCEA	DW41	0.010162	0.005346	0.74809	0.4165	1.796	PCEA	DW41	0.7471	0.4106	1.820	0.005327	0.010124	-0.368	-0.369	1.293	-1.407
2-18	5.41	13.7414	0.82	PCEA	900	840	DW42	2.62	2.76	0.4	10.16	PCEA	DW42	0.010166	0.005351	0.74811	0.4171	1.794	PCEA	DW42	0.747	0.4094	1.825	0.005321	0.010118	-0.570	-0.468	1.734	-1.850
4-29	1.88	4.7752	0.98	PCEA	900	840	DW44	3.11	3.28	0.4	10.16	PCEA	DW44	0.010164	0.005342	0.74724	0.4166	1.794	PCEA	DW44	0.7468	0.4045	1.846	0.005293	0.01008	-0.915	-0.831	2.924	-2.898
4-35	0.62	1.5748	1.00	PCEA	900	840	DW45	3.17	3.34	0.4	10.16	PCEA	DW45	0.010171	0.005343	0.75028	0.4169	1.800	PCEA	DW45	0.7497	0.4053	1.850	0.005296	0.010087	-0.891	-0.824	2.761	-2.762
2-10	7.09	18.0086	0.70	IG-110	900	840	EA41	2.21	2.33	0.4	10.16	IG-110	EA41	0.010164	0.005344	0.73465	0.4170	1.762	IG-110	EA41	0.7338	0.4118	1.782	0.005338	0.010138	-0.101	-0.256	1.136	-1.238
2-15	6.04	15.3416	0.78	IG-110	900	840	EA42	2.48	2.61	0.4	10.16	IG-110	EA42	0.010163	0.005345	0.73047	0.4171	1.751	IG-110	EA42	0.7300	0.4111	1.776	0.005337	0.010132	-0.160	-0.306	1.391	-1.435
4-32	1.25	3.175	0.99	IG-110	900	840	EA46	3.15	3.32	0.4	10.16	IG-110	EA46	0.010162	0.005339	0.72820	0.4164	1.749	IG-110	EA46	0.7274	0.4079	1.783	0.005319	0.010106	-0.375	-0.550	1.974	-2.043
2-11	6.88	17.4752	0.71	2114	900	840	TA41	2.27	2.39	0.4	10.16	2114	TA41	0.010154	0.005344	0.75563	0.4153	1.819	2114	TA41	0.755	0.4140	1.824	0.00535	0.010145	0.119	-0.088	0.236	-0.318
2-16	5.83	14.8082	0.79	2114	900	840	TA42	2.52	2.66	0.4	10.16	2114	TA42	0.010173	0.005348	0.75738	0.4180	1.812	2114	TA42	0.7569	0.4155	1.822	0.005356	0.010163	0.137	-0.106	0.532	-0.593
4-28	2.09	5.3086	0.97	2114	900	840	TA44	3.09	3.26	0.4	10.16	2114	TA44	0.01016	0.005345	0.75473	0.4166	1.811	2114	TA44	0.7542	0.4133	1.825	0.005351	0.010141	0.113	-0.188	0.749	-0.813
4-34	0.83	2.1082	1.00	2114	900	840	TA45	3.16	3.33	0.4	10.16	2114	TA45	0.010158	0.005342	0.75448	0.4159	1.814	2114	TA45	0.7544	0.4127	1.828	0.005349	0.010138	0.131	-0.194	0.771	-0.776
[1] Based on histiric flux distribution data for HFIR																											WG		
[2] Based on estimated HTV duration in HFIR																											AG		
[3] Based on actual HTV duration in HFIR cycles 460 and 461																													

Table 13 HTV capsule summary and pre-and post-irradiation examination mass, dimension and density data for design temperature, T_{irr}=1200°C

HTV Capsule Summary and Pre- and Post-Irradiation Examination Mass, Dimensions and Density Data																												
HTV Capsule Summary												Pre-IE Data Summary							PIE Data Summary							(Irr-Unirr)/Unirr			
	Distance from HMP		Est. flux	Graphite	Irr. Temp.			Irr. Dose		Nominal Specimen OD			Spec. Pre-IE Dims							Spec. PIE Dims									
Position	in.	cm	ratio[1]	grade	Design Temp., ºC	Actual Temp., ºC	Spec. No.	Est.Dose dpa[2]	Actual Dose[3], dpa	in.	mm	Spec. No.	Mean Dia, m	Mean Length, m	Mass g	Volume cm³	Bulk Density g/cm³	Young's Modulus (GPa) E=ρ.v²	0.9E	Spec. No.	Mean Dia, m	Mean Length, m	Mass g	Volume cm³	Bulk Density g/cm³	ΔL/Lo %	ΔD/Do %	ΔDEN/DEN %	ΔV/Vo %
8-66	-8.33	-21.1582	0.581429	NBG-17	1200		AA62	1.85	1.95	0.35	8.89	AA62	0.008886	0.005347	0.58097	0.3141	1.8498	14.05039	12.64535	AA62	0.008844	0.005334	0.5805	0.3096	1.8750	-0.249	-0.472	1.360	-1.422
7-56	-5.62	-14.2748	0.809475	NBG-17	1200		AA46	2.57	2.71	0.4	10.16	AA46	0.010168	0.005342	0.77016	0.4172	1.8461	14.28788	12.85909	AA46	0.010077	0.005308	0.7693	0.4047	1.9010	-0.630	-0.899	2.973	-2.995
3-24	3.54	8.9916	0.924406	NBG-17	1200		AA42	2.94	3.09	0.4	10.16	AA42	0.010162	0.005357	0.77138	0.4171	1.8493	14.46086	13.01478	AA42	0.010054	0.005312	0.7705	0.4041	1.9068	-0.830	-1.062	3.105	-3.122
8-72	-9.59	-24.3586	0.445226	NBG-18	1200		BA64	1.41	1.49	0.35	8.89	BA64	0.008894	0.005357	0.58644	0.3153	1.8601	15.26809	13.74128	BA64	0.008879	0.005352	0.5854	0.3131	1.8696	-0.089	-0.164	0.509	-0.683
8-67	-8.54	-21.6916	0.560059	NBG-18	1200		BA63	1.78	1.87	0.35	8.89	BA63	0.008893	0.005332	0.58373	0.3137	1.8605	15.17919	13.66127	BA63	0.008851	0.005313	0.5829	0.3088	1.8878	-0.363	-0.464	1.466	-1.585
7-62	-6.88	-17.4752	0.714467	NBG-18	1200		BA48	2.27	2.39	0.4	10.16	BA48	0.010164	0.005345	0.77642	0.4166	1.8635	15.72623	14.15361	BA48	0.010081	0.00531	0.7756	0.4045	1.9175	-0.665	-0.825	2.898	-2.919
7-57	-5.83	-14.8082	0.794971	NBG-18	1200		BA47	2.52	2.66	0.4	10.16	BA47	0.010166	0.005347	0.77699	0.4168	1.8644	15.63266	14.0694	BA47	0.010067	0.0053	0.7763	0.4034	1.9242	-0.879	-0.974	3.206	-3.192
3-20	4.38	11.1252	0.884275	NBG-18	1200		BA42	2.81	2.96	0.4	10.16	BA42	0.010163	0.005344	0.77405	0.4164	1.8588	15.62159	14.05943	BA42	0.010056	0.005296	0.7732	0.4022	1.9222	-0.909	-1.050	3.413	-3.406
3-25	3.33	8.4582	0.933109	NBG-18	1200		BA43	2.96	3.12	0.4	10.16	BA43	0.010161	0.005344	0.7715	0.4165	1.8522	15.2886	13.75974	BA43	0.010046	0.005299	0.7704	0.4013	1.9198	-0.844	-1.131	3.648	-3.657
7-63	-7.09	-18.0086	0.69677	H-451	1200		CW45	2.21	2.33	0.4	10.16	CW45	0.010168	0.005342	0.70996	0.4169	1.7027	13.22586	11.90328	CW45	0.010147	0.005327	0.7087	0.4120	1.7200	-0.267	-0.206	1.012	-1.178
3-27	2.91	7.3914	0.948918	H-451	1200		CW42	3.01	3.18	0.4	10.16	CW42	0.010162	0.005343	0.71543	0.4163	1.7186	13.26011	11.9341	CW42	0.01013	0.00532	0.7149	0.4093	1.7469	-0.428	-0.312	1.641	-1.687
8-70	-9.17	-23.2918	0.492755	PCEA	1200		DW63	1.56	1.65	0.35	8.89	DW63	0.008893	0.005353	0.5666	0.3153	1.7970	13.13884	11.82496	DW63	0.008862	0.005331	0.5657	0.3104	1.8226	-0.427	-0.343	1.426	-1.562
8-65	-8.12	-20.6248	0.602267	PCEA	1200		DW62	1.91	2.02	0.35	8.89	DW62	0.008891	0.00535	0.56627	0.3149	1.7980	13.12698	11.81428	DW62	0.008844	0.005324	0.5654	0.3088	1.8308	-0.481	-0.528	1.823	-1.941
7-60	-6.46	-16.4084	0.748265	PCEA	1200		DW49	2.38	2.50	0.4	10.16	DW49	0.010161	0.005343	0.74965	0.4166	1.7993	13.64687	12.28218	DW49	0.010069	0.005294	0.7491	0.4033	1.8575	-0.909	-0.900	3.236	-3.206
7-55	-5.41	-13.7414	0.823448	PCEA	1200		DW48	2.62	2.76	0.4	10.16	DW48	0.010173	0.005342	0.75054	0.4176	1.7972	13.63078	12.26771	DW48	0.010077	0.005289	0.7493	0.4036	1.8563	-0.987	-0.936	3.291	-3.346
3-23	3.75	9.525	0.915172	PCEA	1200		DW43	2.91	3.06	0.4	10.16	DW43	0.010161	0.005355	0.7486	0.4170	1.7950	14.25461	12.82915	DW43	0.010049	0.00529	0.7483	0.4018	1.8623	-1.215	-1.106	3.749	-3.652
8-71	-9.38	-23.8252	0.469256	IG-110	1200		EA64	1.49	1.57	0.35	8.89	EA64	0.008901	0.005346	0.55009	0.3153	1.7446	9.675859	8.708274	EA64	0.008884	0.005341	0.5491	0.3126	1.7563	-0.083	-0.193	0.667	-0.841
8-68	-8.75	-22.225	0.538156	IG-110	1200		EA63	1.71	1.80	0.35	8.89	EA63	0.008881	0.005353	0.55216	0.3143	1.7570	9.170769	8.253692	EA63	0.008861	0.005344	0.5511	0.3113	1.7705	-0.166	-0.222	0.773	-0.958
7-61	-6.67	-16.9418	0.731632	IG-110	1200		EA49	2.32	2.45	0.4	10.16	EA49	0.010164	0.005344	0.72879	0.4162	1.7510	9.851574	8.866417	EA49	0.010115	0.005317	0.7284	0.4092	1.7802	-0.505	-0.481	1.672	-1.697
7-58	-6.04	-15.3416	0.779934	IG-110	1200		EA48	2.48	2.61	0.4	10.16	EA48	0.010157	0.005341	0.72923	0.4164	1.7512	9.953103	8.957793	EA48	0.010095	0.005314	0.728	0.4057	1.7946	-0.511	-0.619	2.474	-2.579
3-19	4.59	11.6586	0.872912	IG-110	1200		EA43	2.77	2.92	0.4	10.16	EA43	0.010161	0.005345	0.7261	0.4169	1.7415	9.405673	8.465105	EA43	0.010099	0.005318	0.7247	0.4067	1.7818	-0.511	-0.612	2.313	-2.449
3-21	4.17	10.5918	0.895106	IG-110	1200		EA44	2.84	3.00	0.4	10.16	EA44	0.010162	0.005335	0.72617	0.4159	1.7461	9.733231	8.759908	EA44	0.010083	0.005304	0.7254	0.4050	1.7912	-0.577	-0.781	2.585	-2.623
3-26	3.12	7.9248	0.94128	IG-110	1200		EA45	2.99	3.15	0.4	10.16	EA45	0.010164	0.005341	0.72948	0.4161	1.7531	9.788972	8.810074	EA45	0.010099	0.005312	0.7289	0.4076	1.7881	-0.547	-0.643	1.996	-2.035
8-69	-8.96	-22.7584	0.515722	2114	1200		TA64	1.64	1.73	0.35	8.89	TA64	0.008892	0.005338	0.57003	0.3141	1.8147	11.08034	9.972305	TA64	0.00887	0.00533	0.5696	0.3112	1.8301	-0.149	-0.250	0.847	-0.915
8-64	-7.91	-20.0914	0.622574	2114	1200		TA63	1.98	2.08	0.35	8.89	TA63	0.008901	0.005346	0.57284	0.3154	1.8164	11.09348	9.984135	TA63	0.008875	0.00534	0.5712	0.3120	1.8309	-0.119	-0.297	0.800	-1.077
7-59	-6.25	-15.875	0.764365	2114	1200		TA48	2.43	2.56	0.4	10.16	TA48	0.010161	0.005345	0.75598	0.4165	1.8149	11.01014	9.909124	TA48	0.010102	0.005323	0.7554	0.4079	1.8518	-0.422	-0.581	2.029	-2.064
3-22	3.96	10.0584	0.905405	2114	1200		TA43	2.88	3.03	0.4	10.16	TA43	0.01017	0.005344	0.75715	0.4176	1.8132	10.92811	9.835301	TA43	0.010098	0.00532	0.7569	0.4075	1.8574	-0.463	-0.706	2.439	-2.413

[1] Based on histiric flux distribution data for HFIR

[2] Based on estimated HTV duration in HFIR

[3] Based on actual HTV duration in HFIR cycles 460 and 461

WG

AG

Table 14 HTV capsule summary and pre- and post-irradiation examination mass, dimension and density data for design temperature, T_{irr}=1500°C

HTV Capsule Summary and Pre- and Post-Irradiation Examination Mass, Dimensions and Density Data																															
Capsule Layout												Pre-IE Data Summary									PIE Data Summary							(Irr-UnIrr)/UnIrr			
	Distance from HMP				Irr. Temp			Irr. Dose		Nominal Specimen OD			Spec. Pre-IE Dims		Mass	Volume	Bulk Density	Young's Modulus (GPa)				Spec. Pre-IE Dims		Mass	Volume	Bulk Density	ΔL/Lo	ΔD/Do	ΔDEN/DEN	ΔV/Vo
Position	in.	cm	Est. flux ratio[1]	Graphite grade	Design Temp., °C	Actual Temp., °C	Spec. No.	Est. Fluence dpa[2]	Actual Dose[3], dpa	in.	mm	Spec. No.	Mean Dia, m	Mean Length, m	g	cm^3	g/cm^3	E=ρ.v[2]	0.9E	Spec. No.	Mean Dia, m	Mean Length, m	g	cm^3	g/cm^3	%	%	%	%
1-8	8.12	20.62	0.602	NBG-17	1500		AA51	1.91	2.02	0.300	7.62	AA51	0.007629	0.005351	0.4177	0.2271	1.839	13.80	12.42	AA51	0.007534	0.005294	0.4169	0.2180	1.913	-1.068	-1.249	3.985	-4.019
6-51	-3.96	-10.06	0.905	NBG-17	1500		AA61	2.88	3.03	0.350	8.89	AA61	0.008897	0.005363	0.5833	0.3161	1.845	13.96	12.56	AA61	0.008711	0.005278	0.5822	0.2973	1.958	-1.581	-2.091	6.126	-5.952
5-41	-1.25	-3.18	0.991	NBG-17	1500		AA45	3.15	3.32	0.400	10.16	AA45	0.010163	0.005345	0.7708	0.4162	1.852	14.50	13.05	AA45	0.009948	0.005268	0.7699	0.3926	1.961	-1.443	-2.112	5.906	-5.690
1-3	9.17	23.29	0.493	NBG-18	1500		BA51	1.56	1.65	0.300	7.62	BA51	0.007633	0.005358	0.4204	0.2281	1.843	14.80	13.32	BA51	0.007556	0.00531	0.4192	0.2198	1.907	-0.895	-1.007	3.470	-3.620
1-9	7.91	20.09	0.623	NBG-18	1500		BA52	1.98	2.08	0.300	7.62	BA52	0.007622	0.005344	0.4191	0.2268	1.848	14.78	13.30	BA52	0.007527	0.005282	0.4177	0.2167	1.928	-1.159	-1.250	4.312	-4.452
6-52	-4.17	-10.59	0.895	NBG-18	1500		BA66	2.84	3.00	0.350	8.89	BA66	0.008887	0.005352	0.5851	0.3148	1.859	15.07	13.56	BA66	0.008698	0.005251	0.5839	0.2945	1.982	-1.881	-2.122	6.640	-6.423
6-47	-3.12	-7.92	0.941	NBG-18	1500		BA65	2.99	3.15	0.350	8.89	BA65	0.008891	0.005354	0.5870	0.3152	1.862	15.37	13.83	BA65	0.008696	0.005255	0.586	0.2952	1.985	-1.856	-2.200	6.630	-6.373
5-42	-1.46	-3.71	0.987	NBG-18	1500		BA46	3.14	3.30	0.400	10.16	BA46	0.010172	0.005347	0.7797	0.4176	1.867	15.32	13.79	BA46	0.009951	0.005253	0.7789	0.3912	1.991	-1.758	-2.172	6.635	-6.320
5-37	-0.41	-1.04	0.999	NBG-18	1500		BA45	3.17	3.34	0.400	10.16	BA45	0.010171	0.005344	0.7772	0.4169	1.864	15.12	13.61	BA45	0.009957	0.005254	0.7768	0.3914	1.985	-1.693	-2.110	6.459	-6.120
1-6	8.54	21.69	0.560	H-451	1500		CW51	1.78	1.87	0.300	7.62	CW51	0.007625	0.005361	0.3831	0.2276	1.683	11.97	10.78	CW51	0.007558	0.0053	0.382	0.2179	1.753	-1.131	-0.883	4.160	-4.262
6-53	-4.38	-11.13	0.884	H-451	1500		CW61	2.81	2.96	0.350	8.89	CW61	0.008902	0.00535	0.5418	0.3162	1.714	12.77	11.49	CW61	0.008743	0.00523	0.5407	0.2968	1.822	-2.243	-1.790	6.306	-6.127
5-43	-1.67	-4.24	0.983	H-451	1500		CW44	3.12	3.29	0.400	10.16	CW44	0.01016	0.005341	0.7100	0.4158	1.708	13.22	11.89	CW44	0.009975	0.005222	0.7089	0.3902	1.817	-2.241	-1.819	6.385	-6.150
1-1	9.59	24.36	0.445	PCEA	1500		DW51	1.41	1.49	0.300	7.62	DW51	0.007633	0.005354	0.4072	0.2275	1.790	12.57	11.31	DW51	0.007567	0.005303	0.4062	0.2203	1.844	-0.955	-0.857	3.011	-3.164
1-7	8.33	21.16	0.581	PCEA	1500		DW52	1.85	1.95	0.300	7.62	DW52	0.007625	0.005344	0.4051	0.2268	1.786	13.10	11.79	DW52	0.007505	0.00526	0.4042	0.2147	1.882	-1.586	-1.574	5.383	-5.317
6-50	-3.75	-9.53	0.915	PCEA	1500		DW61	2.91	3.06	0.350	8.89	DW61	0.008896	0.005346	0.5670	0.3148	1.801	12.99	11.69	DW61	0.008641	0.005178	0.5663	0.2874	1.971	-3.142	-2.869	9.419	-8.723
5-45	-2.09	-5.31	0.974	PCEA	1500		DW47	3.09	3.26	0.400	10.16	DW47	0.010171	0.005346	0.7529	0.4177	1.802	13.69	12.32	DW47	0.009889	0.005191	0.7512	0.3810	1.972	-2.898	-2.772	9.379	-8.775
5-40	-1.04	-2.64	0.993	PCEA	1500		DW46	3.16	3.33	0.400	10.16	DW46	0.01017	0.005342	0.7508	0.4173	1.799	13.64	12.28	DW46	0.009869	0.005176	0.7502	0.3791	1.979	-3.109	-2.960	9.994	-9.152
1-2	9.38	23.83	0.469	IG-110	1500		EA51	1.49	1.57	0.300	7.62	EA51	0.007633	0.005341	0.3959	0.2272	1.743	9.48	8.53	EA51	0.007556	0.005296	0.3952	0.2194	1.801	-0.844	-1.007	3.380	-3.430
1-4	8.96	22.76	0.516	IG-110	1500		EA52	1.64	1.73	0.300	7.62	EA52	0.007624	0.005348	0.3981	0.2272	1.752	9.50	8.55	EA52	0.00753	0.005293	0.3972	0.2172	1.829	-1.033	-1.233	4.401	-4.422
6-48	-3.33	-8.46	0.933	IG-110	1500		EA62	2.96	3.12	0.350	8.89	EA62	0.008889	0.005339	0.5475	0.3138	1.745	9.68	8.71	EA62	0.008666	0.005237	0.5467	0.2923	1.870	-1.903	-2.508	7.200	-6.856
6-46	-2.91	-7.39	0.949	IG-110	1500		EA61	3.01	3.18	0.350	8.89	EA61	0.0089	0.00534	0.5522	0.3149	1.754	9.21	8.29	EA61	0.008669	0.005251	0.5511	0.2931	1.880	-1.659	-2.590	7.209	-6.913
5-38	-0.62	-1.57	0.998	IG-110	1500		EA47	3.17	3.34	0.400	10.16	EA47	0.010161	0.005337	0.7300	0.4159	1.755	9.97	8.97	EA47	0.00992	0.005228	0.7295	0.3861	1.890	-2.058	-2.375	7.662	-7.174
1-5	8.75	22.23	0.538	2114	1500		TA51	1.71	1.80	0.300	7.62	TA51	0.007635	0.005352	0.4125	0.2279	1.810	10.81	9.73	TA51	0.007545	0.005308	0.4118	0.2196	1.876	-0.819	-1.181	3.617	-3.664
6-54	-4.59	-11.66	0.873	2114	1500		TA62	2.77	2.92	0.350	8.89	TA62	0.00889	0.005354	0.5722	0.3150	1.816	10.96	9.86	TA62	0.00874	0.005292	0.5717	0.2996	1.908	-1.158	-1.687	5.063	-4.899
6-49	-3.54	-8.99	0.924	2114	1500		TA61	2.94	3.09	0.350	8.89	TA61	0.008896	0.005356	0.5730	0.3156	1.816	10.77	9.69	TA61	0.008752	0.005311	0.5726	0.3016	1.899	-0.830	-1.627	4.575	-4.445
5-44	-1.88	-4.78	0.979	2114	1500		TA47	3.11	3.28	0.400	10.16	TA47	0.010162	0.005338	0.7544	0.4163	1.812	11.06	9.96	TA47	0.010003	0.005282	0.7542	0.3968	1.900	-1.065	-1.568	4.874	-4.673
5-39	-0.83	-2.11	0.996	2114	1500		TA46	3.16	3.33	0.400	10.16	TA46	0.010166	0.005345	0.7577	0.4164	1.819	11.15	10.03	TA46	0.010001	0.005298	0.757	0.3991	1.897	-0.873	-1.624	4.259	-4.172

[1] Based on histiric flux distribution data for HFIR

[2] Based on estimated HTV duration in HFIR

[3] Based on actual HTV duration in HFIR cycles 460 and 461

WG

AG

Table 15 HTV capsule summary and pre- and post-irradiation examination specimen inner hole diameter growth data for design temperature, T_{irr}=900°C

HTV Capsule Summary, Pre-IE and PIE Specimen Inner Hole Diameter Data																			
Capsule Summary											PreIE				PIE			Hole Diameter (ID) Dimensional change, mm	Hole Diameter (ID) Dimensional change, %
	Distance from HMP		Est. flux ratio[1]	Graphite grade	Design Temp., °C	Spec. No.	Est. dose dpa[2]	Actual dose[3], dpa	Nominal Specimen OD		Graphite Grade	Specimen Number	Hole Diameter, in. Allowable:0.0815-.0820		Specimen Number	Hole Diameter, in.			
Position	in.	cm							in.	mm			H1, ins	H2, ins		H1,ins	H2, ins		
2-13	6.46	16.4084	0.75	NBG-17	900	AA41	2.38	2.50	0.4	10.16	NBG-17	AA41	0.07920	0.07910	AA41	0.08255	0.08225	0.083	4.11
4-30	1.67	4.2418	0.98	NBG-17	900	AA43	3.12	3.29	0.4	10.16	NBG-17	AA43	0.07975	0.07970	AA43	0.08320	0.08285	0.084	4.14
4-36	0.41	1.0414	1.00	NBG-17	900	AA44	3.17	3.34	0.4	10.16	NBG-17	AA44	0.07975	0.07935	AA44	0.08170	0.08175	0.055	2.73
2-14	6.25	15.875	0.76	NBG-18	900	BA41	2.43	2.56	0.4	10.16	NBG-18	BA41	0.07960	0.07945	BA41	0.08245	0.08235	0.073	3.62
4-31	1.46	3.7084	0.99	NBG-18	900	BA44	3.14	3.30	0.4	10.16	NBG-18	BA44	0.08010	0.07995	BA44	0.08255	0.08250	0.064	3.12
2-17	5.62	14.2748	0.81	H-451	900	CW41	2.57	2.71	0.4	10.16	H-451	CW41	0.07975	0.07985	CW41	0.08225	0.08220	0.062	3.04
4-33	1.04	2.6416	0.99	H-451	900	CW43	3.16	3.33	0.4	10.16	H-451	CW43	0.07980	0.07970	CW43	0.08220	0.08200	0.060	2.95
2-12	6.67	16.9418	0.73	PCEA	900	DW41	2.32	2.45	0.4	10.16	PCEA	DW41	0.07960	0.07955	DW41	0.08225	0.08215	0.067	3.30
2-18	5.41	13.7414	0.82	PCEA	900	DW42	2.62	2.76	0.4	10.16	PCEA	DW42	0.07975	0.07975	DW42	0.08270	0.08275	0.076	3.73
4-29	1.88	4.7752	0.98	PCEA	900	DW44	3.11	3.28	0.4	10.16	PCEA	DW44	0.07915	0.07890	DW44	0.08145	0.08195	0.068	3.39
4-35	0.62	1.5748	1.00	PCEA	900	DW45	3.17	3.34	0.4	10.16	PCEA	DW45	0.08000	0.07970	DW45	0.08170	0.08140	0.043	2.13
2-10	7.09	18.0086	0.70	IG-110	900	EA41	2.21	2.33	0.4	10.16	IG-110	EA41	0.07810	0.07845	EA41	0.08405	0.08400	0.146	7.35
2-15	6.04	15.3416	0.78	IG-110	900	EA42	2.48	2.61	0.4	10.16	IG-110	EA42	0.07825	0.07820	EA42	0.08420	0.08440	0.154	7.77
4-32	1.25	3.175	0.99	IG-110	900	EA46	3.15	3.32	0.4	10.16	IG-110	EA46	0.07865	0.07825	EA46	0.08350	0.08355	0.129	6.47
2-11	6.88	17.4752	0.71	2114	900	TA41	2.27	2.39	0.4	10.16	2114	TA41	0.08005	0.08015	TA41	0.08240	0.08260	0.061	3.00
2-16	5.83	14.8082	0.79	2114	900	TA42	2.52	2.66	0.4	10.16	2114	TA42	0.07880	0.07860	TA42	0.08350	0.08355	0.123	6.13
4-28	2.09	5.3086	0.97	2114	900	TA44	3.09	3.26	0.4	10.16	2114	TA44	0.07850	0.07865	TA44	0.08360	0.08370	0.129	6.46
4-34	0.83	2.1082	1.00	2114	900	TA45	3.16	3.33	0.4	10.16	2114	TA45	0.07935	0.07935	TA45	0.08405	0.08410	0.120	5.95
																			WG
																			AG

Table 16 HTV capsule summary and pre- and post-irradiation examination specimen inner hole diameter growth data for design temperature, T_{irr}=1200°C

HTV Capsule Summary, Pre-IE and PIE Specimen Inner Hole Diameter Data																			
Capsule Summary											Pre-IE				PIE				
	Distance from HMP		Est. flux	Graphite	Design		Est. Fluence	Actual Dose[3],	Nominal Specimen OD		Graphite	Specimen	Hole Diameter, in. Allowable:0.0815-.0820		Specimen	Hole Diameter, in.		Hole Diameter Dimensional	Hole Diameter (ID) Dimensional
Position	in.	cm	ratio[1]	grade	Temp., °C	Spec. No.	dpa[2]	dpa	in.	mm	Grade	Number	H1	H2	Number	H1	H2	change, mm	change, %
1-8	8.12	20.62	0.602	NBG-17	1500	AA51	1.91	2.02	0.300	7.62	NBG-17	AA51	0.08045	0.08030	AA51	0.08235	0.08160	0.041	1.99
6-51	-3.96	-10.06	0.905	NBG-17	1500	AA61	2.88	3.03	0.350	8.89	NBG-17	AA61	0.07975	0.07985	AA61	0.08035	0.08035	0.014	0.69
5-41	-1.25	-3.18	0.991	NBG-17	1500	AA45	3.15	3.32	0.400	10.16	NBG-17	AA45	0.08010	0.07985	AA45	0.07950	0.07960	-0.011	-0.53
1-3	9.17	23.29	0.493	NBG-18	1500	BA51	1.56	1.65	0.300	7.62	NBG-18	BA51	0.07930	0.07935	BA51	0.08235	0.08250	0.079	3.91
1-9	7.91	20.09	0.623	NBG-18	1500	BA52	1.98	2.08	0.300	7.62	NBG-18	BA52	0.07935	0.07915	BA52	0.08270	0.08265	0.087	4.32
6-52	-4.17	-10.59	0.895	NBG-18	1500	BA66	2.84	3.00	0.350	8.89	NBG-18	BA66	0.07965	0.07970	BA66	0.08110	0.08115	0.037	1.82
6-47	-3.12	-7.92	0.941	NBG-18	1500	BA65	2.99	3.15	0.350	8.89	NBG-18	BA65	0.07975	0.07950	BA65	0.07965	0.07980	0.003	0.13
5-42	-1.46	-3.71	0.987	NBG-18	1500	BA46	3.14	3.30	0.400	10.16	NBG-18	BA46	0.07935	0.07910	BA46	0.08025	0.08150	0.042	2.08
5-37	-0.41	-1.04	0.999	NBG-18	1500	BA45	3.17	3.34	0.400	10.16	NBG-18	BA45	0.07995	0.07990	BA45	0.08135	0.08145	0.037	1.85
1-6	8.54	21.69	0.560	H-451	1500	CW51	1.78	1.87	0.300	7.62	H-451	CW51	0.07950	0.07980	CW51	0.08625	0.08595	0.164	8.10
6-53	-4.38	-11.13	0.884	H-451	1500	CW61	2.81	2.96	0.350	8.89	H-451	CW61	0.07870	0.07865	CW61	0.08050	0.08030	0.044	2.19
5-43	-1.67	-4.24	0.983	H-451	1500	CW44	3.12	3.29	0.400	10.16	H-451	CW44	0.07980	0.07975	CW44	0.08210	0.08210	0.059	2.91
1-1	9.59	24.36	0.445	PCEA	1500	DW51	1.41	1.49	0.300	7.62	PCEA	DW51	0.08030	0.08025	DW51	0.08235	0.08225	0.051	2.52
1-7	8.33	21.16	0.581	PCEA	1500	DW52	1.85	1.95	0.300	7.62	PCEA	DW52	0.07985	0.07980	DW52	0.08210	0.08200	0.057	2.79
6-50	-3.75	-9.53	0.915	PCEA	1500	DW61	2.91	3.06	0.350	8.89	PCEA	DW61	0.08030	0.08035	DW61	0.07855	0.07905	-0.039	-1.90
5-45	-2.09	-5.31	0.974	PCEA	1500	DW47	3.09	3.26	0.400	10.16	PCEA	DW47	0.07845	0.07855	DW47	0.08190	0.08215	0.090	4.49
5-40	-1.04	-2.64	0.993	PCEA	1500	DW46	3.16	3.33	0.400	10.16	PCEA	DW46	0.07805	0.07850	DW46	0.08010	0.07985	0.043	2.17
1-2	9.38	23.83	0.469	IG-110	1500	EA51	1.49	1.57	0.300	7.62	IG-110	EA51	0.07980	0.07975	EA51	0.08220	0.08205	0.060	2.95
1-4	8.96	22.76	0.516	IG-110	1500	EA52	1.64	1.73	0.300	7.62	IG-110	EA52	0.07890	0.07900	EA52	0.08330	0.08280	0.104	5.19
6-48	-3.33	-8.46	0.933	IG-110	1500	EA62	2.96	3.12	0.350	8.89	IG-110	EA62	0.08030	0.08040	EA62	0.07900	0.07910	-0.033	-1.62
6-46	-2.91	-7.39	0.949	IG-110	1500	EA61	3.01	3.18	0.350	8.89	IG-110	EA61	0.08000	0.07995	EA61	0.07975	0.07945	-0.010	-0.47
5-38	-0.62	-1.57	0.998	IG-110	1500	EA47	3.17	3.34	0.400	10.16	IG-110	EA47	0.07915	0.07915	EA47	0.08255	0.08220	0.082	4.07
1-5	8.75	22.23	0.538	2114	1500	TA51	1.71	1.80	0.300	7.62	2114	TA51	0.08030	0.08040	TA51	0.08135	0.08125	0.024	1.18
6-54	-4.59	-11.66	0.873	2114	1500	TA62	2.77	2.92	0.350	8.89	2114	TA62	0.07985	0.07985	TA62	0.08165	0.08185	0.048	2.38
6-49	-3.54	-8.99	0.924	2114	1500	TA61	2.94	3.09	0.350	8.89	2114	TA61	0.07985	0.07995	TA61	0.08160	0.08165	0.044	2.16
5-44	-1.88	-4.78	0.979	2114	1500	TA47	3.11	3.28	0.400	10.16	2114	TA47	0.07850	0.07850	TA47	0.08260	0.08225	0.100	5.00
5-39	-0.83	-2.11	0.996	2114	1500	TA46	3.16	3.33	0.400	10.16	2114	TA46	0.08020	0.08030	TA46	0.08000	0.07995	-0.007	-0.34
																			WG
																			AG

Table 17 HTV capsule summary and pre- and post-irradiation examination specimen inner hole diameter growth data for design temperature, T_{irr}=1500°C

HTV Capsule Summary, Pre-IE and PIE Specimen Inner Hole Diameter Data																			
Capsule Summary											Pre-IE				PIE				
	Distance from HMP		Est. flux	Graphite	Design		Est. Fluence	Actual Dose[3],	Nominal Specimen OD		Graphite	Specimen	Hole Diameter, in. Allowable:0.0815-.0820		Specimen	Hole Diameter, in.		Hole Diameter Dimensional	Hole Diameter (ID) Dimensional
Position	in.	cm	ratio[1]	grade	Temp., °C	Spec. No.	dpa[2]	dpa	in.	mm	Grade	Number	H1	H2	Number	H1	H2	change, mm	change, %
1-8	8.12	20.62	0.602	NBG-17	1500	AA51	1.91	2.02	0.300	7.62	NBG-17	AA51	0.08045	0.08030	AA51	0.08235	0.08160	0.041	1.99
6-51	-3.96	-10.06	0.905	NBG-17	1500	AA61	2.88	3.03	0.350	8.89	NBG-17	AA61	0.07975	0.07985	AA61	0.08035	0.08035	0.014	0.69
5-41	-1.25	-3.18	0.991	NBG-17	1500	AA45	3.15	3.32	0.400	10.16	NBG-17	AA45	0.08010	0.07985	AA45	0.07950	0.07960	-0.011	-0.53
1-3	9.17	23.29	0.493	NBG-18	1500	BA51	1.56	1.65	0.300	7.62	NBG-18	BA51	0.07930	0.07935	BA51	0.08235	0.08250	0.079	3.91
1-9	7.91	20.09	0.623	NBG-18	1500	BA52	1.98	2.08	0.300	7.62	NBG-18	BA52	0.07935	0.07915	BA52	0.08270	0.08265	0.087	4.32
6-52	-4.17	-10.59	0.895	NBG-18	1500	BA66	2.84	3.00	0.350	8.89	NBG-18	BA66	0.07965	0.07970	BA66	0.08110	0.08115	0.037	1.82
6-47	-3.12	-7.92	0.941	NBG-18	1500	BA65	2.99	3.15	0.350	8.89	NBG-18	BA65	0.07975	0.07950	BA65	0.07965	0.07980	0.003	0.13
5-42	-1.46	-3.71	0.987	NBG-18	1500	BA46	3.14	3.30	0.400	10.16	NBG-18	BA46	0.07935	0.07910	BA46	0.08025	0.08150	0.042	2.08
5-37	-0.41	-1.04	0.999	NBG-18	1500	BA45	3.17	3.34	0.400	10.16	NBG-18	BA45	0.07995	0.07990	BA45	0.08135	0.08145	0.037	1.85
1-6	8.54	21.69	0.560	H-451	1500	CW51	1.78	1.87	0.300	7.62	H-451	CW51	0.07950	0.07980	CW51	0.08625	0.08595	0.164	8.10
6-53	-4.38	-11.13	0.884	H-451	1500	CW61	2.81	2.96	0.350	8.89	H-451	CW61	0.07870	0.07865	CW61	0.08050	0.08030	0.044	2.19
5-43	-1.67	-4.24	0.983	H-451	1500	CW44	3.12	3.29	0.400	10.16	H-451	CW44	0.07980	0.07975	CW44	0.08210	0.08210	0.059	2.91
1-1	9.59	24.36	0.445	PCEA	1500	DW51	1.41	1.49	0.300	7.62	PCEA	DW51	0.08030	0.08025	DW51	0.08235	0.08225	0.051	2.52
1-7	8.33	21.16	0.581	PCEA	1500	DW52	1.85	1.95	0.300	7.62	PCEA	DW52	0.07985	0.07980	DW52	0.08210	0.08200	0.057	2.79
6-50	-3.75	-9.53	0.915	PCEA	1500	DW61	2.91	3.06	0.350	8.89	PCEA	DW61	0.08030	0.08035	DW61	0.07855	0.07905	-0.039	-1.90
5-45	-2.09	-5.31	0.974	PCEA	1500	DW47	3.09	3.26	0.400	10.16	PCEA	DW47	0.07845	0.07855	DW47	0.08190	0.08215	0.090	4.49
5-40	-1.04	-2.64	0.993	PCEA	1500	DW46	3.16	3.33	0.400	10.16	PCEA	DW46	0.07805	0.07850	DW46	0.08010	0.07985	0.043	2.17
1-2	9.38	23.83	0.469	IG-110	1500	EA51	1.49	1.57	0.300	7.62	IG-110	EA51	0.07980	0.07975	EA51	0.08220	0.08205	0.060	2.95
1-4	8.96	22.76	0.516	IG-110	1500	EA52	1.64	1.73	0.300	7.62	IG-110	EA52	0.07890	0.07900	EA52	0.08330	0.08280	0.104	5.19
6-48	-3.33	-8.46	0.933	IG-110	1500	EA62	2.96	3.12	0.350	8.89	IG-110	EA62	0.08030	0.08040	EA62	0.07900	0.07910	-0.033	-1.62
6-46	-2.91	-7.39	0.949	IG-110	1500	EA61	3.01	3.18	0.350	8.89	IG-110	EA61	0.08000	0.07995	EA61	0.07975	0.07945	-0.010	-0.47
5-38	-0.62	-1.57	0.998	IG-110	1500	EA47	3.17	3.34	0.400	10.16	IG-110	EA47	0.07915	0.07915	EA47	0.08255	0.08220	0.082	4.07
1-5	8.75	22.23	0.538	2114	1500	TA51	1.71	1.80	0.300	7.62	2114	TA51	0.08030	0.08040	TA51	0.08135	0.08125	0.024	1.18
6-54	-4.59	-11.66	0.873	2114	1500	TA62	2.77	2.92	0.350	8.89	2114	TA62	0.07985	0.07985	TA62	0.08165	0.08185	0.048	2.38
6-49	-3.54	-8.99	0.924	2114	1500	TA61	2.94	3.09	0.350	8.89	2114	TA61	0.07985	0.07995	TA61	0.08160	0.08165	0.044	2.16
5-44	-1.88	-4.78	0.979	2114	1500	TA47	3.11	3.28	0.400	10.16	2114	TA47	0.07850	0.07850	TA47	0.08260	0.08225	0.100	5.00
5-39	-0.83	-2.11	0.996	2114	1500	TA46	3.16	3.33	0.400	10.16	2114	TA46	0.08020	0.08030	TA46	0.08000	0.07995	-0.007	-0.34
																			WG
																			AG

APPENDIX B. : ELASTIC MODULUS DATA

Table 18 HTV capsule summary and pre- and post-irradiation examination Young's modulus data and post irradiation examination TOF and velocity data for design temperature, T_{irr}=900°C

HTV Capsule Summary and Pre- and Post-Irradiation Examiation Young's Modulus Data																							
CAPSULE LAYOUT							Pre-IE		PIE														
	Irr. Temp.				Irr. Dose		Young's Modulus (GPa)		Average Thickness*		Density		Measurement 1		Measurement 2		Measurement 3		Mean Velocity	Young's Modulus (Pa)		Young's Modulus, GPa	Fractioal Change, [(EI/E0)-1]
Position	Design Temp.,°C	Actual Temp.,°C	Graphite grade	Spec. No.	Est. dose[1] dpa	Actual dose[2], dpa	E=ρ.v^2	0.9E	m	10^{-3} m	kg/m^3	g/cm^3	TOF (s)	Vel (m/s)	TOF (s)	Vel (m/s)	TOF (s)	Vel (m/s)	m/s	E=ρ.v^2	0.9E	0.9E	(0.9E used)
2-13	900	840	NBG-17	AA41	2.38	2.50	14.05	12.65	0.005356	5.356	1858.412	1.858	1.70E-06	3150.534	1.70E-06	3150.534	1.70E-06	3150.534	3150.534	1.84E+10	1.66E+10	16.60	0.31
4-30	900	840	NBG-17	AA43	3.12	3.29	14.38	12.94	0.00534	5.340	1871.815	1.872	1.62E-06	3296.316	1.61E-06	3316.79	1.61E-06	3316.79	3309.966	2.05E+10	1.85E+10	18.46	0.43
4-36	900	840	NBG-17	AA44	3.17	3.34	14.52	13.07	0.005337	5.337	1876.413	1.876	1.57E-06	3399.677	1.59E-06	3356.914	1.59E-06	3356.914	3371.168	2.13E+10	1.92E+10	19.19	0.47
2-14	900	840	NBG-18	BA41	2.43	2.56	15.56	14.00	0.005339	5.339	1870.684	1.871	1.68E-06	3178.213	1.68E-06	3178.213	1.68E-06	3178.213	3178.213	1.89E+10	1.70E+10	17.01	0.21
4-31	900	840	NBG-18	BA44	3.14	3.30	15.21	13.69	0.005329	5.329	1869.711	1.870	1.61E-06	3309.691	1.59E-06	3351.322	1.60E-06	3330.377	3330.463	2.07E+10	1.87E+10	18.66	0.36
2-17	900	840	H-451	CW41	2.57	2.71	13.15	11.84	0.005326	5.326	1729.111	1.729	1.57E-06	3392.599	1.57E-06	3392.599	1.57E-06	3392.599	3392.599	1.99E+10	1.79E+10	17.91	0.51
4-33	900	840	H-451	CW43	3.16	3.33	13.34	12.01	0.005327	5.327	1716.377	1.716	1.57E-06	3393.205	1.57E-06	3393.205	1.57E-06	3393.205	3393.205	1.98E+10	1.78E+10	17.79	0.48
2-12	900	840	PCEA	DW41	2.32	2.45	13.79	12.41	0.005327	5.327	1819.539	1.820	1.68E-06	3170.653	1.68E-06	3170.653	1.68E-06	3170.653	3170.653	1.83E+10	1.65E+10	16.46	0.33
2-18	900	840	PCEA	DW42	2.62	2.76	13.79	12.41	0.005321	5.321	1824.678	1.825	1.67E-06	3186.217	1.67E-06	3186.217	1.67E-06	3186.217	3186.217	1.85E+10	1.67E+10	16.67	0.34
4-29	900	840	PCEA	DW44	3.11	3.28	13.61	12.24	0.005293	5.293	1846.272	1.846	1.61E-06	3287.604	1.61E-06	3287.604	1.61E-06	3287.604	3287.604	2.00E+10	1.80E+10	17.96	0.47
4-35	900	840	PCEA	DW45	3.17	3.34	13.65	12.29	0.005296	5.296	1849.575	1.850	1.63E-06	3248.824	1.63E-06	3248.824	1.64E-06	3229.014	3242.22	1.94E+10	1.75E+10	17.50	0.42
2-10	900	840	IG-110	EA41	2.21	2.33	9.68	8.71	0.005338	5.338	1781.735	1.782	1.82E-06	2933.037	1.82E-06	2933.037	1.82E-06	2933.037	2933.037	1.53E+10	1.38E+10	13.79	0.58
2-15	900	840	IG-110	EA42	2.48	2.61	9.62	8.66	0.005337	5.337	1775.797	1.776	1.84E-06	2900.466	1.84E-06	2900.466	1.84E-06	2900.466	2900.466	1.49E+10	1.34E+10	13.45	0.55
4-32	900	840	IG-110	EA46	3.15	3.32	9.76	8.78	0.005319	5.319	1783.443	1.783	1.74E-06	3056.941	1.74E-06	3056.941	1.74E-06	3056.941	3056.941	1.67E+10	1.50E+10	15.00	0.71
2-11	900	840	2114	TA41	2.27	2.39	11.14	10.02	0.00535	5.350	1823.644	1.824	1.82E-06	2939.666	1.82E-06	2939.666	1.82E-06	2939.666	2939.666	1.58E+10	1.42E+10	14.18	0.42
2-16	900	840	2114	TA42	2.52	2.66	11.04	9.94	0.005356	5.356	1821.745	1.822	1.79E-06	2991.95	1.79E-06	2991.95	1.79E-06	2991.95	2991.95	1.63E+10	1.47E+10	14.68	0.48
4-28	900	840	2114	TA44	3.09	3.26	10.99	9.89	0.005351	5.351	1824.994	1.825	1.73E-06	3093.331	1.70E-06	3147.919	1.71E-06	3129.51	3123.587	1.78E+10	1.60E+10	16.03	0.62
4-34	900	840	2114	TA45	3.16	3.33	11.11	10.00	0.005349	5.349	1828.158	1.828	1.69E-06	3165.043	1.69E-06	3165.043	1.69E-06	3165.043	3165.043	1.83E+10	1.65E+10	16.48	0.65
[1] Based on estimated HTV duration in HFIR																							
[2] Based on actual HTV duration in HFIR cycles 460 and 461																						WG	

Table 19 HTV capsule summary and pre- and post-irradiation examination Young's modulus data and post irradiation examination TOF and velocity data for design temperature, T_{irr}=1200°C

HTV Capsule Summary and pre- and post-irradiation Examination Young's Modulus Data																							
CAPSULE LAYOUT							PreIE		PIE														
	Irr, Temp				Irr Dose		Young's Modulus (GPa)		Average Thickness*		Density		Measurement 1		Measurement 2		Measurement 3		Mean Velocity	Young's Modulus (Pa)		Young's Modulus, GPa	Fractioal Change, [(EI/E0)-1]
Position	Design Temp., °C	Actual Temp., °C	Graphite grade	Spec. No.	Est.Dose[1] dpa	Actual Dose[2], dpa	E=ρ.v^2	0.9E	m	10^{-3} m	kg/m^3	g/cm^3	TOF (s)	Vel (m/s)	TOF (s)	Vel (m/s)	TOF (s)	Vel (m/s)	m/s	E=ρ.v^2	0.9E	0.9E	(0.9E used)
8-66	1200		NBG-17	AA62	1.85	1.95	14.05039	12.64535	0.005334	5.334	1875.0	1.8750	1.77E-06	3013.38	1.77E-06	3013.38	1.77E-06	3013.38	3013.38	1.70E+10	1.53E+10	15.32	0.21
7-56	1200		NBG-17	AA46	2.57	2.71	14.28788	12.85909	0.005308	5.308	1901.0	1.9010	1.68E-06	3159.503	1.68E-06	3159.503	1.68E-06	3159.503	3159.503	1.90E+10	1.71E+10	17.08	0.33
3-24	1200		NBG-17	AA42	2.94	3.09	14.46086	13.01478	0.005312	5.312	1906.8	1.9068	1.68E-06	3162.149	1.68E-06	3162.149	1.68E-06	3162.149	3162.149	1.91E+10	1.72E+10	17.16	0.32
8-72	1200		NBG-18	BA64	1.41	1.49	15.26809	13.74128	0.005352	5.352	1869.6	1.8696	1.75E-06	3058.16	1.75E-06	3058.16	1.75E-06	3058.16	3058.16	1.75E+10	1.57E+10	15.74	0.15
8-67	1200		NBG-18	BA63	1.78	1.87	15.17919	13.66127	0.005313	5.313	1887.8	1.8878	1.74E-06	3053.474	1.74E-06	3053.474	1.74E-06	3053.474	3053.474	1.76E+10	1.58E+10	15.84	0.16
7-62	1200		NBG-18	BA48	2.27	2.39	15.72623	14.15361	0.005310	5.310	1917.5	1.9175	1.72E-06	3087.134	1.72E-06	3087.134	1.72E-06	3087.134	3087.134	1.83E+10	1.64E+10	16.45	0.16
7-57	1200		NBG-18	BA47	2.52	2.66	15.63266	14.0694	0.005300	5.300	1924.2	1.9242	1.64E-06	3231.53	1.64E-06	3231.53	1.64E-06	3231.53	3231.53	2.01E+10	1.81E+10	18.08	0.29
3-20	1200		NBG-18	BA42	2.81	2.96	15.62159	14.05943	0.005296	5.296	1922.2	1.9222	1.67E-06	3171.198	1.67E-06	3171.198	1.67E-06	3171.198	3171.198	1.93E+10	1.74E+10	17.40	0.24
3-25	1200		NBG-18	BA43	2.96	3.12	15.2886	13.75974	0.005299	5.299	1919.8	1.9198	1.67E-06	3173.289	1.67E-06	3173.289	1.67E-06	3173.289	3173.289	1.93E+10	1.74E+10	17.40	0.26
7-63	1200		H-451	CW45	2.21	2.33	13.22586	11.90328	0.005327	5.327	1720.0	1.7200	1.72E-06	3097.286	1.72E-06	3097.286	1.72E-06	3097.286	3097.286	1.65E+10	1.49E+10	14.85	0.25
3-27	1200		H-451	CW42	3.01	3.18	13.26011	11.9341	0.005320	5.320	1746.9	1.7469	1.63E-06	3264.017	1.60E-06	3325.217	1.60E-06	3325.217	3304.817	1.91E+10	1.72E+10	17.17	0.44
8-70	1200		PCEA	DW63	1.56	1.65	13.13884	11.82496	0.005331	5.331	1822.6	1.8226	1.78E-06	2994.667	1.78E-06	2994.667	1.78E-06	2994.667	2994.667	1.63E+10	1.47E+10	14.71	0.24
8-65	1200		PCEA	DW62	1.91	2.02	13.12698	11.81428	0.005324	5.324	1830.8	1.8308	1.75E-06	3042.376	1.75E-06	3042.376	1.75E-06	3042.376	3042.376	1.69E+10	1.53E+10	15.25	0.29
7-60	1200		PCEA	DW49	2.38	2.50	13.64687	12.28218	0.005294	5.294	1857.5	1.8575	1.73E-06	3060.296	1.73E-06	3060.296	1.73E-06	3060.296	3060.296	1.74E+10	1.57E+10	15.66	0.27
7-55	1200		PCEA	DW48	2.62	2.76	13.63078	12.26771	0.005289	5.289	1856.3	1.8563	1.74E-06	3039.789	1.74E-06	3039.789	1.74E-06	3039.789	3039.789	1.72E+10	1.54E+10	15.44	0.26
3-23	1200		PCEA	DW43	2.91	3.06	14.25461	12.82915	0.005290	5.290	1862.3	1.8623	1.69E-06	3130.099	1.69E-06	3130.099	1.69E-06	3130.099	3130.099	1.82E+10	1.64E+10	16.42	0.28
8-71	1200		IG-110	EA64	1.49	1.57	9.675859	8.708274	0.005341	5.341	1756.3	1.7563	1.90E-06	2811.212	1.90E-06	2811.212	1.90E-06	2811.212	2811.212	1.39E+10	1.25E+10	12.49	0.43
8-68	1200		IG-110	EA63	1.71	1.80	9.170769	8.253692	0.005344	5.344	1770.5	1.7705	1.94E-06	2754.722	1.94E-06	2754.722	1.94E-06	2754.722	2754.722	1.34E+10	1.21E+10	12.09	0.47
7-61	1200		IG-110	EA49	2.32	2.45	9.851574	8.866417	0.005317	5.317	1780.2	1.7802	1.90E-06	2798.679	1.90E-06	2798.679	1.90E-06	2798.679	2798.679	1.39E+10	1.25E+10	12.55	0.42
7-58	1200		IG-110	EA48	2.48	2.61	9.953103	8.957793	0.005314	5.314	1794.6	1.7946	1.88E-06	2826.594	1.88E-06	2826.594	1.88E-06	2826.594	2826.594	1.43E+10	1.29E+10	12.90	0.44
3-19	1200		IG-110	EA43	2.77	2.92	9.405673	8.465105	0.005318	5.318	1781.8	1.7818	1.89E-06	2813.655	1.89E-06	2813.655	1.89E-06	2813.655	2813.655	1.41E+10	1.27E+10	12.69	0.50
3-21	1200		IG-110	EA44	2.84	3.00	9.733231	8.759908	0.005304	5.304	1791.2	1.7912	1.87E-06	2836.277	1.87E-06	2836.277	1.87E-06	2836.277	2836.277	1.44E+10	1.30E+10	12.97	0.48
3-26	1200		IG-110	EA45	2.99	3.15	9.788972	8.810074	0.005312	5.312	1788.1	1.7881	1.84E-06	2887.007	1.84E-06	2887.007	1.84E-06	2887.007	2887.007	1.49E+10	1.34E+10	13.41	0.52
8-69	1200		2114	TA64	1.64	1.73	11.08034	9.972305	0.005330	5.330	1830.1	1.8301	1.85E-06	2881.012	1.85E-06	2881.012	1.84E-06	2896.67	2886.231	1.52E+10	1.37E+10	13.72	0.38
8-64	1200		2114	TA63	1.98	2.08	11.09348	9.984135	0.005340	5.340	1830.9	1.8309	1.85E-06	2886.486	1.85E-06	2886.486	1.85E-06	2886.486	2886.486	1.53E+10	1.37E+10	13.73	0.38
7-59	1200		2114	TA48	2.43	2.56	11.01014	9.909124	0.005323	5.323	1851.8	1.8518	1.82E-06	2924.489	1.82E-06	2924.489	1.82E-06	2924.489	2924.489	1.58E+10	1.43E+10	14.25	0.44
3-22	1200		2114	TA43	2.88	3.03	10.92811	9.835301	0.005320	5.320	1857.4	1.8574	1.82E-06	2922.919	1.82E-06	2922.919	1.82E-06	2922.919	2922.919	1.59E+10	1.43E+10	14.28	0.45
[1] Based on estimated HTV duration in HFIR																							
[2] Based on actual HTV duration in HFIR cycles 460 and 461																						WG	

Table 20 HTV capsule summary and pre- and post- irradiation examination Young's modulus data and post irradiation examination TOF and velocity data for design temperature, T_{irr}=1500°C

HTV Capsule Summary and Pre- and Posr-Irradiatiom Examination Young's Modulus Data																							
CAPSULE LAYOUT							PreIE		PIE														
	Irr. Temp.				Irr. dose		Young's Modulus (GPa)		Average Thickness*		Density		Measurement 1		Measurement 2		Measurement 3		Mean Velocity	Young's Modulus (Pa)		Young's Modulus, GPa	Fractioal Change, [(EI/E0)-1]
Position	Design Temp., °C	Actual Temp., °C	Graphite grade	Spec. No.	Est.Dose[1] dpa	Actual Dose[2], dpa	E=p.v^2	0.9E	m	10^{-3} m	kg/m^3	g/cm^3	TOF (s)	Vel (m/s)	TOF (s)	Vel (m/s)	TOF (s)	Vel (m/s)	m/s	E=p.v^2	0.9E	0.9E	(0.9E used)
1-8	1500		NBG-17	AA51	1.91	2.02	13.80	12.42	0.005294	5.294	1912.6	1.913	1.77E-06	2991.137	1.77E-06	2991.137	1.77E-06	2991.137	2991.137	17112111982	15400900784	15.40	0.24
6-51	1500		NBG-17	AA61	2.88	3.03	13.96	12.56	0.005278	5.278	1958.4	1.958	1.74E-06	3033.402	1.73E-06	3050.936	1.73E-06	3050.936	3045.092	18159022334	16343120101	16.34	0.30
5-41	1500		NBG-17	AA45	3.15	3.32	14.50	13.05	0.005268	5.268	1961.3	1.961	1.69E-06	3117.136	1.66E-06	3173.47	1.66E-06	3173.47	3154.692	19518587496	17566728746	17.57	0.35
1-3	1500		NBG-18	BA51	1.56	1.65	14.80	13.32	0.005310	5.310	1907.1	1.907	1.70E-06	3123.453	1.70E-06	3123.453	1.70E-06	3123.453	3123.453	18605453023	16744907721	16.74	0.26
1-9	1500		NBG-18	BA52	1.98	2.08	14.78	13.30	0.005282	5.282	1927.5	1.928	1.71E-06	3088.662	1.71E-06	3088.662	1.71E-06	3088.662	3088.662	18388166710	16549350039	16.55	0.24
6-52	1500		NBG-18	BA66	2.84	3.00	15.07	13.56	0.005251	5.251	1982.4	1.982	1.68E-06	3125.863	1.67E-06	3144.581	1.67E-06	3144.581	3138.342	19524959517	17572463566	17.57	0.30
6-47	1500		NBG-18	BA65	2.99	3.15	15.37	13.83	0.005255	5.255	1985.4	1.985	1.66E-06	3165.628	1.66E-06	3165.628	1.66E-06	3165.628	3165.628	19895981630	17906383467	17.91	0.29
5-42	1500		NBG-18	BA46	3.14	3.30	15.32	13.79	0.005253	5.253	1991.2	1.991	1.63E-06	3222.917	1.63E-06	3222.917	1.63E-06	3222.917	3222.917	20683468897	18615122007	18.62	0.35
5-37	1500		NBG-18	BA45	3.17	3.34	15.12	13.61	0.005254	5.254	1984.5	1.985	1.63E-06	3223.112	1.63E-06	3223.112	1.63E-06	3223.112	3223.112	20616219455	18554597509	18.55	0.36
1-6	1500		H-451	CW51	1.78	1.87	11.97	10.78	0.005300	5.300	1753.4	1.753	1.77E-06	2994.366	1.77E-06	2994.366	1.77E-06	2994.366	2994.366	15721490985	14149341886	14.15	0.31
6-53	1500		H-451	CW61	2.81	2.96	12.77	11.49	0.005230	5.230	1821.6	1.822	1.76E-06	2971.511	1.76E-06	2971.511	1.76E-06	2971.511	2971.511	16084523128	14476070816	14.48	0.26
5-43	1500		H-451	CW44	3.12	3.29	13.22	11.89	0.005222	5.222	1816.6	1.817	1.77E-06	2950.059	1.77E-06	2950.059	1.77E-06	2950.059	2950.059	15809355397	14228419857	14.23	0.20
1-1	1500		PCEA	DW51	1.41	1.49	12.57	11.31	0.005303	5.303	1844.0	1.844	1.77E-06	2995.801	1.77E-06	2995.801	1.77E-06	2995.801	2995.801	16549370197	14894433177	14.89	0.32
1-7	1500		PCEA	DW52	1.85	1.95	13.10	11.79	0.005260	5.260	1882.3	1.882	1.76E-06	2988.469	1.77E-06	2971.585	1.77E-06	2971.585	2977.213	16684203455	15015783110	15.02	0.27
6-50	1500		PCEA	DW61	2.91	3.06	12.99	11.69	0.005178	5.178	1970.7	1.971	1.68E-06	3082.018	1.68E-06	3082.018	1.68E-06	3082.018	3082.018	18719510763	16847559686	16.85	0.44
5-45	1500		PCEA	DW47	3.09	3.26	13.69	12.32	0.005191	5.191	1971.5	1.972	1.66E-06	3126.992	1.66E-06	3126.992	1.66E-06	3126.992	3126.992	19277535937	17349782343	17.35	0.41
5-40	1500		PCEA	DW46	3.16	3.33	13.64	12.28	0.005176	5.176	1978.6	1.979	1.64E-06	3155.834	1.64E-06	3155.834	1.64E-06	3155.834	3155.834	19705868339	17735281505	17.74	0.44
1-2	1500		IG-110	EA51	1.49	1.57	9.48	8.53	0.005296	5.296	1801.4	1.801	1.96E-06	2702.152	1.96E-06	2702.152	1.95E-06	2716.009	2706.771	13198510860	11878659774	11.88	0.39
1-4	1500		IG-110	EA52	1.64	1.73	9.50	8.55	0.005293	5.293	1828.8	1.829	1.97E-06	2686.662	1.97E-06	2686.662	1.97E-06	2686.662	2686.662	13200526999	11880474299	11.88	0.39
6-48	1500		IG-110	EA62	2.96	3.12	9.68	8.71	0.005237	5.237	1870.2	1.870	1.90E-06	2756.568	1.90E-06	2756.568	1.90E-06	2756.568	2756.568	14210705582	12789635023	12.79	0.47
6-46	1500		IG-110	EA61	3.01	3.18	9.21	8.29	0.005251	5.251	1880.3	1.880	1.89E-06	2778.377	1.89E-06	2778.377	1.89E-06	2778.377	2778.377	14515072026	13063564824	13.06	0.58
5-38	1500		IG-110	EA47	3.17	3.34	9.97	8.97	0.005228	5.228	1889.6	1.890	1.81E-06	2888.198	1.81E-06	2888.198	1.80E-06	2904.243	2893.546	15821009791	14238908812	14.24	0.59
1-5	1500		2114	TA51	1.71	1.80	10.81	9.73	0.005308	5.308	1875.6	1.876	1.87E-06	2838.654	1.88E-06	2823.555	1.88E-06	2823.555	2828.588	15006130084	13505517076	13.51	0.39
6-54	1500		2114	TA62	2.77	2.92	10.96	9.86	0.005292	5.292	1908.2	1.908	1.83E-06	2891.803	1.83E-06	2891.803	1.83E-06	2891.803	2891.803	15957372500	14361635250	14.36	0.46
6-49	1500		2114	TA61	2.94	3.09	10.77	9.69	0.005311	5.311	1898.7	1.899	1.78E-06	2983.965	1.78E-06	2983.965	1.78E-06	2983.965	2983.965	16906236969	15215613272	15.22	0.57
5-44	1500		2114	TA47	3.11	3.28	11.06	9.96	0.005282	5.282	1900.5	1.900	1.70E-06	3106.831	1.70E-06	3106.831	1.71E-06	3088.662	3100.775	18272841632	16445557469	16.45	0.65
5-39	1500		2114	TA46	3.16	3.33	11.15	10.03	0.005298	5.298	1896.9	1.897	1.70E-06	3116.729	1.70E-06	3116.729	1.70E-06	3116.729	3116.729	18426514770	16583863293	16.58	0.65
[1] Based on estimated HTV duration in HFIR																							
[2] Based on actual HTV duration in HFIR cycles 460 and 461																						WG	

9. REFERENCES

[1] Thrower P A and Meyer R M, Review article: point defects and self-diffusion in graphite, *Phys. Status Solidi (a)*, 14, 11-37 (1978)

[2] Kelly B. T., Physics of Graphite, Applied Science Publishers, London (1981)

[3] Burchell T.D, Radiation damage in carbon materials. In *Physical Processes of the Interaction of Fusion Plasmas with Solids*, ed. W.O. Hoffer and J. Roth, Academic Press, San Diego, 1996, pp.341-384

[4] Burchell, T. D. Fission Reactor Applications of Carbon, In: Carbon Materials for Advanced Technologies, Burchell, T. D., Ed., Pub. Elsevier Science, Oxford, UK (1999).

[5] Kelly B T, Carbon Vol.15, pp. 117-127 (1977)

[6] Engle G B and Eatherly W P, Irradiation Behavior of Graphite at High Temperatures, *High Temperatures-High Pressures* 4, 119-158 (1972)

[7] Burchell, T. D. and Snead, L. L. Journal of Nuclear Materials, 371, 18–27 (2007)

[8] Price R J, High-temperature neutron irradiation of highly oriented carbons and graphites, Carbon 12, 159-169 (1974)

[9] Burchell, T. D. and Eatherly, W. P. Journal of Nuclear Materials, 170-181, 205-208 (1991)

[10] ORNL/TM-2012/517, Tim Burchell and Joe Strizak, HTV irradiation Capsule Specimen Pre-IE Report, February 2013

[11] ASTM C559-16, Standard Test Method for Bulk Density by Physical Measurement of Manufactured Carbon and Graphite Articles, Annual Book of Standards, Vol. 05.05, 2017

[12] ASTM C769-15, Standard Test Method For Sonic Velocity in Manufactured Carbon and Graphite Materials for Use in Obtaining Young's Modulus, Annual Book of Standards, Vol. 05.05, 2017

[13] ASTM E228-11, Standard Test Method for Linear Thermal Expansion of Solid Materials With a Push-Rod Dilatometer, Annual Book of Standards, 2011

[14] ASTM C611-98 (Reapproved 2016), Standard Test Method for Electrical Resistivity of Manufactured Carbon and Graphite Articles at Room Temperature, Annual Book of Standards, Vol. 05.05, 2017

[15] ORNL/TM-2012/10, Tim Burchell, Joe Strizak, Joel McDuffee and Ken Thoms, Experimental Plan for HFIR High Temperature Graphite Irradiation capsule (HTV), April 2012

[16] Thomas Daly and Joel McDuffee, Experimental And Computational Study Of The Flux Spectrum In Materials Irradiation Facilities Of
The High Flux Isotope Reactor, In PHYSOR 2012 Advances in Reactor Physics Linking Research, Industry, and Education, Knoxville, Tennessee, USA, April 15-20, 2012, on CD-ROM, American Nuclear Society, LaGrange Park, IL (2012)

[17] Campbell, A.A., W.D. Porter, Y. Katoh, and L.L. Snead, "Method for Analyzing Passive SiC Thermometry with a Continuous Dilatometer to Determine Irradiation Temperature", *NIMB*, 370, 49-58 (2016)

[18] DAC-18-13-HTV01, Rev.0, J. L. McDuffee, Design Analysis for the HTV High Temperature Graphite Target Experiment, April 2014

[19] ORNL/TM-2011/497 Tim Burchell and Joe Strizak, "Post-Irradiation Examination Data for PCEA Irradiated at 900°C in HFIR" May 2012

[20] T. D. Burchell and J. P. Strizak, The Effect of Neutron Irradiation on the Fracture Toughness of Graphite*, Nuclear Engineering and Design* 271 (2014) pp. 262-269

[21] International Database on Irradiated Nuclear Graphite Properties, 2009 version. International Atomic Energy Agency